FABRICATION OF REDUCED GRAPHENE OXIDE QUANTUM DOTS VIA HYDROTHERMAL PROCESS AND THEIR APPLICATION IN SUPERCAPACITORS

TANATCHAYA SEESAN

A THESIS SUBMITTED IN PARTIAL FULFILLMENT OF THE REQUIREMENT FOR THE
DEGREE OF MASTER OF SCIENCE IN PHYSICS
DEPARTMENT OF PHYSICS SCHOOL OF SCIENCE
KING MONGKUT'S INSTITUTE OF TECHNOLOGY LADKRABANG
2025
KMITL-2025-SC-M-030-025

Thesis Title Fabrication of Reduced Graphene Oxide Quantum Dots Via Hydrothermal Process and Their Application in Supercapacitors
Student Tanatchaya Seesan
Student ID 66056036
Degree Master of Science (Applied Physics)
Department Physics
Year 2025
Advisor Prof. Dr. Chesta Ruttanapun

Abstract

This study presents the hydrothermal synthesis, characterization, and application of reduced graphene oxide quantum dots (rGO-QDs) as functional materials in supercapacitor electrolytes. The rGO-QDs were synthesized through oxidative cutting of graphene oxide followed by hydrothermal reduction, with synthesis parameters systematically optimized across five experimental trials. The optimized rGO-QDs exhibited blue fluorescence, nanometer-scale dimensions (~4 nm), and distinct graphitic lattice features, confirming successful quantum dot formation with restored π-conjugated domains.

Comprehensive characterization was performed using UV-Vis absorption, photoluminescence spectroscopy, XRD, TEM, Raman spectroscopy, and Hall effect measurements. The results demonstrated that the rGO-QDs possess tunable optical and electronic properties, which are highly sensitive to synthesis conditions such as ultrasonication time, pH adjustment, and purification steps.

For application, the rGO-QDs were dispersed in a 3 M KOH solution and utilized as a hybrid electrolyte in symmetric coin-cell supercapacitors. The rGO-QD-enhanced electrolyte significantly improved the specific capacitance to 55 F/g compared to the pure KOH system. This enhancement is attributed to increased ionic conductivity, improved ion mobility, and additional pseudocapacitive contributions from the functional groups on the rGO-QD surfaces.

The findings highlight the multifunctionality of rGO-QDs, combining high dispersibility, tunable bandgap, and surface activity for both optical and electrochemical applications. This work provides a scalable synthesis route and establishes rGO-QDs as promising candidates for next-generation energy storage systems.

Keywords: Reduced Graphene Oxide Quantum Dots, Hydrothermal Synthesis, Optical Properties, Supercapacitor

Acknowledgements

This thesis is based on the works which the author have attended to as a Master's student of Department of Physics, School of Science, King Mongkut’s Institute of Technology Ladkrabang, Ladkrabang. This thesis would not have been possible without the kind help of many people.

First, I shall be grateful to my supervisor, Assoc. Prof. Dr. Chesta Ruttanapun. He provides me the best environment for research and is a good mentor. Thanks to School of Science, King Mongkut’s Institute of Technology Ladkrabang, Ladkrabang for awarding me a RA/TA [RA/TA-2566-M-016], providing me with the financial means to complete this project.

I would like to express my sincere gratitude to my supervisor in Japan Prof. Yoshiaki Yasuno, who is a principle investigator of Computational Optics Group (COG), University of Tsukuba, Japan, for your patience, guidance, and support. I have benefited greatly from your wealth of knowledge and meticulous editing. I am extremely grateful that you took me on as a student and continued to have faith in me over the years.

I would like to thank anonymous reviewers of the Graphene community for their careful reading of our manuscript and their insightful comments and suggestions.

Finally I would like to thank my family. My parents and sister are not only patrons to get higher education, but also great supporter in my life.

Miss Tanatchaya Seesan

Table of contents

Page

List of tables

Page

List of figures

Abbreviations/Symbols

AC	Attenuation Coefficient
C_{dl}	Double-layer capacitance
C_{sp}	Specific capacitance
CCC	Charge Carrier Concentration
CD	Carbon Dot
CNTs	Carbon Nanotubes
CV	Cyclic Voltammetry
DFT	Density Functional Theory
DLS	Dynamic Light Scattering
E_a	Activation Energy
E_{bg}	Bandgap of bulk material
EDLC	Electric Double-Layer Capacitance
EDX	Energy Dispersive X-ray Spectroscopy
EIS	Electrochemical Impedance Spectroscopy
FT-IR	Fourier Transform Infrared Spectroscopy
FWHM	Full Width at Half Maximum
GCD	Galvanostatic Charge–Discharge
GNR	Graphene Nanoribbon
GO	Graphene Oxide
GQD	Graphene Quantum Dot
h	Planck’s constant
HRTEM	High-Resolution Transmission Electron Microscopy
I_D/I_G	Intensity Ratio of D-band to G-band
I	Discharge Current
k	Boltzmann constant
KOH	Potassium Hydroxide
L	Distance between electrodes
LED	Light-Emitting Diode
$m_e,\ m_h$	Effective Mass of Electron and Hole

NMP	N-Methyl-2-Pyrrolidone
PL	Photoluminescence
PVDF	Polyvinylidene Fluoride
QD	Quantum Dot
QY	Quantum Yield
R_{ct}	Charge Transfer Resistance
rGO	Reduced Graphene Oxide
rGO-QD	Reduced Graphene Oxide Quantum Dot
R_H	Hall Coefficient
R_s	Sheet Resistance
SEM	Scanning Electron Microscopy
sp^2	sp^2-hybridized Carbon
T	Absolute Temperature
TE	Thermoelectric
TEM	Transmission Electron Microscopy
UV-Vis	Ultraviolet-Visible Spectroscopy
XPS	X-ray Photoelectron Spectroscopy
XRD	X-ray Diffraction
ZT	Thermoelectric Figure of Merit
Z_W	Warburg Impedance
S	Seebeck Coefficient
ω	Angular Frequency
σ	Ionic Conductivity
σ_W	Warburg Coefficient

Chapter 1

Introduction

1.1 Background and motivation

In the pursuit of high-efficiency and sustainable energy technologies, the development of novel nanomaterials has become a central focus across various research disciplines. Among these, graphene-based materials have garnered significant attention owing to their extraordinary mechanical strength, thermal and electrical conductivity, and high surface area. Their two-dimensional sp^2-hybridized carbon lattice and modifiable surface chemistry make them highly versatile for use in applications ranging from energy storage and optoelectronics to sensing and nanomedicine [1].

One particularly promising member of the graphene family is reduced graphene oxide quantum dots (rGO-QDs) zero-dimensional (0D) nanostructures that combine the high conductivity of reduced graphene oxide (rGO) with the unique size-dependent optical and electronic properties of quantum dots. Due to quantum confinement effects, rGO-QDs exhibit tunable photoluminescence, strong light absorption, and modifiable bandgap energies [2,3]. These properties, along with oxygen-containing functional groups on their surfaces, contribute to high dispersibility, enhanced electrochemical activity, and effective charge transfer, making them suitable for advanced optoelectronic, sensing, and energy applications [2,3].

This research was initially conceived with the goal of enhancing the thermoelectric performance of bismuth telluride (Bi_2Te_3), a well-known thermoelectric material used for converting heat into electricity. However, its performance is limited by intrinsic trade-offs namely, the simultaneous requirement for high electrical conductivity and low thermal conductivity, a challenge governed by the Wiedemann-Franz law and the Pisarenko relation. Recent studies have proposed that incorporating graphene-based quantum dots can overcome these limitations by introducing additional phonon scattering centers and improving carrier mobility, leading to enhanced thermoelectric figure of merit (ZT) in Bi_2Te_3 composites [4,5].

Although early synthesis and integration of rGO-QDs into Bi_2Te_3 were successful, difficulties in reproducibility and limitations in thermoelectric property analysis necessitated a shift in research direction. Rather than abandoning the material altogether, the focus was strategically redirected toward investigating the fundamental properties of rGO-QDs and their application in energy storage systems, particularly in electrolyte supercapacitors. In this context, rGO-QDs offer substantial benefits: their ultrasmall size increases effective surface area for ion transport, while their oxygenated functional groups enhance electrolyte wettability and interfacial charge transfer [6].

This redirection enables a broader evaluation of rGO-QDs as multifunctional nanomaterials. Their potential extends beyond thermoelectricity into domains requiring high power density, rapid charge/discharge rates, and stable ionic conduction, such as next-generation supercapacitors and hybrid electrochemical devices. Therefore, even though the application has changed, the core investigation of rGO-QDs as high-performance functional materials remains intact and scientifically relevant.

1.2 Objectives of the study

1) Synthesize and characterize composite materials made of rGO-QDs and Bi_2Te_3.
2) Investigate how rGO-QDs affect the key thermoelectric properties of Bi_2Te_3: Seebeck coefficient, electrical conductivity, and thermal conductivity.
3) To reduce the thermal conductivity while maintaining its high electrical conductivity.
4) To synthesize and characterize the optical properties of rGO-QDs using UV-Vis spectroscopy, photoluminescence (PL), and Raman spectroscopy to confirm their quantum confinement effect.
5) To evaluate the ionic conduction behavior of rGO-QDs in KOH-based electrolyte solutions using electrochemical impedance spectroscopy (EIS).
6) To analyze the electrochemical performance of rGO-QDs as an electrolyte additive in supercapacitor devices, focusing on capacitance, charge storage, and internal resistance.

1.3 Scopes of the study

1) Synthesis of rGO-QDs by using a hydrothermal process.
2) Characterization and properties measurements of synthesis rGO–QDs and rGO–QDs/ Bi_2Te_3.

3) Enhanced thermoelectric properties of Bi_2Te_3 by using rGO-QDs composite nanomaterial.
4) Structural, optical, and electrochemical characterization of rGO-QDs using techniques such as TEM, XRD, Raman spectroscopy, UV-Vis, fluorescence spectroscopy, Hall effect, and EIS.
5) Investigation of rGO-QDs as an additive in electrolyte systems for supercapacitors, and evaluation of their effect on device performance metrics.

1.4 Benefits of the study

1) Develop thermoelectric materials with potentially superior properties compared to pure Bi_2Te_3.
2) Provides a deeper understanding of the mechanisms behind thermoelectric behavior in composite materials.
3) Balancing high electrical conductivity for efficient heat-to-electricity conversion with low thermal conductivity to minimize heat loss.
4) The study investigates the potential of rGO-QDs in KOH-based electrolytes to enhance electrolyte performance in supercapacitors by improving ionic conductivity, reducing internal resistance, and increasing charge storage efficiency.
5) The study provides insights into the ionic conduction mechanism of rGO-QDs by analyzing ion transport behavior in rGO-QD-enhanced electrolytes, contributing to the development of advanced energy storage materials.
6) It expands the application of rGO-QDs in energy storage by advancing nanomaterials for supercapacitor electrolytes, paving the way for future research in next-generation energy storage technologies.

Chapter 2

Theory and Literature Reviews

2.1 Graphene-Based Materials and Quantum Dots: Structure and Properties.

Graphene-based materials have gained significant attention due to their unique structural, electronic, and optical properties, making them highly versatile for various applications, including energy storage, optoelectronics, and nanomedicine. Among these materials, graphene, GO, and rGO exhibit distinct characteristics that influence their performance in different applications. More recently, rGO-QDs, a quantum-confined nanomaterial derived from rGO, have emerged as a particularly promising subclass. Their tunable size, high surface-to-volume ratio, and edge-dominated surface chemistry provide multifunctional behavior that is especially attractive for use in electrochemical systems and optoelectronic devices [2,6].

GO and rGO are essential materials in nanotechnology and materials science due to their remarkable physicochemical properties, structural versatility, and functional tunability. GO is a chemically modified form of graphene synthesized through the oxidation of graphite. This process introduces oxygen-containing functional groups, such as hydroxyl (-OH), epoxy (-O-), and carboxyl (-COOH), which significantly alter its electronic structure, solubility, and reactivity [7,8]. These oxygen functionalities enhance GO's dispersion in aqueous and polar solvents, making it suitable for various applications, including biomedical imaging, composite materials, and catalysis [7]. However, the introduction of oxygen groups also disrupts the sp^2 hybridization of carbon atoms, leading to a significant decrease in electrical conductivity [9].

rGO is derived from GO through various reduction processes aimed at removing oxygen-containing groups while partially restoring the π-conjugated system of graphene. The reduction process enhances the electrical conductivity, mechanical strength, and chemical stability of the material, making it suitable for applications in energy storage, optoelectronics, and flexible electronics. The extent of reduction significantly influences the final properties of rGO, as incomplete reduction leaves residual oxygen groups that affect conductivity and electrochemical behavior [10,11]

The synthesis and transformation of GO into rGO are crucial steps in tailoring these materials for specific applications. The level of oxidation and subsequent reduction dictate their structural and electrical properties, which can be optimized for energy devices such as supercapacitors and batteries. Building upon this foundation, this section further explores the structural evolution from GO to rGO and ultimately to rGO-QDs, along with their implications for electrical conductivity, surface functionality, and nanoscale behavior relevant to advanced energy and sensing applications.

2.1.1 Structure and Properties of GO rGO and rGO-QDs

GO and rGO are both derived from pristine graphene, yet their physicochemical properties diverge substantially due to differences in oxidation level and defect concentration. In GO, oxygen-containing functional groups—predominantly hydroxyl and epoxy groups on the basal planes and carboxyl groups at the edges- are introduced during oxidation. These groups increase the interlayer spacing and disrupt the continuous sp^2-hybridized carbon lattice, converting portions of the conjugated network into sp^3-hybridized areas. As a consequence, GO exhibits considerably lower electrical conductivity compared to graphene, but it also displays enhanced hydrophilicity and colloidal stability, making it well-suited for applications that benefit from surface functionalization, such as nanocomposite matrices, catalyst supports, and biomedical platforms [12].

The reduction of GO to form rGO is achieved through chemical, thermal, or electrochemical methods aimed at removing a portion of the oxygen functionalities. This process partially restores the π-conjugated framework, thereby enhancing the electrical conductivity, mechanical strength, and chemical stability of the material. However, the method of reduction critically influences the defect landscape of the resulting rGO. Thermal reduction, for example, can lead to rapid gas evolution that may generate lattice vacancies and folds, while chemical or electrochemical reduction offers better control over residual functional groups but might leave behind impurities or unremoved oxygen groups [13]. The resultant rGO thus typically possesses a hybrid structure that combines reformed sp^2 domains with residual oxidized regions, allowing its properties to be fine-tuned for applications such as flexible electronics, supercapacitor electrodes, and biosensors.

When rGO is further scaled down to form quantum dots (rGO-QDs), additional phenomena arising from quantum confinement and high edge-to-surface atom ratios come into play. Although the nanometric dimensions of rGO-QDs lead to an increase in defect density relative to bulk rGO, these defects-comprising vacancies, edge sites, and remnant oxygenated groups-contribute to tunable optical properties and enhanced electrochemical activity. The synthesis typically involves hydrothermal treatment of GO to simultaneously reduce the material and fragment it into quantum-sized domains, resulting in rGO-QDs with relatively narrow size distributions, good water dispersibility, intrinsic photoluminescence, and adequate electrical conductivity for supporting rapid electron transfer processes [14]. Therefore, while GO is typically favored for its high density of surface functional groups and dispersibility, rGO and its quantum dot derivatives strike an optimal balance between electrical conductivity and surface reactivity, enabling their use across a range of energy-related and electronic applications.

2.1.1.1 Fundamental Structure of Graphene-Based Materials

Graphene is a two-dimensional (2D) carbon allotrope, consists of a single layer of sp^2-hybridized carbon atoms arranged in a hexagonal honeycomb lattice. This unique structure yields an uninterrupted π-conjugated network with delocalized electrons across its plane, which is central to its exceptional mechanical strength, high thermal and electrical conductivity, and unusual electronic properties such as massless Dirac fermion behavior and high charge carrier mobility [15]. The ideal atomic arrangement of graphene is foundational to its remarkable in-plane electron transport and extraordinary flexibility.

GO is obtained through the oxidative treatment of graphite. In the oxidation process, oxygen-containing functional groups such as hydroxyl (–OH) and epoxy (–O–) groups are predominantly introduced onto the basal planes, while carboxyl (–COOH) groups tend to localize at the sheet edges. These functional groups disrupt the continuous sp^2-hybridized carbon lattice by converting portions of the aromatic network into sp^3-hybridized regions, thereby increasing interlayer spacing and generating structural defects. Consequently, the loss of an extended π-conjugated system severely impairs electrical conductivity, effectively transforming graphene into an insulating material; however, this functionalization simultaneously augments the hydrophilicity of the material, which facilitates its dispersion in aqueous and other polar solvents and enables subsequent chemical modifications [1].

The subsequent reduction of GO to form rGO aims to remove a portion of the oxygen functionalities through chemical, thermal, or electrochemical strategies, thereby partially restoring the π-conjugated network. While such reduction improves properties such as electrical conductivity, mechanical strength, and chemical stability compared to GO, it is typically incomplete. Residual oxygen groups and defects (e.g., vacancies, wrinkles, edge disruptions) remain, resulting in a hybrid structure where restored sp^2 domains coexist with oxidized regions. The precise properties of rGO are highly sensitive to both the degree of reduction and the method employed; for instance, thermal reduction can enhance conductivity via effective oxygen removal but may also introduce additional lattice defects, whereas chemical or electrochemical routes offer greater control over the surface chemistry [16].

Moreover, rGO-QDs, which are synthesized from rGO, possess lateral sizes typically below 10 nm. Their nanoscale dimensions result in discrete energy levels, distinguishing them structurally and electronically from their larger counterparts. When rGO is further downscaled into quantum dots (rGO-QDs), the material not only preserves fragments of the sp^2-hybridized carbon lattice but also exhibits new properties attributable to quantum confinement effects and a high edge-to-surface atom ratio. These rGO-QDs inherit a complex structure: while small sp^2 domains in these nanostructures allow for relatively efficient electron transport, the edge-dominated chemistry and residual oxygenated sites provide opportunities for tunable optical emission and enhanced electrochemical activity. This combination of features results in rGO-QDs being highly attractive for applications that span from optoelectronic devices to energy storage systems, where both their electronic conductivity and surface reactivity are critical [17]. Overall, the continuum of structural modifications from pristine graphene through GO and rGO to rGO-QDs illustrates a trade-off between processability, functionalizability, and electronic performance, and emphasizes the importance of atomic-level control in tailoring material properties for specific technological applications.

2.1.1.2 Functional Groups and π-Conjugation Restoration

GO is produced by the oxidative treatment of graphite, a process that introduces a wide range of oxygen-containing functional groups into the carbon lattice. Predominantly, hydroxyl (–OH) and epoxy (–O–) groups are grafted onto the basal planes, while carboxyl (–COOH) and carbonyl (C=O) groups tend to localize at the sheet edges. The incorporation of these polar groups disrupts the planar sp^2-hybridization characteristic of pristine graphene, converting regions of the conjugated aromatic network into sp^3-hybridized domains. This structural transformation results in an increased interlayer spacing and creates a high density of defects that hinder electron delocalization, thereby diminishing the electrical conductivity of GO. However, these oxygen functionalities also confer excellent hydrophilicity and chemical reactivity, promoting robust dispersion in aqueous and other polar solvents, while facilitating chemical modifications for applications in composites, biomedicine, and catalysis [18].

The reduction of GO to yield rGO is a pivotal step in partially restoring the π-conjugated network that underpins graphene’s superior electrical and mechanical properties. Reduction methods, including thermal annealing, chemical reduction (using agents such as hydrazine, ascorbic acid, or sodium borohydride), and electrochemical approaches, aim to remove oxygen functionalities. Thermal reduction generally achieves greater deoxygenation, improving electrical conductivity; however, it may also induce structural damage due to rapid gas evolution. In contrast, chemical and electrochemical reductions allow for more selective deoxygenation, thus preserving some residual oxygen groups that can be beneficial for subsequent functionalization, albeit at the expense of complete restoration of the sp^2 network [16]. The resulting rGO typically exhibits a composite architecture of restored conductive regions interspersed with defect-rich, oxygenated areas, thereby offering a tunable balance between electrical performance and chemical activity. In the case of rGO-QDs, the restoration of π-conjugation is localized due to the limited domain size. However, this partial recovery still significantly enhances the optical and electronic properties of the quantum dots, particularly their ability to exhibit photoluminescence and support electron delocalization.

When rGO is further processed into quantum dots, its physicochemical behavior becomes more complex due to additional size-dependent quantum confinement effects and an increased edge-to-surface atom ratio. The heterogeneous and incomplete restoration of π-conjugation in rGO persists in the rGO-QDs, with residual oxygen functional groups and structural defects influencing their optoelectronic properties. These localized electronic states are crucial for defining the photoluminescence, charge transport, and chemical reactivity of the quantum dots, which are vital parameters for applications in imaging, sensing, and energy storage [14]. Consequently, understanding the distribution and transformation of oxygen-containing groups from GO to rGO and subsequently to rGO-QDs is essential for tailoring the balance between conductivity and functionality to meet specific device requirements.

2.1.1.3 Synthesis and Properties of rGO-QDs

rGO-QDs are a class of carbon-based nanomaterials that combine the distinctive electronic characteristics of graphene with the quantum confinement effect of quantum dots. These nanostructures typically possess lateral sizes in the range of 2 to 10 nanometers and exhibit a range of desirable features, such as high surface area, tunable optical emission, excellent dispersibility, and notable electrical conductivity [2,6]. The high dispersibility and chemical reactivity of these nanodots are attributed to their partially restored sp^2-hybridized carbon networks and the presence of residual oxygenated functional groups, which not only ensure stability in polar media but also serve as reactive sites for further conjugation [6,14].

The synthesis of rGO-QDs typically begins with the preparation of GO, which is then reduced and fragmented into quantum-sized domains using physical or chemical methods. A commonly employed method is the hydrothermal technique, where an aqueous suspension of GO is sealed in a Teflon-lined autoclave and heated at 160–200 °C for several hours. This process not only reduces oxygen functionalities but also cleaves the GO sheets into well-dispersed quantum dots with narrow size distribution [14]. Other methods include oxidative fragmentation followed by chemical reduction using agents such as hydrazine, sodium borohydride, or ascorbic acid. Ultrasonic-assisted exfoliation is another strategy that uses shear force to break GO sheets into nanoscale pieces. Each synthesis method differs in particle uniformity, yield, surface chemistry, and potential by-products, but all aim to produce nanodots with useful optical and electronic features [2,14]. The hydrothermal approach is often preferred for its one-step simplicity and relatively high yield, making it attractive for scalable synthesis. Reaction parameters such as pH, precursor concentration, temperature, and duration significantly influence the size, fluorescence, and surface properties of the resulting QDs.

The confirmation that the synthesized material is indeed rGO-QDs typically involves a combination of structural, chemical, morphological, and optical analyses. Transmission electron microscopy (TEM) plays a pivotal role in analyzing the nanoscale morphology of rGO-QDs, typically revealing lattice fringes that show an interlayer spacing of approximately 0.34 nm. This spacing is characteristic of graphitic domains, confirming the presence of sp^2 hybridized carbon structures (TEM, HRTEM) which are essential for the electrical and optical properties of graphene-related materials [19]. X-ray Diffraction (XRD) is employed to identify the crystallographic structure of rGO-QDs. The broad peak around 24° to 26° (2θ) correlates to the (002) plane of reduced graphene oxide, indicating a restoration of the sp^2 carbon network, which is crucial for enhancing conductivity and electronic properties [14]. Furthermore, Raman spectroscopy significantly contributes to understanding the quality of the synthesized rGO-QDs. The intensity ratio of the D and G bands (ID/IG) is evaluated; an increase in the D band intensity suggests the presence of defects that are often found at the edges of quantum dots, which is pivotal in affirming quantum dot formation [3]. Fourier Transform Infrared (FTIR) spectroscopy complements these findings by providing insights into the chemical composition, wherein the reduced peaks associated with oxygen-containing functional groups like –OH and C=O indicate effective reduction relative to graphene oxide [12]. Moreover, X-ray Photoelectron Spectroscopy (XPS) quantitatively assesses the reduction effectiveness by demonstrating a decline in oxygen functionalities and an increase in C=C bonds associated with graphitic domains, providing evidence of the chemical alterations occurring during the reduction process [12]. Optical properties are also essential for identifying rGO-QDs. UV-Vis absorption spectroscopy typically showcases a π–π^* transition peak between 260 to 270 nm, a characteristic feature that reveals the extent of conjugation and the degree of quantum confinement in the QDs [14]. Photoluminescence (PL) studies are instrumental in confirming the quantum dot nature, characterized by excitation-dependent emissions and a blue shift in emission wavelengths compared to bulk rGO, which corroborates the size-induced quantum confinement effects that boost the photoluminescent properties of the material [2]. Additionally, Dynamic Light Scattering (DLS) and zeta potential measurements may provide quantitative data on the size distribution and colloidal stability of rGO-QDs, further indicating successful synthesis [20]. These analytical techniques collectively verify the nanoscale dimensions, partial reduction, and preserved π-conjugation in rGO-QDs, ensuring their suitability for optoelectronic and electrochemical applications.

In terms of optical properties, rGO-QDs display strong and tunable photoluminescence, which is influenced by both quantum confinement and surface/edge state effects. As the particle size decreases, quantum confinement causes a blue shift in the emission spectrum, while the presence of oxygenated functional groups at the edges introduces additional defect-related states that modulate emission intensity and wavelength. The emission profile can be tuned from blue to red by adjusting the synthesis parameters such as temperature, pH, and reaction duration. Ultraviolet-visible (UV–Vis) absorption spectra of rGO-QDs typically show a primary peak around 230 nm, corresponding to π–π^* transitions in the aromatic C=C bonds, and a shoulder between 300 and 350 nm, attributed to n–π^* transitions of oxygenated groups [2,6].

Beyond their optical performance, rGO-QDs exhibit improved electrical conductivity compared to unreduced GO or insulating carbon quantum dots. This enhancement is attributed to the partial restoration of the π-conjugated network, which allows for more efficient charge carrier transport. When integrated into electrochemical systems particularly as additives in supercapacitor electrolytes rGO-QDs improve interfacial charge transfer and facilitate ion diffusion through their high surface area and enhanced electrolyte wettability [6]. Furthermore, the coexistence of conductive sp^2 domains and reactive oxygenated edges makes rGO-QDs highly versatile for applications across optoelectronics, energy conversion, catalysis, and biosensing. Importantly, their synthesis scalability, tunable emission, and environmental compatibility give rGO-QDs a competitive edge over traditional semiconductor QDs in green nanotechnology development.

Compared to other types of quantum dots, such as traditional semiconductor-based QDs (e.g., CdSe, PbS) or carbon dots (CDs), rGO-QDs offer the advantage of chemical stability, environmental compatibility, and dual functionality in both electron transport and optical modulation. Their performance can be tailored via synthesis conditions, enabling integration into next-generation devices that require a synergistic balance of conductivity, fluorescence, and surface reactivity.

2.1.1.4 Electrical Conductivity and Defect Structure of GO, rGO, and rGO-QDs

The electrical conductivity of graphene-based is a fundamental property governing their utility in electronics, energy storage, and electrochemical applications. Pristine graphene exhibits outstanding conductivity ($\sim 10^4$–10^5 S/m), attributed to its extended sp^2-hybridized carbon lattice and high charge carrier mobility. However, oxidation to form GO introduces oxygen-containing functional groups (e.g., hydroxyl, epoxy, carboxyl), disrupting the π-conjugated system and converting sp^2 carbons into sp^3 hybridizations. This structural alteration drastically lowers GO’s conductivity, typically to the range of 10^{-2} to 10^2 S/m [12].

rGO is obtained by partially removing these oxygen groups through chemical, thermal, or electrochemical reduction, leading to a partial restoration of the conductive sp^2 domains. The conductivity of rGO varies widely depending on the reduction method, often ranging from 10^2 to 10^3 S/m [21,22]. For instance, thermal reduction can restore more extended π-networks but may introduce structural vacancies, while chemical reduction tends to be milder but may leave residual defects and functional groups that scatter electrons.

Characterization of these materials is commonly performed using techniques such as Raman spectroscopy and X-ray Photoelectron Spectroscopy (XPS). Raman spectra provide insights into structural disorder through the D and G bands. The D band, associated with lattice defects, increases in intensity relative to the G band when disorder is present. The I_D/I_G ratio serves as a metric for defect density and graphitization. XPS complements this by quantifying elemental compositions and bonding states; a high oxygen-to-carbon ratio in GO indicates extensive oxidation, while a reduced ratio in rGO signifies restoration of graphitic structure [12,21]. In general, rGO’s electrical conductivity represents a trade-off between restored sp^2 regions and defect-induced scattering, which can be strategically tuned for specific applications.

When GO is further downscaled to reduced graphene oxide quantum dots (rGO-QDs), their electrical properties are further influenced by size effects, edge chemistry, and quantum confinement. Although rGO-QDs typically exhibit lower bulk conductivity than extended rGO sheets due to their limited sp² domain size, they possess significant advantages in interfacial electron transfer processes. Their conductivity, while modest, is sufficient for roles in electrochemical devices like sensors and supercapacitors, where rapid redox activity is more critical than bulk electron transport [14,23]. The localized electronic states arising from edge defects and oxygen-containing groups can support hopping conduction and increase electrochemical surface area [24].

Moreover, as rGO-QDs are quantum-confined structures (2–10 nm), their high surface-to-volume ratios amplify the influence of defects and surface states on electronic behavior. Optical and electrochemical properties become tunable through controlled synthesis conditions, which modify the density of defect sites and the degree of sp² restoration. Raman I_D/I_G ratios in rGO-QDs often reflect increased disorder compared to rGO, indicating their edge-dominated nature. This defect-induced heterogeneity, while detrimental to bulk conductivity, proves beneficial for applications requiring high charge transfer kinetics and functional reactivity. Thus, understanding and manipulating defect structures and edge chemistry are key to optimizing rGO-QDs for high-performance nanoelectronic and energy-related devices.

2.2 Application-Relevant Properties of rGO-QDs: Thermoelectric and Electrochemical Perspectives

2.2.1 Thermoelectric Role of rGO-QDs in Bi_2Te_3 Composites

Thermoelectric (TE) materials convert heat differentials into electricity, quantified by the dimensionless figure of merit ZT. This figure is defined as:

$$\mathrm{ZT} = \frac{\sigma S^2 T}{\kappa} \tag{1}$$

where σ is electrical conductivity, S is the Seebeck coefficient, T is absolute temperature, and κ is the thermal conductivity [25]. An equivalent term, the power factor (PF), is often used and defined as σS^2, since maximizing PF while minimizing κ is key to high ZT. Bismuth telluride (Bi_2Te_3) is a well-known TE material near room temperature with ZT≈ 1, and research has focused on enhancing its performance through nanostructuring and composite approaches [26,27]. Incorporating rGO-QDs into Bi_2Te_3 matrices has emerged as an effective strategy to boost TE performance via phonon scattering and carrier energy filtering mechanisms.

At the nanoscale, quantum confinement of carriers and abundant interfaces can profoundly influence TE transport. Reducing material dimensions increases boundary phonon scattering (lowering lattice thermal conductivity, κ_L) and can create discrete energy levels that affect charge transport [28]. In the case of Bi_2Te_3/rGO-QD composites, the rGO-QDs serve as nanoinclusions that disrupt phonon propagation, significantly reducing κ without severely harming electrical transport [29]. Li *et al.* (2017) demonstrated that Bi_2Te_3 nanosheets embedded with 20 nm graphene QDs showed a marked drop in thermal conductivity along with an enhanced power factor, owing to optimized electron scattering at Bi_2Te_3–GQD interfaces. The Seebeck coefficient (S) in such hybrids can also be tuned by energy filtering: low-energy carriers are selectively scattered at the Bi_2Te_3/GQD interface, allowing higher-energy (hotter) carriers to dominate transport, which raises S. As a result of these combined effects, the Bi_2Te_3/GQD (20 nm) hybrids achieved a maximum $ZT \approx 0.55$ at 425 K, higher than pristine Bi_2Te_3 under the same conditions. This improvement illustrates how rGO-QDs can play a thermoelectric role as performance enhancers in a bulk matrix.

Mechanistically, the interface density and size of QDs are critical design parameters. Smaller and more numerous QDs increase interface area for phonon scattering, but if too many or too small, they may introduce electron barriers that reduce σ. Li *et al*. noted that varying the GQD size allows tuning of their dispersion and density, which in turn optimized the TE transport properties. There exists an optimal QD size/content that maximizes phonon blocking while either preserving or even improving carrier transport via modulation doping. In addition to thermal effects, graphene-based inclusions can also enhance mechanical robustness; studies have found that adding graphene (even in nanoplate form) reduces grain size and can improve the mechanical stability of Bi_2Te_3 composites [26]. This is advantageous for device fabrication, as a small fraction of graphene or QDs can not only boost ZT but also strengthen the composite against thermal stress and deformation. This improvement can be partially attributed to the quantum confinement effects in rGO-QDs, which enhance the density of electronic states near the Fermi level, thereby improving the Seebeck coefficient and overall energy conversion efficiency.

It is important to note that quantum and nanoscale effects in rGO-QDs complement the intrinsic TE properties of Bi_2Te_3. Graphene QDs in particular have shown unique TE phenomena such as coherent thermopower. For instance, Zhao *et al.* (2019) observed thermopower generation from quasi-bound states in graphene QDs, highlighting that confined charges can exhibit resonant thermoelectric effects at room temperature [28]. While such quantum-coherent effects are typically studied in model systems, they underscore the broader point that rGO-QDs bring quantum confinement benefits to composites. In practical Bi_2Te_3/rGO-QD composites, carriers remain largely diffusive, but the energy filtering due to band offset at Bi_2Te_3 graphene interfaces can mimic a "mini-bandgap" filter for charge carriers, thus boosting Seebeck coefficient without enormous conductivity loss. The overall result is an improved PF and reduced κ_L, a win–win for ZT [29].

Finally, rGO-QDs are attractive because they retain high electrical conductivity (when well-reduced) and can form percolative networks inside the matrix. Unlike insulating oxide nanoparticles, carbon-based QDs can provide conductive pathways between Bi_2Te_3 grains, mitigating the drop in σ. Therefore, the thermoelectric role of rGO-QDs in Bi_2Te_3 is two-fold: (1) thermal conductivity suppression via interface phonon scattering and (2) power factor enhancement through carrier energy spectrum modulation. This synergistic effect leads to higher TE efficiency as evidenced by recent reports [29], making rGO-QDs promising nanoscale inclusions for next-generation high-performance thermoelectrics.

2.2.2 Electrochemical Properties for Energy Storage Applications

Beyond thermoelectrics, rGO-QDs exhibit noteworthy electrochemical properties that are advantageous for energy storage devices such as supercapacitors and batteries. In electrochemical applications, high surface area, electrical conductivity, and accessible active sites are paramount. Graphene-based quantum dots tick all these boxes: they are extremely small (few nm) – offering a large surface-to-volume ratio – and, when derived from GO, come decorated with edge and surface functional groups (e.g. hydroxyl, carboxyl). Upon reduction, rGO-QDs regain good conductivity while still retaining defects and functional moieties that can participate in Faradaic reactions. This combination leads to excellent double-layer capacitive behavior augmented by some pseudocapacitance from residual functional groups.

A prime example is the use of graphene QD electrodes in electric double-layer capacitors (EDLCs). Zhang *et al.* (2018) prepared uniform GQDs (<5 nm) by a top-down oxidative cutting of GO, followed by thermal reduction [30]. The resulting rGO-QDs had abundant edge sites but minimized excess oxygen, preventing them from restacking – a problem that plagues larger graphene sheets. When tested as electrode material, these GQDs exhibited nearly ideal EDLC behavior, with a high specific capacitance of ~296.7 F/g and an energy density of 41.2 Wh/kg at 1 A/g. Such performance metrics are on par with or exceeding conventional activated carbon-based supercapacitors, demonstrating the effectiveness of nanoscopic graphene in storing charge. The high capacitance arises from the EDLC mechanism – a nanoscopic charge separation at the interface between the GQD surface and electrolyte. Because the QDs are so small, nearly every atom lies at or near a surface; this means a greater fraction of atoms participate in charge storage (either via non-Faradaic double-layer charging or Faradaic redox if functional groups are present). Additionally, the curvature and defects of rGO-QDs can serve as redox-active sites, contributing pseudocapacitance that boosts the total stored charge beyond a purely physical Helmholtz double layer.

Several intrinsic properties of rGO-QDs benefit ion transport and charge storage kinetics. First, their nanometer size shortens ion diffusion paths: electrolyte ions only need to travel a short distance to adsorb/desorb on a QD surface, enabling rapid charging and discharging (low RC time constants). Second, rGO-QDs, being conductive, facilitate fast electron transport to all those numerous surface sites, evidenced by the low internal resistance observed in GQD supercapacitors. Third, the presence of functional groups (though reduced) can provide additional Faradaic reactions. For example, quinone-like oxygen or residual hydroxyl groups at QD edges can undergo redox reactions, effectively increasing capacitance (this is similar to how functionalized carbon provides pseudocapacitance in acid electrolytes). However, because the QDs have been “purified” by thermal treatment, they strike a balance: enough defects for extra capacity, but not so many as to severely impede conductivity.

Comparatively, rGO-QDs vs. bulk rGO sheets offer a trade-off between accessible surface and conductivity. Bulk graphene or rGO sheets have superb conductivity but tend to restack, reducing accessible surface area. Quantum-sized graphene dots resist restacking (they behave almost like pillared spacers when mixed with larger sheets, keeping them apart) [30]. Moreover, QDs can insert into porous structures or composite electrodes more uniformly. For instance, rGO-QDs have been combined with conducting polymers (like polypyrrole) to form composite electrodes with significantly improved capacitance, leveraging the QDs' role as a nanoscopic conductor and spacer [31]. In batteries, rGO-QDs have also been explored as conductive additives or even as active materials. Their ability to provide a percolating conductive network can improve the rate capability of battery electrodes, and their functional edges can host lithium ions or other charge carriers in high numbers. One study on a graphene QD/Si anode showed that GQDs helped accommodate Si expansion and provided conductive channels, enhancing cyclability of the lithium-ion battery anode [32]. Thus, whether in supercapacitors or battery electrodes, the electrochemical role of rGO-QDs is to furnish a high-surface-area, highly conductive, and chemically interactive platform for charge storage.

In summary, rGO-QDs are ideal nanoscale building blocks for energy storage: they combine the advantages of carbon nanostructures (chemical stability, high conductivity after reduction, and robust cycling) with the quantum-size effect of exposing a maximal surface for charge accumulation. The result is electrode materials with high capacitance, excellent power density (fast charging) and good lifecycle stability [30]. These properties make rGO-QDs promising for advanced supercapacitors, micro-power sources, and even as catalyst supports in fuel cells or electrolyzers, where their high surface area and conductivity improve electrochemical reactions. The insights from recent studies firmly establish that carefully engineered rGO-QD electrodes can outperform traditional carbon materials, supporting their integration in next-generation energy storage devices.

2.2.3 Optical Properties and Bandgap Tuning

One of the most intriguing aspects of graphene-based quantum dots is their tunable optical properties, particularly the ability to exhibit size-dependent photoluminescence (PL) and adjustable bandgaps. While pristine graphene is a semimetal with zero bandgap, it acquires a finite bandgap when confined into nanometer-scale dots due to quantum confinement and edge effects. In reduced graphene oxide quantum dots (rGO-QDs), the electrons and holes are confined within discrete sp^2 carbon domain, leading to discrete energy levels much like in a semiconductor quantum dot.

The bandgap E_g of a graphene QDs is inversely related to its size: the square of their size. Smaller QDs, with fewer conjugated π-domains, exhibit more widely spaced energy levels, resulting in larger bandgaps. Conversely, larger QDs have more delocalized states and thus narrower gaps. This principle is illustrated by experimental studies and theoretical calculations [33,34,34,35]. In particular, Figure 2.2.1 shows a linear relationship between the emission energy $h\nu$ and the inverse square of QD diameter ($1/a^{-2}$), which is consistent with the quantum confinement model. As the QD size decreases, the photon emission energy increases, confirming the presence of strong size-dependent bandgap tuning.

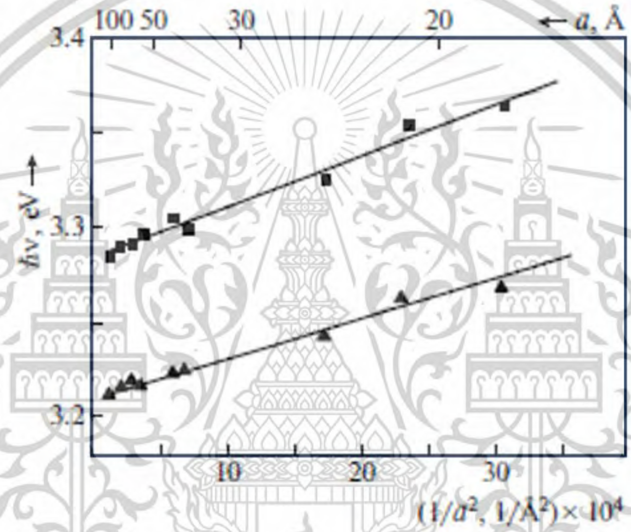

Figure 2.2.1 Relationship between emission energy and QD size ($1/a^{-2}$) [34].

In practical terms, this size-dependent bandgap manifests as PL emission that shifts with QD size. Quantum dots tend to emit light at higher energies (bluer colors) when they are smaller, and emit lower-energy (redder) light when larger. Graphene QDs follow this trend: for example, a batch of GQDs with average size ~6 nm might emit blue light, whereas 10 nm GQDs could emit green. Experimental studies have indeed observed that by controlling the size of graphene QDs (through techniques like size-selective dialysis or filtration), one can tune the PL peak wavelength [35]. In one study, four different GQD sizes (~6.5, 8.4, 9.3, and 10.3 nm) were isolated, and the smallest GQDs showed the strongest and most blue-shifted emission, whereas larger ones had slightly red-shifted PL peaks. The trend corresponds to calculated gaps: DFT (Density Functional Theory) calculations confirm that GQD bandgap drops rapidly as diameter increases up to ~5–6 nm, then saturates for larger sizes. Thus, there is a pronounced quantum confinement regime for GQDs below about 5 nm where optical properties are highly size-tunable, whereas beyond that, adding more carbon atoms yields diminishing changes in bandgap.

Apart from size, the edge chemistry and functionalization of rGO-QDs also critically affect their optical behavior. Graphene QDs can have predominantly zigzag or armchair edge configurations, or be functionalized with oxygen, hydrogen, etc. Zigzag edges introduce localized states that can even be mid-gap; armchair edges tend to open a gap. As seen in Figure 2.2.2, zigzag-edged GQDs have a smaller gap than armchair-edged ones of the same size due to differing π-bond topology. Chemical doping is another powerful tuning knob: introducing heteroatoms like nitrogen or sulfur into GQDs modulates their electronic structure. Doping can either create new emissive recombination centers or alter the bandgap by changing the electron density. For instance, nitrogen-doped GQDs often show shifted PL and higher quantum yield due to new radiative recombination paths. Researchers have leveraged this by doping GQDs to achieve multicolor emission or to enhance brightness (quantum yield). Surface passivation (e.g., attaching polymer or organic ligands) is yet another method to tune optical output, often resulting in brighter emission by mitigating nonradiative recombination at surface defects.

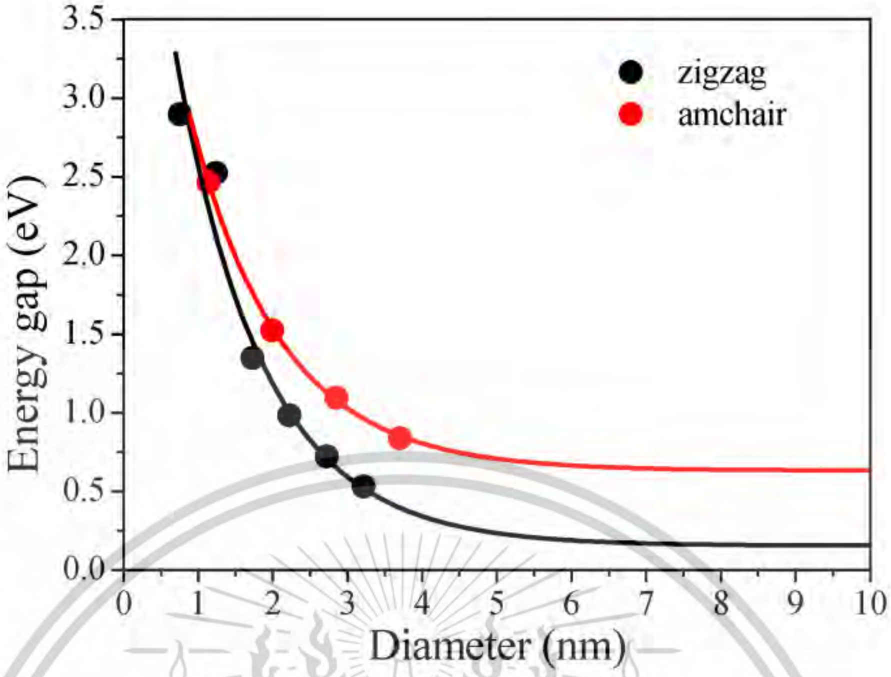

Figure 2.2.2 DFT-calculated energy gap vs. GQD diameter for zigzag and armchair edges [35].

Beyond photoluminescence, rGO-QDs exhibit notable absorption properties. They typically show an absorption band in the UV due to the $\pi - \pi^*$ transitions of the aromatic carbon core. As the size (and conjugation length) of the QD increases, this absorption edge red-shifts (lower photon energy), consistent with a decreasing bandgap. In some reports, an optical Tauc analysis is used to estimate the bandgap of GQDs from UV-Vis absorption. For example, one study found a GQD film had an optical bandgap of ~4.1 eV [33], aligning with other reports for small (<5 nm) GQDs. When those GQDs were embedded in a polymer (PVA), the composite's effective bandgap slightly increased (to ~4.10 eV from 4.06 eV for pure PVA), indicating that the GQDs' quantum confinement widens the gap of the host matrix. The authors attributed this to the quantum confinement effect of the dots, which widen the energy difference between filled and empty states in the composite. In essence, by introducing quantum dots, one can tune the optical bandgap of materials in a predictable way: adding smaller dots raises the effective bandgap and blue-shifts optical transitions, while larger dots or fewer dots have the opposite effect.

From an application perspective, the optical tunability of rGO-QDs is valuable for designing optoelectronic and sensing devices. Their stable photoluminescence and size-dependent emission make them candidates for multicolor bio-imaging tags, LEDs, and even solar spectrum tuning. Moreover, the fact that graphene usually lacks a bandgap but GQDs have one means GQDs could be used in electronics where graphene falls short – for instance, GQDs in a polymer LED can act as the emissive semiconductor. The PL is also excitation-dependent in many GQDs (different excitation wavelengths yield different emission peaks due to distributions of sizes and surface states), which can be leveraged for white-light emission or ratiometric sensors. In this work, the size-dependent optical features of rGO-QDs were experimentally confirmed by UV-Vis absorption and fluorescence spectroscopy, as discussed in Chapter 4. These tunable optical properties not only validate the quantum-confined structure of the synthesized rGO-QDs but also support their integration into optoelectronic and electrochemical systems.

2.2.4 Synergistic Design Considerations for Multifunctional Devices

Harnessing the full potential of reduced graphene oxide quantum dots (rGO-QDs) within multifunctional devices necessitates a synergistic design approach that effectively integrates multiple functionalities, including thermoelectric, electrochemical, and optical properties. Achieving this integration poses challenges as the properties beneficial for one functionality may inadvertently affect another. Here we explore several key design considerations to optimize the utility of rGO-QDs in various applications.

Optimal Loading and Dispersion: The performance of multifunctional composites is highly dependent on the optimal loading and uniform dispersion of nanofillers such as reduced graphene oxide quantum dots (rGO-QDs). Although direct studies on rGO-QDs remain limited, related research on GQDs and rGO-based systems provides insight into design strategies that may apply similarly to rGO-QDs.

In thermoelectric composites, a small amount of GQDs (typically 1–5 wt%) incorporated into Bi_2Te_3 matrices has been shown to reduce lattice thermal conductivity due to enhanced phonon scattering and interfacial disruption, while maintaining or slightly improving electrical conductivity [29]. However, excessive loading can result in charge carrier percolation pathways that short-circuit the thermoelectric gradient, ultimately reducing the Seebeck coefficient and power factor [36]. Although these studies involved GQDs, rGO-QDs possess similar size-dependent transport behavior due to quantum confinement and surface defect states, suggesting that a comparable optimal range might exist.

In electrochemical applications, especially in supercapacitor electrodes, increased loading of rGO or carbon-based QDs generally enhances double-layer capacitance due to increased surface area. However, beyond a certain threshold, particle agglomeration becomes prominent, blocking active sites and reducing electrolyte accessibility [37]. For rGO-QDs, which retain surface functional groups from their GO origin, proper dispersion also ensures uniform electron pathways and minimizes interparticle resistance. Achieving this balance often requires surface modification or hybridization with conductive additives.

Therefore, while optimal loading must be tailored case-by-case, studies on analogous materials indicate that both thermoelectric and electrochemical performances follow a non-linear trend with filler content: low loading underutilizes the potential of rGO-QDs, whereas overloading introduces interfacial saturation and performance loss. Fine-tuning the weight fraction of rGO-QDs and ensuring nanoscale dispersion are thus crucial to unlocking their multifunctional potential.

Interface Engineering: Interface engineering plays a critical role in optimizing the multifunctional performance of nanocomposites, particularly when integrating carbon-based nanomaterials like reduced graphene oxide quantum dots (rGO-QDs). Although direct studies on interface phenomena involving rGO-QDs are still emerging, related findings from graphene, rGO, and GQD systems offer applicable insights.

Well-designed interfaces enhance charge carrier mobility, reduce recombination losses, and promote mechanical and thermal stability within composite systems. In photocatalytic and thermoelectric composites, surface-functionalized GQDs have been shown to establish efficient charge transfer pathways with the host matrix, significantly improving conductivity and overall performance [38,39]. Similarly, rGO when hybridized with polymers or semiconductors can reduce interfacial resistance and form percolated networks that facilitate electron flow [40]. For rGO-QDs, the presence of residual oxygenated groups inherited from GO precursors allows for further functionalization, enabling compatibility with a range of host materials. This is particularly important in electrochemical devices, where uniform interfaces help maximize electrolyte interaction, minimize charge transfer resistance, and ensure mechanical adhesion to electrodes. Interface engineering strategies may include surface ligand modification, in-situ synthesis onto host substrates, or incorporation into polymeric matrices to improve dispersion and bonding.

Thus, while systematic studies on interface behavior of rGO-QDs remain limited, design strategies borrowed from similar carbon nanomaterials suggest that engineering strong, stable, and conductive interfaces is essential for achieving synergistic functionality in optoelectronic, electrochemical, and energy-conversion devices.

Mechanical and Thermal Integration: Integrating mechanical flexibility and thermal robustness is vital in the development of multifunctional devices using reduced graphene oxide quantum dots (rGO-QDs), especially for wearable electronics and energy systems. While rGO-QDs are primarily studied for their optical and electronic properties, insights from graphene oxide (GO), reduced graphene oxide (rGO), and graphene quantum dots (GQDs) provide a foundational understanding of how these carbon nanomaterials contribute to mechanical and thermal enhancement in composites.

The incorporation of carbon-based nanostructures into thermoelectric materials such as Bi_2Te_3 has shown to improve fracture toughness and elasticity of the matrix, allowing the fabrication of flexible thermoelectric films [41,42]. These enhancements are largely attributed to the ability of sp^2-hybridized carbon domains to dissipate stress, reinforce the matrix, and prevent crack propagation. Although specific studies on rGO-QDs are limited, their small size and high surface area suggest that, when properly dispersed, they could offer similar reinforcement effects by interacting at the microstructural level.

In addition to mechanical benefits, rGO and related nanomaterials can support thermal stability and manage heat dissipation. The high thermal conductivity of graphitic domains helps distribute localized heat, which is crucial in maintaining device performance under fluctuating temperatures. Moreover, when embedded in polymers or hybrid films, rGO-based materials assist in controlling thermal gradients and enhancing thermal fatigue resistance [43].

For rGO-QDs, the combination of quantum confinement and residual functional groups may also contribute to interfacial energy dissipation and matrix bonding, potentially making them suitable candidates for thermally resilient and flexible device platforms. Nonetheless, further dedicated studies are needed to explicitly confirm these effects for rGO-QDs.

Self-Powering and Multi-Modal Operation: The development of self-powering devices systems capable of generating, storing, and utilizing energy autonomously has gained momentum in recent years, especially for wearable and remote electronics. Reduced graphene oxide quantum dots (rGO-QDs), owing to their multifunctional properties, have emerged as promising candidates for realizing such integrated systems.

In thermoelectric applications, incorporating rGO-QDs into composite materials can improve the Seebeck coefficient and electrical conductivity, thereby boosting the overall thermoelectric performance [29]. These properties are essential for harvesting waste heat and converting it into usable electricity, forming the basis of self-powered systems.

Moreover, rGO-QDs can also function as efficient electrode materials in micro-supercapacitors due to their high surface area, tunable conductivity, and electrochemical stability. This dual role energy harvesting and energy storage opens the door for integrated devices that combine thermoelectric generators with supercapacitors into a compact, flexible platform [44,45]. For instance, thermoelectric thin films based on Bi_2Te_3-rGO-QD composites have been used to power micro-supercapacitors embedded with carbon nanomaterials, achieving real-time energy conversion and utilization without the need for external circuits [43].

Such hybrid configurations not only reduce system complexity but also enhance energy efficiency by enabling simultaneous multi-functional operation such as sensing, storage, and communication within a single compact device. The small size and surface functionalization potential of rGO-QDs further allow their integration into soft electronics, where conformal contact with the body or surface is necessary.

Though direct studies on rGO-QDs for fully integrated self-powered systems remain limited, extrapolations from research on GQDs, rGO, and related carbon nanomaterials suggest that rGO-QDs could serve as key building blocks for next-generation multi-modal platforms.

Thermal and Optical Synergy: Integrating thermal and optical functionalities into a single material system is a key design goal for multifunctional devices, especially in applications such as wearable electronics, optoelectronic sensors, and energy management platforms. Reduced graphene oxide quantum dots (rGO-QDs) offer a unique combination of thermal conductivity and photoluminescent properties that enable such synergistic integration.

Thermally, rGO-QDs benefit from their partial sp^2 carbon domains, which facilitate moderate heat conduction. When embedded in thermoelectric composites like Bi_2Te_3, rGO-QDs can contribute to lowering lattice thermal conductivity through enhanced phonon scattering, while still maintaining reasonable electrical transport—a balance essential for thermoelectric performance [29]. Optically, rGO-QDs exhibit strong, stable photoluminescence with excitation-dependent emission. This allows them to act as optical sensors or active layers in light-emitting devices. The combination of photoluminescence and thermal responsiveness offers potential for real-time temperature sensing through spectral shift monitoring, or for dynamic displays in heat-responsive systems [46].

Moreover, their lightweight nature and minimal addition to composite mass make them ideal for integration in flexible substrates or textiles where simultaneous optical signaling and heat dissipation are desired. This is particularly advantageous in applications such as smart fabrics or optothermal feedback systems in wearable devices.

Several studies also suggest the feasibility of rGO-QDs in optical-thermal regulation systems where light absorption can be tuned for controlled heating, while maintaining visual signaling functions. For instance, materials with embedded rGO-QDs have demonstrated temperature-dependent changes in optical output, allowing for adaptive thermal display or early overheating detection in electronics [47].

Though further experimental studies are needed specifically on rGO-QDs, extrapolations from GQDs and related carbon nanomaterials support the potential of rGO-QDs as effective thermal-optical dual-function materials in next-generation adaptive and intelligent systems. Table 2.2.1 summarizes the key multifunctional roles of rGO-QDs across various application domains, along with corresponding design considerations essential for their effective integration.

Table 2.2.1 Design considerations and multifunctional roles of rGO-QDs in thermoelectric, electrochemical, optical, and mechanical applications.

Property/Function	Role of rGO-QDs	Design Considerations
Thermoelectric (in Bi_2Te_3)	▪ Scatter phonons to reduce lattice thermal conductivity ▪ Introduce energy filtering to enhance Seebeck coefficient ▪ Preserve electrical pathways for high σ	▪ Optimize QD loading (typically ~1–5 wt%) to avoid percolation issues or short circuits ▪ Surface-functionalize QDs to improve interfacial compatibility with Bi_2Te_3 matrix
Electrochemical (Supercap)	▪ Provide high surface area for double-layer charge storage ▪ Enable fast electron transport ▪ Contribute pseudocapacitance via defect-rich edges	▪ Maintain optimal dispersion to prevent agglomeration ▪ Use porous binders that do not hinder ionic pathways ▪ Combine with conductive support matrix for structural reinforcement
Optical (PL/Bandgap)	▪ Offer size-dependent bandgap and tunable PL ▪ Enable defect-state emission for sensing ▪ Serve as transparent conductors in thin films	▪ Adjust QD size and doping for specific emission wavelengths ▪ Passivate surfaces to enhance quantum yield and minimize non-radiative losses ▪ Integrate into host without PL quenching

Mechanical/Flexibility	▪ Improve mechanical strength and prevent grain growth in host matrix ▪ Introduce flexibility in otherwise brittle thermoelectric or polymer composites	▪ Ensure uniform dispersion to minimize stress concentration ▪ Use rGO-sheet–QD hybrids for synergistic reinforcement and flexible percolation networks

2.3 Literature Reviews

2.3.1 Research on Graphene Quantum Dots (GQDs) and rGO-QDs

Graphene quantum dots (GQDs) are nanoscale fragments of graphene (typically <10 nm in diameter and a few layers thick) that combine the 0D quantum confinement of carbon dots with the crystallinity and conductivity of graphene [48]. Their discovery in the early 2010s opened new avenues in nanocarbon research, as GQDs exhibit unique size-dependent properties absent in bulk graphene. Notably, GQDs possess a tunable bandgap (whereas pristine graphene is gapless) due to quantum confinement and edge effects, leading to photoluminescence (PL) that can span from blue to red depending on size and surface chemistry [1] (Zhu *et al.*, 2014). Multiple synthesis routes for GQDs have been developed. Top-down methods start from larger carbon allotropes (graphite, GO, carbon fibers, etc.) and break them down via chemical oxidation, laser ablation, or electrochemical exfoliation [49]. For example, Pan *et al.* (2010) [50] oxidized graphene sheets and then hydrothermally cut them into ~5 nm fluorescent GQDs, one of the first demonstrations of graphene’s quantum-dot behavior. These approaches can yield GQDs in bulk, though controlling size and surface groups can be challenging. In contrast, bottom-up methods build GQDs from molecular precursors (e.g. polycyclic aromatic hydrocarbons or biomass fragments) through solvothermal reactions or microwave-assisted carbonization. Bottom-up synthesis offers fine control over GQD size, doping, and functionalization, at the expense of more complex chemistry.

Fundamental properties of GQDs have been extensively characterized. Structurally, GQDs consist of sp^2-bonded carbon domains with abundant edge sites terminated by functional groups (–COOH, –OH, etc., especially if derived from GO). They often display a lattice fringe spacing around 0.21–0.24 nm in high-resolution TEM, corresponding to graphene's (100) lattice planes [51]. Optical behavior is a hallmark of GQDs: they show strong π–π^* absorption in the UV (usually a peak ~270 nm) and excitation-dependent PL emissions in the visible range. Smaller or highly oxidized GQDs tend to emit in the blue/green, while larger or heteroatom-doped GQDs can exhibit red-shifted or even white-light emission [52]. This tunable PL arises from a combination of quantum confinement (smaller GQDs have larger bandgaps) and surface/edge states. Bandgap engineering is possible by controlling GQD size, shape, and defects: as one study showed, adding heteroatoms like N can introduce mid-gap states and modify both optical and electronic properties [49]. For instance, nitrogen-doped GQDs were found to exhibit different emission colors and enhanced electron delocalization, implying potential for tailored optoelectronic behavior [49].

Reduced graphene oxide quantum dots (rGO-QDs) are a closely related class, typically produced by first synthesizing GO-derived quantum dots and then chemically reducing them to partially restore conductivity. rGO-QDs share the quantum confined size of GQDs but with fewer oxygen functional groups (higher C:O ratio). This generally leads to improved electrical conductivity and more graphitic domains, while still retaining significant surface functionality. Buatong *et al.* (2023) demonstrated a hydrothermal route to obtain rGO-QDs ~4–5 nm in size, confirming by XRD and Raman that the GO precursor's interlayer spacing contracts upon reduction and the I_D/I_G defect ratio decreases (to ~0.9) as sp^2 carbon networks are restored. The rGO-QDs exhibited tunable photoluminescence similar to GQDs, indicating quantum confinement was preserved despite reduction. Interestingly, that study also noted the rGO-QDs showed paramagnetic behavior, attributed to remaining unpaired electron spins at defect sites, highlighting how adjusting the oxidation level of GQDs can unlock new properties. Overall, the past decade's research on GQDs and rGO-QDs has established their synthesis techniques and fundamental properties – from zero-dimensional quantum-confined electronic structure to high surface area with abundant active sites which underpin their applications in various fields.

2.3.2 Application of rGO-QDs in Thermoelectric Composites

One prominent application of graphene-based quantum dots is in thermoelectric (TE) composites, where the goal is to improve the material's dimensionless figure of merit (ZT) by decoupling electrical conductivity, Seebeck coefficient, and thermal conductivity. Graphene QDs can be incorporated into TE matrices (such as bismuth telluride or metal oxides) to introduce nanostructured interfaces that scatter heat-carrying phonons and potentially energy-filter charge carriers. Li *et al.* (2017) [29] provided an early demonstration of this strategy by embedding 20 nm GQDs into Bi_2Te_3 nanosheets [29]. The Bi_2Te_3/GQD hybrid showed a significantly reduced thermal conductivity alongside an enhanced power factor ($S^2\sigma$), yielding a maximum ZT≈0.55 at 425 K higher than pristine Bi_2Te_3 [29]. The improvements were attributed to the GQD–Bi_2Te_3 interfaces, which acted as effective phonon scattering centers (lowering lattice thermal conductivity) while maintaining good electrical transport. By tuning the size and dispersion of GQDs, Li *et al.* were able to optimize the density of these interfaces, illustrating a key principle: smaller, well-dispersed quantum dots create more interface area for scattering phonons without overly disrupting the electron percolation network. This concept of interface engineering has since been explored with various host materials and carbon nanostructures.

Recent research by Choi *et al.* (2024) generalized these findings by incorporating low-oxidation graphene QDs into a 3D porous ZnO framework. As illustrated in Figure 2.3.1, this configuration achieved enhanced Seebeck coefficient and suppressed thermal conductivity, resulting in a fourfold improvement in ZT values.

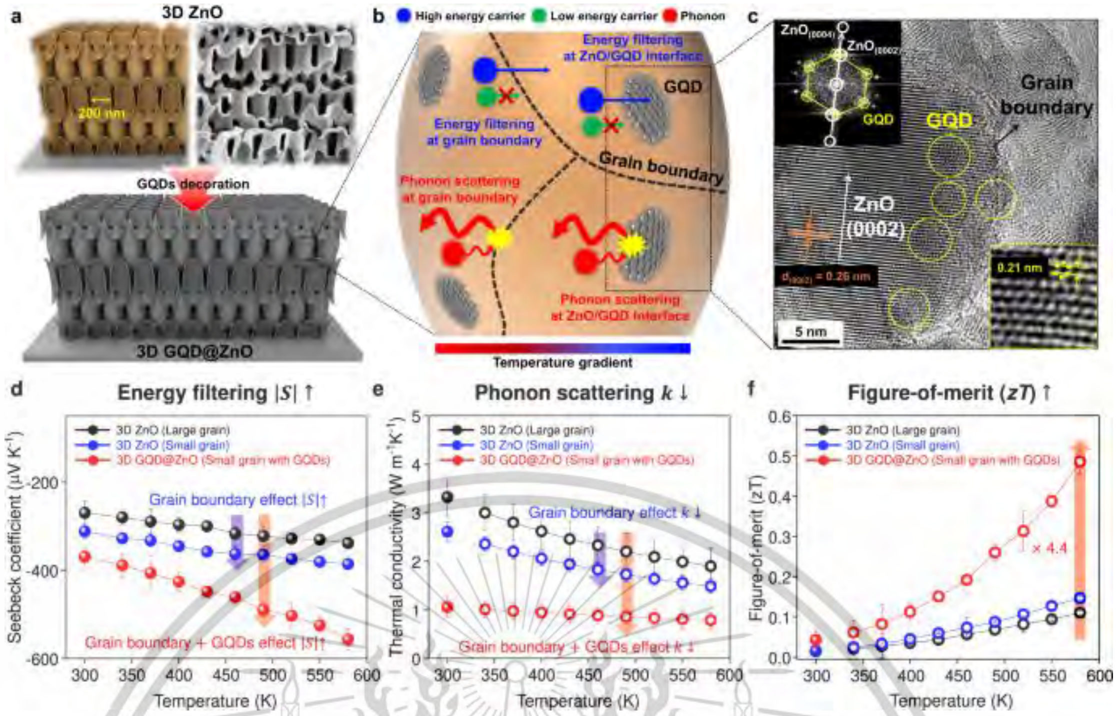

Figure 2.3.1 Schematic illustration and experimental results from Choi *et al.* (2024) showing how GQDs at grain boundaries in a 3D ZnO nanostructure introduce energy filtering and phonon scattering. (a) 3D porous ZnO framework before and after GQD decoration; (b) illustration of low-energy electrons being filtered at GQD/ZnO interfaces and phonons scattered at interfaces and grain boundaries; (c) TEM image confirming ~5 nm GQDs attached to ZnO (FFT patterns indicate lattice of GQD vs. ZnO). (d–f) Temperature-dependent TE properties: GQDs raise the Seebeck coefficient via energy filtering, markedly reduce thermal conductivity, and thereby boost ZT (~4.4× increase at 500 K) compared to ZnO alone.

The GQD-decorated ZnO achieved the highest ZT ever reported for ZnO (~0.48 at 580 K, a 4-fold increase) [53]. The mechanism was elucidated as twofold: (1) Enhanced phonon scattering the GQD/ZnO heterointerfaces and native grain boundaries reflect phonons, lowering the thermal conductivity; and (2) Electron energy filtering – band offset at the GQD–ZnO interface preferentially impedes low-energy (low Seebeck coefficient) electrons, thereby increasing the Seebeck coefficient. This dual benefit relies on the ability to distribute GQDs uniformly across the host matrix. Notably, GQDs excel in this role compared to larger carbon additives. As Choi *et al.* (2024) pointed out, among carbon nanostructures, graphene QDs offer an interfacing advantage over graphene sheets or CNTs due to their high density of active sites that enable uniform coverage of the host material. Graphene sheets or carbon nanotubes, while providing conductivity, cannot be dispersed at as fine a length scale and thus create fewer, larger interfaces. GQDs/rGO-QDs, in contrast, act as ultra-fine “nanoprecipitates” decorating grains and grain boundaries. This leads to a TE composite where heat transport is interrupted at countless 0D inclusions, yet electrical connectivity can be maintained or even enhanced by the percolative network of conductive dots. Indeed, several studies on Bi_2Te_3, PbTe, and oxide TEs report that introducing nanoscale carbon (including GQDs) yields a net gain in ZT via reduced κ and modestly improved or unchanged σ and Seebeck [29,53]. In summary, prior research on graphene derivatives quantum dots in thermoelectrics has established them as effective phonon-scattering centers and energy filters. This opens a pathway to engineer higher-performance TE materials by judiciously adding carbon quantum dots, provided their size, band alignment, and dispersion are carefully controlled to maximize interfacial scattering without introducing too many charge-carrier traps.

2.3.3 Electrochemical Energy Storage Applications of rGO-QDs

Beyond thermoelectrics, rGO-QDs have attracted considerable interest in electrochemical energy storage, including supercapacitors and battery electrodes. Their small size, high surface-to-volume ratio, and tunable surface chemistry make them appealing as electrode additives or even as active materials to enhance capacitance and charge transport. In supercapacitors, two primary charge storage mechanisms exist: electric double-layer capacitance (EDLC), which is surface ion adsorption, and pseudocapacitance, which involves fast reversible redox reactions. Graphene-based materials are known for EDLC, but they typically lack pseudocapacitance. rGO-QDs can introduce pseudocapacitive functionalities due to their abundant edge defects and functional groups (e.g. –COOH, –OH, =O), while also improving ion transport and electrical connectivity.

Early studies by Liu *et al.* (2014) [2] and Zhu *et al.* (2014) [1] demonstrated that incorporating graphene QDs into carbon electrodes can significantly boost supercapacitor performance. For example, Zhu *et al.* (2014) reported that adding GQDs to activated carbon electrodes simultaneously increased the specific capacitance and rate capability of the device. They attributed this to two effects: (1) the GQDs introduce numerous additional active sites for charge storage (faradaic reactions at functional groups and enhanced EDLC on their large surface), and (2) the GQDs improve the wettability of the electrode material in the electrolyte. Enhanced wettability means electrolyte ions can access the internal surfaces more easily, reducing ion transport resistance. These findings have been echoed in other works for instance, Zhu *et al.* (2014) prepared carbon/GQD composites and observed improved capacitive behavior owing to the GQDs' polar oxygenated surfaces increasing ion affinity. Likewise, Liu *et al.* (2014) showed that GQDs could serve as solution-processable pseudocapacitive materials, yielding electrodes with higher capacitance than those using graphene alone, thanks to faradic reactions at the GQD surfaces.

One creative utilization of GQDs is as an electrolyte additive in supercapacitors, as opposed to an electrode additive. Zhang *et al.* (2016) [8] pioneered this approach by using oxygen-rich GQDs dispersed in KOH as a hybrid electrolyte [8]. The GQDs, having many weakly acidic functional groups, release mobile protons (H_3O^+) when neutralized by KOH, effectively functioning as a pseudocapacitive proton source in the electrolyte. The study found that neutralizing GQD solutions with KOH dramatically increased ionic conductivity and improved the capacitive performance of test supercapacitors, compared to pure KOH electrolyte. The mechanism is that fully ionizing the –COOH/-OH groups on GQDs yields a high concentration of mobile ions and additionally these functionalized GQDs can shuttle charge or adsorb/desorb ions themselves, contributing to capacitance. Zhang *et al.* achieved solid-state devices with GQD-based electrolyte films that had comparable capacitance (~42 F/g) to liquid electrolyte cells, and with excellent rate capability at moderate scan rates. This concept using GQDs as quasi-ion carriers in the electrolyte is novel and inspired further work. Our thesis builds on a similar idea: leveraging rGO-QDs to enhance ionic conductivity in the electrolyte (see Chapter 4), though direct studies using rGO-QDs in this role remain limited.

rGO-QDs have been explored primarily for their structural, optical, and electrochemical properties relevant to supercapacitor applications. For instance, Buatong *et al.* (2023) synthesized rGO-QDs via a hydrothermal process and characterized their size, photoluminescence, and magnetic properties. Although they did not directly construct hybrid electrodes, their findings support the potential of rGO-QDs for electrochemical applications due to their high dispersibility, surface functionality, and quantum confinement effects. In previous literature, the combination of graphene-based quantum dots with pseudocapacitive materials such as transition-metal oxides has shown promise. For example, some studies demonstrated that introducing carbon QDs can create conductive pathways and increase electroactive surface area when combined with metal oxides. These composite electrodes delivered high specific capacitance and maintained cycle stability, thanks to enhanced charge transfer and volume-buffering effects. While Buatong *et al.* (2023) did not test such a composite directly, the physicochemical properties they reported such as nanometric size, oxygen-containing surface groups, and structural defects are relevant to future designs of pseudocapacitor materials.

Beyond supercapacitors, GQDs and potentially rGO-QDs have been investigated in battery electrodes (e.g. as additives in Li-ion battery anodes to improve capacity and cyclability) and in ion-storage mechanisms broadly defined as “iontronics” [53]. Their small size allows them to intercalate or accommodate ions in ways bulk carbons cannot. For instance, GQDs have been embedded in SnO_2 and TiO_2 anodes to improve Na-ion storage, where they help form conductive networks and prevent large volume expansion. In all these cases, the recurring benefits of rGO-QDs are: (i) introduction of pseudocapacitive reactions (due to reversible redox of surface functional groups), (ii) improvement of ion mobility (by providing more ion-accessible porosity or by functioning as ion reservoirs in electrolytes), and (iii) enhanced electronic conductivity (since well-graphitized QDs can form percolating paths among insulating or poorly percolating matrices). Thus, rGO-QDs are emerging as versatile components in energy storage design from electrodes to electrolytes enabling higher capacitances, faster charge–discharge, and in some cases new device architectures (e.g. fully solid-state proton supercapacitors). The works of Liu (2014), Zhu (2014), Zhang (2016), and Buatong (2023, in characterization context), among others, collectively highlight these mechanisms, which form a foundation for the approaches pursued in this thesis. Notably, our research expands the application scope by adapting rGO-QDs as electrolyte additives a concept inspired by the GQD studies mentioned above.

2.3.4 Optical and Electronic Behavior in rGO-QDs-Based Systems

Reduced graphene oxide quantum dots have garnered considerable attention due to their distinctive optical and electronic properties, which arise from their quantum-confined structure, tunable surface functionalities, and nanoscale size. These properties make rGO-QDs attractive candidates for applications in optoelectronic devices, sensors, and memory systems.

Numerous studies have reported that rGO-QDs exhibit strong absorption in the ultraviolet region, attributed to π–π^* transitions in aromatic sp^2 domains, along with a visible-range absorption tail corresponding to n–π^* transitions from oxygen-containing groups [14,54]. Their photoluminescence (PL) is commonly excitation-dependent, which is indicative of quantum confinement and surface-related emissive trap states. Specifically, smaller rGO-QDs (approximately 2 nm in diameter) typically emit in the UV-blue region, while larger dots or those with specific edge functionalization can shift emission toward the green-red spectrum [3].

This size and edge-dependent tunability of PL has been widely utilized in sensing applications. For example, edge-enriched rGO-QDs functionalized with carboxyl or hydroxyl groups have shown enhanced PL quantum yields and selective sensitivity toward metal ions such as Fe^{3+}, primarily due to analyte-induced quenching effects [2,55]. Electrochemiluminescent behavior has also been observed in rGO-QDs, with several studies demonstrating stable luminescence under electrochemical stimulation, a property that enables their use in metal ion detection at nanomolar levels [56].

In terms of electronic behavior, rGO-QDs occupy an intermediate regime between molecular systems and bulk graphene. Their discrete energy levels and moderate conductivity, arising from π-conjugated domains, have positioned them as tunable semiconductors with reported band gaps ranging from approximately 2 to 4 eV depending on size and reduction degree [12]. Applications in optoelectronic devices have been increasingly reported. Thin films of rGO-QDs have been used in photodetectors capable of broad-spectrum photoresponse, driven by their strong and tunable optical absorption properties [21]. In light-emitting diodes (LEDs), rGO-QDs have functioned as emissive layers or as phosphors for white light emission. Notably, Tan *et al.* (2015) [57] demonstrated that defect-rich GQDs could emit balanced red, green, and blue components, resulting in white electroluminescence, which illustrates the capability of tailoring emission through edge-state engineering.

In addition to photodetection and lighting, rGO-QDs have been integrated into non-volatile memory devices as charge-trapping layers. Their quantum dot nature enables electron or hole storage, which modulates the threshold voltage of field-effect transistors. This charge retention has been shown to depend on the oxidation level and structural integrity of the QDs [23]. Photovoltaic applications have also benefited from the inclusion of rGO-QDs. Studies report that embedding QDs into photoanodes such as TiO_2 in dye-sensitized solar cells (DSSCs) enhances photocurrent output, as the QDs extend light absorption and improve interfacial electron transfer efficiency [24].

In summary, the literature strongly supports the multifunctional role of rGO-QDs in optoelectronic systems. Their excitation-dependent PL, tunable band gaps, surface-sensitive luminescence, and moderate conductivity have been widely leveraged in fluorescent sensors, light-emitting devices, memory elements, and solar cells. These properties, governed by quantum confinement and edge chemistry, establish rGO-QDs as a promising class of nanomaterials for future device integration.

2.3.5 Comparative Insights: rGO-QDs vs. Other Carbon Nanostructures

The rGO-QDs belong to the broad family of carbon nanomaterials, and it is instructive to compare them with other members – such as bulk graphene/GO, carbon dots, and carbon nanotubes (CNTs) – to highlight their distinct advantages. GO itself is a 2D platelet (typically micrometer-sized) with abundant functional groups. While GO offers a high surface area and hydrophilicity, its large lateral size means it lacks the quantum confinement effects of GQDs and can face restacking issues. rGO-QDs, being nanoscale, do not restack into graphite-like structures; they remain well-dispersed and stable in colloids [8]. This enables them to more uniformly combine with or coat other materials. For example, in composites, GO sheets might aggregate or create micron-scale phase separation, whereas rGO-QDs form homogeneous mixtures down to the nanometer scale [53]. Moreover, GO is an electrical insulator in its as-made form, requiring reduction to restore conductivity. rGO-QDs, by definition, are already in a reduced state to a certain degree, so they provide conductive pathways more readily than GO sheets. In thermoelectric or electrode composites, GO would primarily act as a phonon scatterer or insulator unless reduced in situ. In contrast, rGO-QDs can scatter phonons (or store charge) and conduct electrons, a dual function that is highly desirable.

Carbon quantum dots (carbon dots, CDs) are another 0D carbon nanostructure, typically derived from organic carbonization (such as citric acid pyrolysis). They are usually amorphous or polycrystalline and often contain a significant fraction of oxygen and hydrogen. CDs and GQDs share photoluminescence properties, but GQDs (and rGO-QDs) generally have a more graphitic crystalline core [48]. This difference leads to higher electrical conductivity and chemical stability in GQDs. Tian *et al.* (2018) [58] discussed that GQDs combine the advantageous fluorescence and surface chemical properties of carbon dots with the excellent carrier mobility associated with graphene domains, making them highly promising for optoelectronic and energy-related applications. In supercapacitors, for instance, undoped carbon dots can enhance capacitance but often at the cost of added series resistance (due to their insulating nature). GQDs, especially reduced ones, mitigate this by contributing less resistance. Additionally, rGO-QDs have better-defined graphitic π-structure, which can facilitate π–π stacking or coupling with other aromatic systems (useful in composite electrodes or sensor interfaces) more effectively than largely amorphous carbon dots. In short, compared to generic carbon dots, rGO-QDs typically offer superior charge transport and a more controllable structure, albeit with slightly lower quantum yields in photoluminescence if overly reduced (trade-off between conductivity and luminescence).

Carbon nanotubes (CNTs) are one-dimensional tubular graphene structures (with diameters ~1–2 nm for single-walled CNTs and lengths up to microns). CNTs have excellent electrical conductivity and high mechanical strength, and have been widely used to enhance composite materials. However, when comparing CNTs to rGO-QDs in contexts like composite functional materials, there are clear differences. CNTs, due to their high aspect ratio, tend to form percolating networks at relatively low loadings and can bridge electrical connections across a matrix. Yet, this same feature means they do not uniformly decorate a host matrix at the atomic scale; there will be regions without CNT coverage, and achieving atomic-scale homogeneity is difficult. rGO-QDs, being zero-dimensional, can uniformly cover a host’s surface in large numbers [53]. Choi *et al.* (2024) explicitly observed that GQDs had an interfacing advantage over CNTs in their ZnO system, as the QDs could densely and evenly attach to the 3D surface, whereas CNTs or graphene sheets could not. Furthermore, CNTs do not provide any quantum confinement effect – they behave either as conductors or semiconductors depending on chirality, but their electronic density of states is not easily tunable by size like QDs. Nor do CNTs inherently have the rich surface functional chemistry that rGO-QDs possess. Thus, CNTs contribute mostly EDLC capacitance (if used in supercapacitors) and phonon scattering (if used in TE composites) but little pseudocapacitance or bandgap-induced electron filtering. rGO-QDs, on the other hand, introduce functional groups and finite bandgaps that can be leveraged for pseudocapacitive reactions and selective carrier scattering. One could say CNTs are excellent for providing a highway for electrons, but rGO-QDs provide a network of hubs where interesting chemistry and quantum effects happen in addition to conducting electrons. Practically, CNTs also face processing challenges – they bundle together due to Van der Waals attraction and often require surfactants or functionalization to disperse, whereas rGO-QDs, owing to their small size and surface groups, disperse readily in solvents and resin matrices.

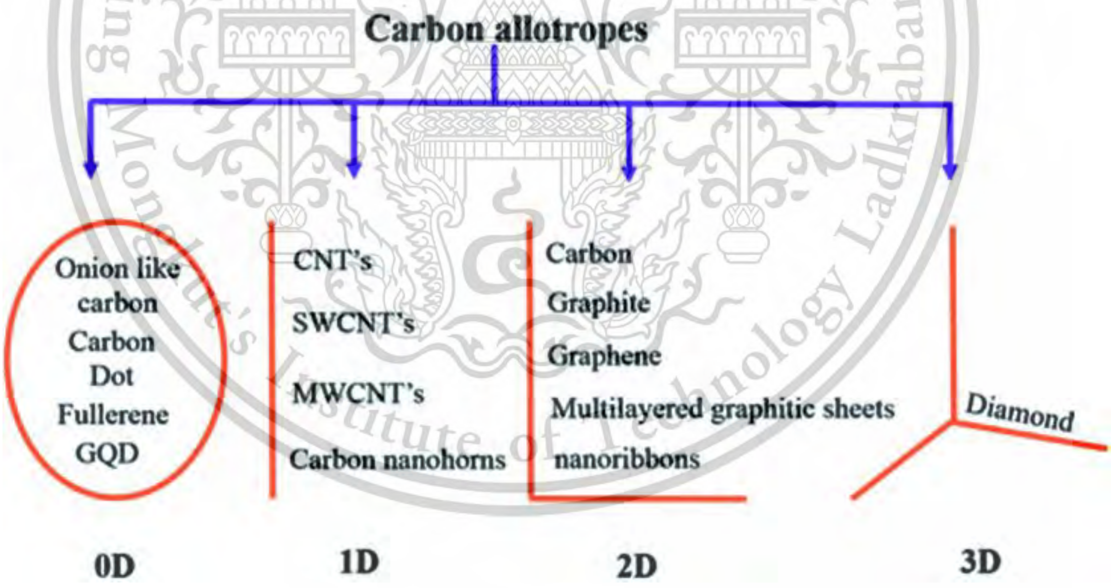

Figure 2.3.2 Classification of carbon allotropes by dimensionality (0D, 1D, 2D, 3D). Graphene quantum dots (GQDs) fall in the 0D category alongside traditional carbon dots and fullerenes, whereas carbon nanotubes (CNTs) are 1D and graphene is 2D. rGO-QDs share the zero-dimensional quantum-confined nature with other 0D carbons but also inherit graphene's crystalline framework. Source: Kumar et al. (2020) [48].

A comparison worth noting is between rGO-QDs and graphene nanoplatelets or graphene nanoribbons (GNRs). GNRs (narrow strips of graphene) do have quantum confinement in one dimension (width), and have been studied for tuning bandgaps in graphene. However, GNRs are still extended in one dimension, so their behavior (particularly in composites) is closer to that of CNTs or graphene sheets than to QDs. GNRs and graphene nanoplatelets primarily improve electrical conductivity and mechanical properties when added to composites, but do not provide the same degree of phonon scattering or surface redox activity as 0D QDs. Meanwhile, fullerenes (0D carbon cages like C_{60}) are another 0D carbon to compare. Fullerenes have a defined molecular structure and a wide bandgap (~1.5–1.8 eV for C_{60}) and have seen use in organic electronics (e.g., as electron acceptors in solar cells). Compared to rGO-QDs, fullerenes are hydrophobic and lack functional groups (unless chemically modified), making them less directly useful in electrochemical applications that require interface with electrolytes. rGO-QDs' rich surface chemistry gives them an edge in aqueous and electrochemical environments, whereas fullerenes shine in dry electronic contexts. Additionally, one can disperse rGO-QDs at higher loading without precipitation in solvents due to their functional groups [8]; fullerenes, by contrast, have limited solubility in anything but organic solvents and tend to crystallize out.

In summary, rGO-QDs distinguish themselves from other carbon nanostructures in a few key ways: (i) dimensionality as 0D particles they can be uniformly distributed and avoid aggregation issues common to 1D/2D materials; (ii) quantum confinement and bandgap unlike graphene or CNTs, they have tunable electronic and optical properties; (iii) abundant edge chemistry they bring functional groups and defects that enable pseudocapacitance and chemical sensing, unlike the relatively inert surface of CNTs or fullerenes; (iv) conductivity when suitably reduced, they still provide good electrical conduction, an advantage over purely amorphous carbon dots. The consensus in literature is that while no single carbon form is “best” for all purposes, rGO-QDs offer a multifunctional balance that is particularly advantageous in nanoscale hybrid materials where interface effects dominate. This justifies the increasing preference for rGO-QDs in nanocomposite design, particularly when multifunctionality, dispersibility, and surface activity are prioritized over single-function conductive additives like CNTs. By using rGO-QDs, we aim to exploit their unique combination of high surface area, quantum-tailored energy levels, and compatibility with solution processing features that set them apart from other carbon allotropes.

2.3.6 Summary of Research Gaps and Opportunities

The above review of literature highlights significant progress in understanding and utilizing rGO-QDs/GQDs, but also reveals key gaps and opportunities that motivate the present thesis. In the thermoelectric domain, studies have shown qualitative benefits of adding GQDs to TE materials (e.g., Bi_2Te_3, ZnO) in terms of phonon scattering and energy filtering [29,53]. However, open questions remain on the optimization and generalization of this approach. For instance, much of the work has focused on unmodified GQDs; there is limited research specifically on reduced GO-QDs in TE composites. rGO-QDs might offer better electrical integration with a host (due to fewer insulating oxides) and could be more effective in modulating carrier concentrations. Yet, the trade-off between defect density and interfacial energy barrier (as noted by Choi *et al.*, a well-aligned band structure is needed) is not fully explored. One gap is the quantitative modeling of how GQD size, loading, and surface chemistry affect TE parameters – most studies report an empirical boost in ZT, but a predictive framework (beyond qualitative energy filtering theory) is lacking. Addressing this could allow rational design of rGO-QD-enhanced TE materials. Additionally, a practical concern is stability: do these quantum dots stay well-dispersed under thermal stress and over time, or do they coalesce or segregate? The literature is thin on long-term stability analysis of GQD-TE composites. While many studies have shifted focus toward energy storage, thermoelectric considerations remain relevant, particularly regarding the unifying concept of employing nanodot additives to manipulate transport phenomena across different domains.

In the supercapacitor and energy storage arena, numerous studies have incorporated GQDs into electrodes, demonstrating improved capacitance and rate performance (sections 2.3.3–2.3.4). However, one research gap is the exploration of rGO-QDs as electrolyte additives an idea only briefly touched by Zhang *et al.* (2016) [8]. Their work showed promise (GQDs acting as solid or liquid electrolytes), but it raises further questions: How do different functional groups on the QD (carboxylate vs sulfonate, etc.) affect ion conduction and electrolyte stability? What is the optimal size/oxidation level of an rGO-QD for maximizing ionic conductivity without sacrificing voltage window or inducing side reactions? And importantly, can this concept be transferred to other types of electrolytes (e.g., organic or ionic liquid electrolytes) to extend the voltage range? Addressing these questions requires systematic investigation of ion conduction behavior in alkaline electrolytes doped with rGO-QDs, such as KOH-based systems, to fill the existing knowledge gap in quantum-dot-enhanced ion transport. Another gap in supercapacitor research is understanding the mechanism of pseudocapacitance in carbon quantum dots. We know functional groups contribute faradaic capacitance, but distinguishing the contributions of different oxygen/nitrogen functionalities (and how they can be controlled via the synthesis of rGO-QDs) is not well documented. This is an opportunity for scientific insight: by comparing capacitance from differently reduced QDs (with different O contents), one can elucidate which functional groups are most beneficial. Future studies could aim to correlate the reduction level of rGO-QDs (e.g., C:O ratio via XPS analysis) with electrochemical performance, in order to identify the optimal surface chemistry for energy storage an area not yet fully explored in existing literature.

Moreover, while rGO-QDs have been applied either in TE or in supercapacitors separately, few if any studies bridge these two fields. A unique opportunity exists in bridging the thermoelectric and supercapacitor fields by exploring how the same nanomaterial rGO-QDs can influence both thermal/electrical conduction and ionic/electrical conduction depending on the application. A broader opportunity emerges here: the multi-functionality of rGO-QDs suggests they could be key components in hybrid systems that scavenge waste heat and store the converted energy. For example, one could envision a device where rGO-QDs enhance a TE generator and the same or connected QDs aid in storing that generated charge in a supercapacitor – essentially an integrated energy harvester-storage system. While such integration is beyond the scope of this thesis, our literature review did not find studies that explicitly connect the dots (no pun intended) between rGO-QD's thermoelectric improvements and their electrochemical benefits. Identifying this gap has sharpened the vision of our research: by deeply understanding rGO-QDs in both contexts, we lay groundwork for future exploration of coupled thermal-electrochemical systems.

Finally, there remain practical challenges and research gaps regarding the scalability and consistency of rGO-QD synthesis. Many lab studies use small batches of QDs with sometimes bespoke syntheses. For rGO-QDs to be viable in real devices (whether TE modules or supercapacitor electrodes), methods to produce them in larger quantity with consistent size and surface chemistry need development. Liu *et al.* (2014) and others have hinted at greener, scalable syntheses (e.g., hydrothermal cutting of biomass into GQDs), but these often yield carbon dots with mixed structures. Buatong *et al.* (2023) achieved a controlled hydrothermal cutting of GO [14], which is a promising route; however, issues like controlling the polydispersity and thoroughly removing residual acids/ions are sometimes glossed over in publications. Recent approaches in synthesis have explored hydrothermal processes combined with purification steps to achieve rGO-QDs with narrow size distributions (~4 nm) and defined surface chemistry, helping bridge the gap between proof-of-concept studies and material reproducibility. By doing so, we hope to provide a reproducible protocol that future researchers can build on, thereby filling the gap between proof-of-concept studies and material reproducibility.

In conclusion, the literature suggests that rGO-QDs are a powerful, multifunctional nanomaterial with demonstrated benefits in thermoelectric and electrochemical systems. Yet, it also exposes gaps in understanding mechanisms (especially in ion conduction and pseudocapacitance), in exploring new application configurations, and in scaling the material. These gaps present promising opportunities for future research. Optimizing rGO-QDs for use in supercapacitor electrolytes remains an underexplored area, with potential synergies derived from their behavior in thermoelectric systems. Advancing the understanding of rGO-QDs in both domains may pave the way for multifunctional energy platforms that integrate energy harvesting and storage.

Chapter 3

Methodology

This chapter details the materials, equipment, and experimental procedures used to synthesize rGO-QDs and optimize their production. Both successful and failed synthesis trials are chronicled, culminating in the final. Characterization techniques used to evaluate the structural, optical, and electrochemical properties of the rGO-QDs are also described. Throughout, preliminary observations (e.g., solution color changes, XRD patterns, or photoluminescence responses) are noted to illustrate the rationale behind each iterative modification in the methodology.

3.1 Materials and Chemicals

The following raw materials and chemicals were used in the synthesis of rGO-QDs and subsequent experiments:

- Sulfuric acid (H_2SO_4, 96%) – Concentrated acid used in GO oxidation and GO fragmentation steps (Carlo Erba)
- Nitric acid (HNO_3, 65%) – Concentrated acid used in combination with H_2SO_4 for oxidative cutting of GO (Supelco)
- Sodium hydroxide (NaOH) Pellets – Used for pH adjustment before hydrothermal reduction (QRéC)
- Potassium hydroxide (KOH) – Used in electrolyte preparation for electrochemical measurements (Merck)
- Deionized water (DI) – Used throughout for dilution, washing, and dialysis.
- Dialysis membrane (MWCO 3,500 Da) – For purification of rGO-QDs after synthesis.
- Organic solvents: N-Methyl-2-pyrrolidone (NMP) and others for electrode preparation (including polyvinylidene fluoride (PVDF) binder).

All chemicals were of analytical grade and used as received without further purification. The GO used as the starting material was supplied by the *Smart Materials Research and Innovation Unit Lab*. This GO was subjected to oxidative cutting and hydrothermal treatment to synthesize rGO-QDs.

3.2 Equipment and Instrumentation

The experimental setup for synthesis and characterization involved the following equipment:

- Ultrasonic Bath (Sonicator): A temperature-controlled ultrasonic bath was used for prolonged ultrasonication of GO in acid. Sonication promotes the fragmentation of GO sheets.
- Teflon-lined Autoclave: A hydrothermal reactor was used for high-temperature, high-pressure.
- Centrifuge: A high-speed centrifuge with appropriate rotor was used for separating solid residues from supernatants. Centrifugation steps were crucial for removing large GO fragments.
- Vacuum Filtration Apparatus: A Buchner funnel with a 47 mm membrane filter (nylon or PTFE) attached to a vacuum flask was used to filter out particulate matter above the quantum dot size.
- Magnetic Stirrer/Hotplate: Used during chemical mixing and for maintaining temperature.
- Muffle Furnace: Used indirectly for drying or any thermal treatment of samples, set at controlled temperatures as needed.
- Analytical Balance: For precise weighing of graphite and reagents (±0.1 mg accuracy).

<u>Characterization Instruments:</u>

- Raman Spectrometer: Thermo Scientific DXR Smart Raman with 532 nm laser excitation was used for Raman analysis.
- X-ray Diffractometer: Rigaku SmartLab XRD system with Cu Kα (λ=1.5406 Å) radiation for phase and structure analysis.
- Transmission Electron Microscope (TEM): High-resolution TEM (Thermo Fisher Scientific Talos, 200 kV) for imaging the size and morphology of QDs.
- UV–Vis Spectrophotometer: Thermo Scientific GENESYS™ 150 for measuring optical absorption spectra of GO/rGO/QDs.

- Fluorescence Spectrometer: Horiba FluoroMax+ for photoluminescence (PL) spectroscopy of rGO-QDs.
- Electrochemical Workstation: A potentiostat/impedance analyzer (Wuhan CorrTest multichannel instrument) for electrochemical impedance spectroscopy (EIS) measurements of electrolytes and supercapacitor cells.

All measurement equipment was calibrated and operated according to manufacturer guidelines. The combination of these instruments enabled both the careful execution of synthesis steps and a comprehensive analysis of the rGO-QDs produced.

3.3 Experimental Design and Considerations

Rationale for Synthesis Strategy: The hydrothermal reduction process was selected as the core synthesis strategy for rGO-QDs due to its effectiveness in simultaneously cutting GO sheets into quantum dots and reducing them to restore graphitic structure. Among various methods (top-down and bottom-up), the hydrothermal approach is especially attractive for producing graphene-based quantum dots because of its relative simplicity and the lack of need for specialized equipment. Under high-temperature, high-pressure conditions in a sealed autoclave, GO can be fragmented into nanoscale pieces and partially reduced, yielding fairly uniform rGO-QDs in one step. This strategy avoids the use of harsh chemical reducing agents (like hydrazine or $NaBH_4$) that are common in chemical reduction methods, thereby minimizing toxic reagents and post-synthesis impurities. Additionally, hydrothermal treatment inherently provides water as a medium, aligning with greener synthesis principles. Alternative approaches such as purely chemical reduction or ultrasonication were considered but deemed less optimal alone. Chemical reduction of GO (using hydrazine or other reducers) can effectively remove oxygen functional groups, but it does not necessarily shear the GO into quantum dots, often requiring a prior cutting step and involving toxic chemicals. Ultrasonication alone can break down carbon materials into nanoscale pieces by cavitation and shear forces, but without a subsequent reduction step the product remains highly oxidized (GOQDs) with lower electrical conductivity. By combining controlled oxidative cutting with hydrothermal reduction, the chosen strategy aims to yield rGO-QDs with well-defined size, good dispersion, and restored π-conjugation domains for optimal optical and electronic properties.

Reference to Previous Methods: This experimental plan builds on insights from earlier rGO-QD synthesis methods, each with known advantages and limitations. Hydrothermal cutting of GO has been reported to yield high-quality rGO-QDs with controllable size distributions and low defect densities. For instance, Buatong *et al.* (2023) demonstrated that increasing the hydrothermal reduction temperature from 90 °C to 180 °C progressively decreases the interlayer spacing and defect density in rGO-QDs [14]. Such findings support the choice of a high-temperature hydrothermal approach in our design. By contrast, chemical reduction methods (a non-hydrothermal route) can effectively restore carbon sp^2 domains but often require strong reducing agents (e.g. hydrazine, hydroquinone) and may leave behind toxic residues or create new defects during oxygen group removal. Previous studies using hydrazine rGO-QDs noted improved electrical conductivity but also introduced nitrogen functionalities and vacancy defects that altered photoluminescence. These drawbacks informed our decision to minimize the use of external reducing agents. Ultrasonication-based methods (often in tandem with chemical or microwave treatments) have shown the ability to produce GQDs rapidly with high yields. Zhu *et al.* (2011) [59] achieved one-step synthesis of GQDs via ultrasonication with $KMnO_4$, obtaining highly luminescent GQDs in a simple, acid-free process. However, purely ultrasonic fragmentation may result in a broad size distribution and predominantly oxidized dots that still require reduction for certain applications. By referencing these methods, we justified a combined strategy: first chemically cut GO into smaller pieces (using acid oxidation and ultrasonication, akin to a strong oxidative “top-down” cut), then apply hydrothermal treatment to simultaneously reduce and further cleave the material under controlled conditions. Each parameter modification in our design was grounded in literature precedents. For example, we chose a strong acid mixture (H_2SO_4:HNO_3) for pre-oxidation based on its success in “opening up” graphene sheets into smaller fragments – a process known to introduce linearly arranged epoxy groups that make the carbon lattice susceptible to rupture upon heating. We introduced a mild alkaline environment (pH~8) during hydrothermal treatment to facilitate deoxygenation and cutting, following Pan *et al.*’s [50] approach for producing bright, blue-emitting GQDs.

Each adjustment (temperature, time, pH, precursor treatment) was thus chosen with a theoretical rationale: to optimize the size of QDs (for quantum confinement), maximize restoration of sp^2 carbon (for conductivity and fluorescence), and minimize structural defects or contaminants, leveraging the best practices reported in earlier rGO-QD syntheses.

Justification for Parameter Modifications: Throughout the experimental design, modifying each parameter was carefully considered to balance the trade-offs between cutting efficiency, reduction quality, and product yield. The hydrothermal temperature was set at 180 °C in the final design because lower temperatures (e.g. 120 °C or 150 °C) in initial trials yielded incomplete reduction (persisting oxygen content and a brownish product) and larger dot sizes with weak photoluminescence. Literature suggests that 180 °C is a critical threshold for efficient “hydrothermal cutting” of GO, as higher temperatures generate reactive oxygen species (from residual functional groups or added H_2O_2) that cleave carbon-carbon bonds more effectively. This is corroborated by the observed trend of shrinking rGO-QD size (from ~22 nm down to ~8 nm) when the hydrothermal temperature is raised to 180 °C. Reaction duration was extended to 12 hours after shorter trials (e.g. 4 h or 6 h) produced insufficient reduction (indicated by residual GO XRD peaks around $2\theta \approx 10°$). A longer dwell at high temperature allows more complete removal of oxygen functional groups and healing of graphitic domains, as indicated by a decrease in the Raman D/G intensity ratio in prolonged treatments. The decision to perform a pre-cutting via acid oxidation and ultrasonication was justified by the need to create defect sites that seed the formation of quantum dots. GO pre-treated with a 1:3 H_2SO_4:HNO_3 mixture is heavily oxygenated and fragmented, which, after ultrasonication, yields small GO pieces (colloidal GOQDs). Without this step, a hydrothermal treatment might only reduce the surface of large GO sheets without thoroughly breaking them into QDs. Each cleaning and purification step (centrifugation to remove unexfoliated debris, dialysis to eliminate residual ions) was kept consistent to ensure that improvements in product quality stemmed from the synthesis modifications rather than differences in post-processing. In summary, the experimental design was iterative and evidence-based, drawing on theoretical rationales and past research to fine-tune the synthesis of rGO-QDs. The combination of a controlled pre-oxidation + ultrasonication step followed by hydrothermal reduction under optimized conditions was expected to yield rGO-QDs with superior structural and optical quality, which formed the foundation for subsequent characterization and application testing.

3.4 Synthesis Trials and Optimization

A series of five synthesis trials (Trial 1 through Trial 5) were conducted to develop an effective route for producing rGO-QDs. Each trial introduced specific modifications in ultrasonication time, pH adjustment, hydrothermal treatment, and purification (centrifugation, dialysis, filtration) to address the shortcomings of the previous attempt. The evolution of the procedure and the corresponding outcomes are detailed below, along with theoretical rationale for the observed successes or failures.

Trial 1: Initial Synthesis with Basic Hydrothermal Reduction

In this initial synthesis trial, graphene oxide (GO) was prepared using the modified Hummers' method and oxidized in a mixture of concentrated H_2SO_4 and HNO_3 in a volume ratio of 1:3. The resulting solution underwent ultrasonication for 10 hours to promote exfoliation and partial oxidative cutting of GO sheets. Afterward, the suspension was diluted with deionized (DI) water and thoroughly washed via repeated centrifugation and decantation until the pH reached neutral (~7). The sediment was then redispersed in DI water, and the dispersion was transferred into a Teflon-lined autoclave for hydrothermal treatment at 180°C for 15 hours. After naturally cooling to room temperature, the product was centrifuged at 8000 rpm for 15 minutes 2 times, and the supernatant was collected and dialyzed using a 3500 Da molecular weight cut-off (MWCO) membrane for 12 hours to remove residual acids and small impurities.

Result: The product appeared brown in ambient light in Figure 3.4.1(a) but exhibited no visible photoluminescence under UV light at 365 nm in Figure 3.4.1(b), indicating the absence of quantum confinement characteristics typically associated with quantum dots. Furthermore, X-ray diffraction (XRD) analysis in Figure 3.4.1(c) revealed dominant peaks at $2\theta \approx 24°$ and $2\theta \approx 43°$, corresponding to the (002) and (100) planes of reduced graphene oxide (rGO), respectively. The lack of peak broadening or shift toward lower angles suggests that the sample retained stacked multilayer graphitic structures and was not successfully fragmented into nanoscale quantum dots. These results indicate that the synthesis conditions in Trial 1 were insufficient for producing rGO quantum dots (rGO-QDs), and further optimization was required.

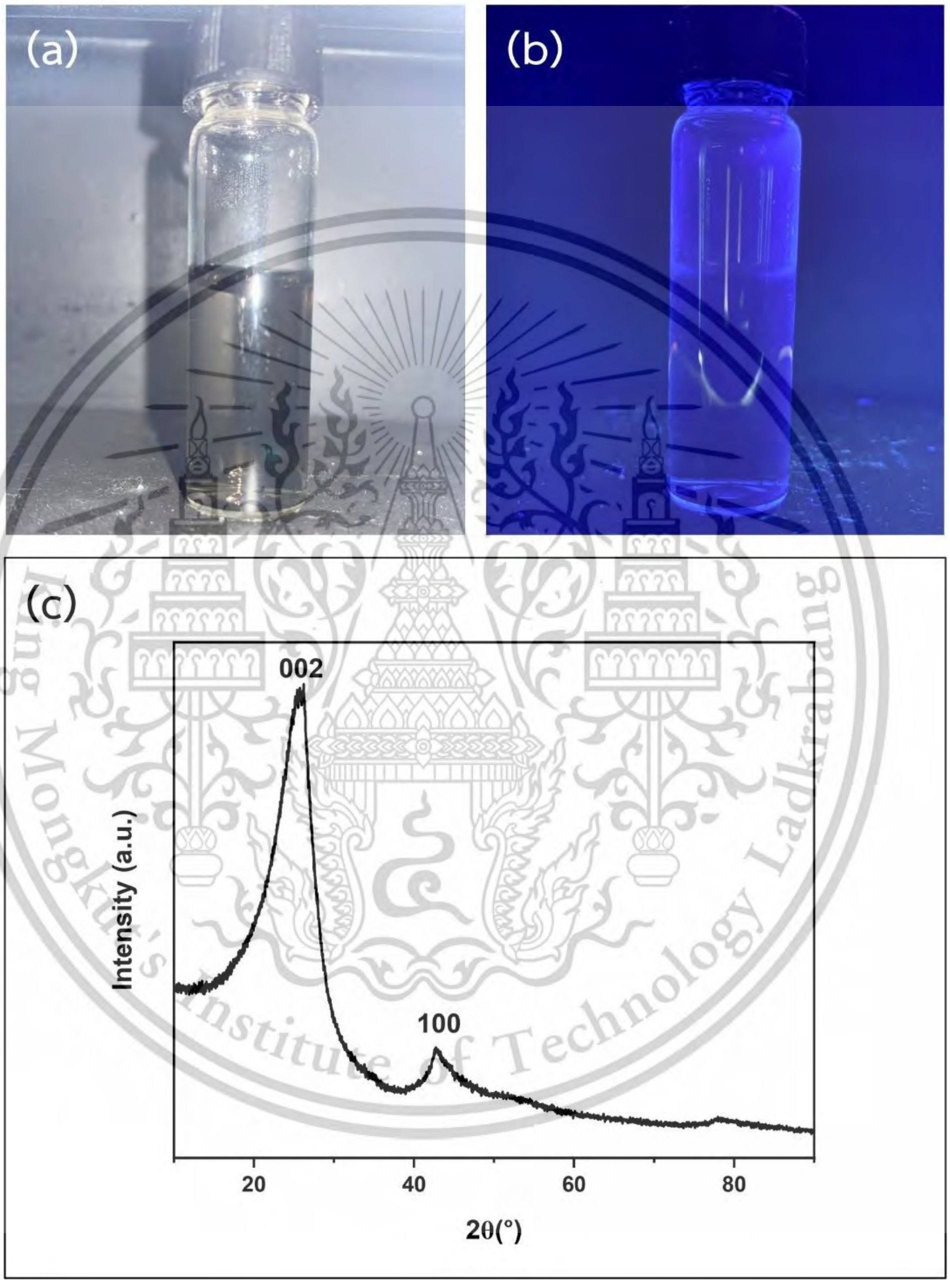

Figure 3.4.1 Visual and structural characterization of the sample synthesized in Trial 1 (a) under ambient light, (b) no photoluminescence is observed under 365 nm UV light, and (c) XRD pattern reveals broad (002) and (100) peaks.

Trial 2: Enhanced Ultrasonication-Assisted Cutting

In Trial 2, the synthesis protocol was modified from Trial 1 by extending the ultrasonication time from 10 hours to 11 hours, aiming to improve the oxidative cutting efficiency of the GO sheets and promote the formation of smaller fragments. GO was first synthesized via the modified Hummers' method and oxidized in a 1:3 mixture of concentrated H_2SO_4 and HNO_3. The mixture was then subjected to ultrasonication for 11 hours to enhance exfoliation and size reduction.

After sonication, the solution was diluted with deionized (DI) water and repeatedly washed through centrifugation until reaching neutral pH (~7). The resulting sediment was redispersed in DI water without pH adjustment. The suspension was hydrothermally treated at 180°C for 15 hours in a Teflon-lined autoclave. After cooling to room temperature, the sample was centrifuged at 8000 rpm for 15 minutes (twice), and the supernatant was collected. Dialysis was then performed using a 3500 Da MWCO membrane for 24 hours to remove residual acids and small molecules.

Result: After increasing the ultrasonication time to 11 hours, the resulting solution remained dark brown and did not exhibit photoluminescence under UV light at 365 nm, as shown in Figure 3.4.2(b). This indicates that quantum confinement and surface state-related emissions were still not achieved. The XRD pattern in Figure 3.4.2(c) continued to show a dominant (002) peak with an additional (100) reflection, characteristic of partially reduced graphene oxide structures rather than discrete quantum dots. The persistence of these broad peaks implies incomplete cutting of the GO sheets and aggregation into stacked domains, suggesting that the applied treatment was insufficient to produce rGO-QDs.

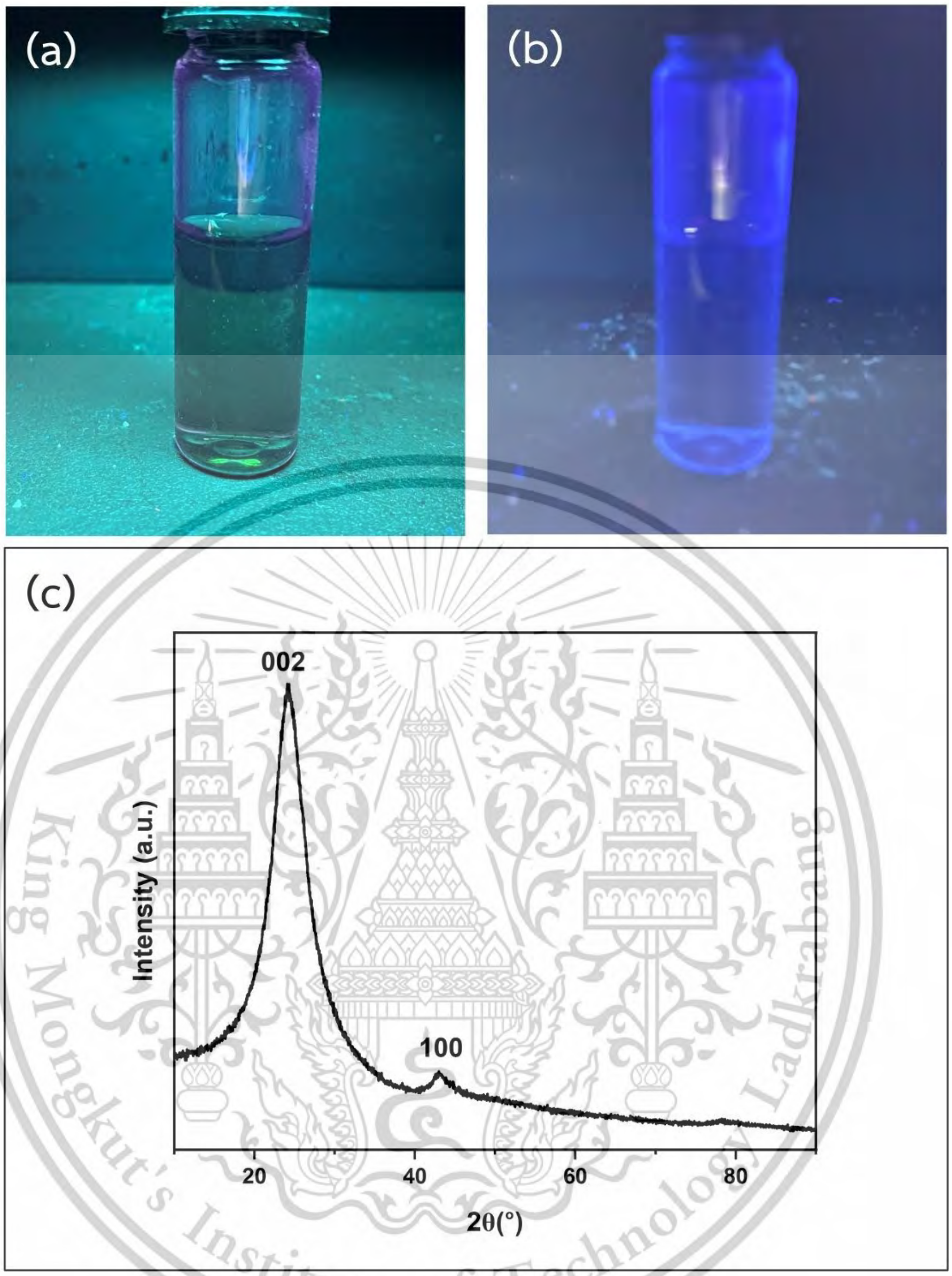

Figure 3.4.2 Visual and structural characterization of the sample synthesized in Trial 2 (a) under ambient light, (b) no photoluminescence under UV light, and (c) XRD pattern reveals broad (002) and (100) peaks.

Trial 3: Prolonged Ultrasonication and pH Adjustment Prior to Hydrothermal Treatment

To further promote the exfoliation and oxidative cutting of graphene oxide (GO) into nanoscale fragments, Trial 3 extended the ultrasonication time to 12 hours, compared to 11 hours in Trial 2. Additionally, the pH of the GO suspension was adjusted to approximately 8 using sodium hydroxide (NaOH) prior to hydrothermal treatment to enhance reduction conditions and support the formation of quantum dot-like domains. The hydrothermal process was conducted at 180°C for 15 hours, followed by centrifugation at 8000 rpm (15 minutes, twice). The resulting supernatant was dialyzed using a 3500 Da MWCO membrane for 24 hours.

Result: The rGO-QD solution obtained in Trial 3 exhibited a light brown color under ambient light (Figure 3.4.3(a)), with no visible fluorescence under UV illumination (Figure 3.4.3(b)). This indicated that the synthesized product lacked the characteristic photoluminescence typically associated with graphene quantum dots. The XRD pattern (Figure 3.4.3(c)) showed a broad and low-intensity peak centered at approximately 24.8°, corresponding to the (002) plane of reduced graphene oxide. The peak was significantly broader than that of graphite or bulk rGO, suggesting the formation of nanoscale graphene domains. However, the absence of photoluminescence implied that the quantum confinement and surface defect states necessary for rGO-QD fluorescence had not yet fully developed under this condition. Overall, the result suggested partial reduction and fragmentation of GO, but not sufficient to yield functional rGO-QDs with quantum dot characteristics.

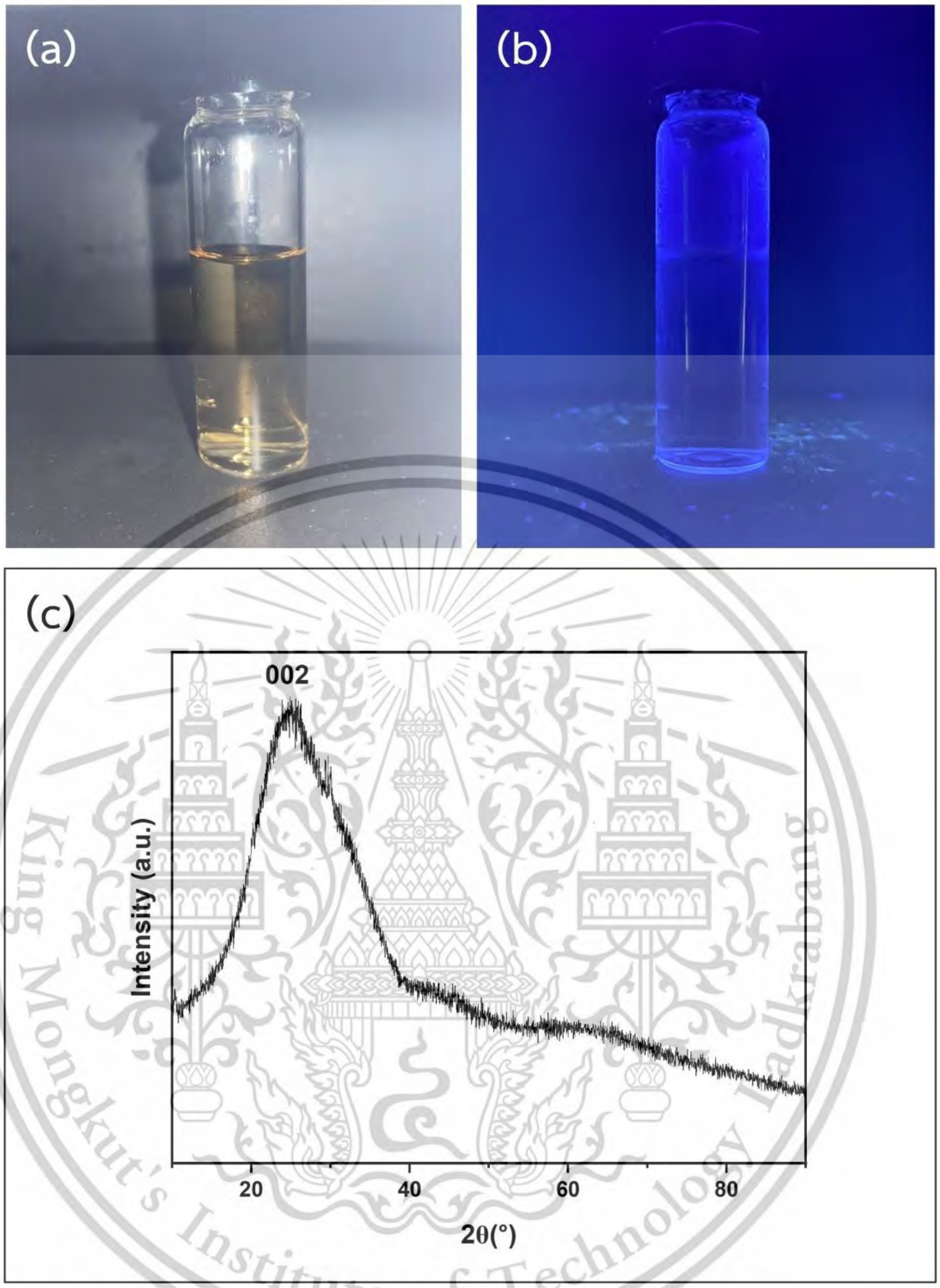

Figure 3.4.3 Visual and structural characterization of the sample synthesized in Trial 3 (a) under ambient light, (b) no photoluminescence under UV light, and (c) XRD pattern showing the broad (002) peak.

Trial 4: Optimization by Vacuum Filtration Instead of Centrifugation

In this trial, the synthesis process was identical to that in Trial 3, except that the post-hydrothermal purification step was modified. Instead of using centrifugation at 8000 rpm, the product was purified using vacuum filtration through a 0.22 μm pore size membrane. The aim was to improve the separation of small-sized quantum dots from larger particulates or aggregated residues.

Result: The resulting solution appeared yellowish under ambient light (Figure 3.4.4(a), and exhibited non-prominent fluorescence under UV illumination (Figure 3.4.4(b), suggesting the formation of luminescent rGO-QDs. The XRD pattern (Figure 3.4.4(c) displayed a broad (002) peak centered around 24°, characteristic of disordered graphitic domains. The absence of sharp peaks and the broad nature of the diffraction suggest a nanoscale, amorphous to semicrystalline structure consistent with reduced graphene oxide quantum dots.

This was the first trial to successfully achieve fluorescence emission, indicating that replacing the centrifugation step with fine vacuum filtration may have effectively removed residual particles while preserving well-dispersed quantum dots in the filtrate.

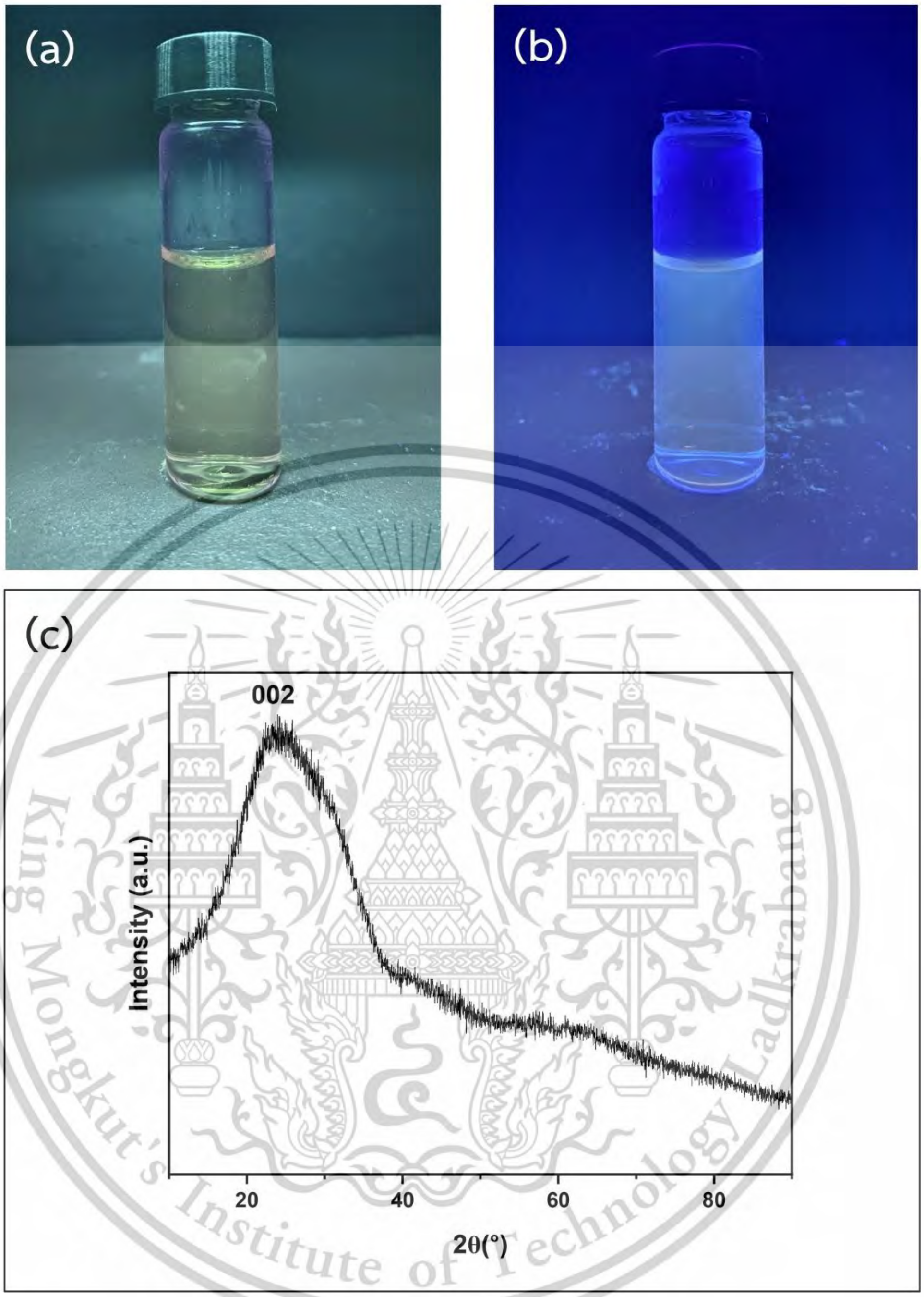

Figure 3.4.4 Visual and structural characterization of the sample synthesized in Trial 4 (a) under ambient light, (b) yellow fluorescence under UV illumination, and (c) XRD pattern showing the broad (002) peak of rGO-QDs.

Trial 5: Optimized Synthesis with Enhanced Purification

In this trial, the synthesis protocol was refined to improve both the optical properties and structural quality of rGO-QDs. GO was oxidized using a 1:3 mixture of H_2SO_4 and HNO_3, followed by 12 hours of ultrasonication to facilitate sheet cutting. The mixture was then diluted, washed thoroughly, and centrifuged at 9000 rpm for 15 minutes to remove larger flakes. The sediment was redispersed in 25 mL of distilled water, and the pH was adjusted to 8 using NaOH. This suspension was subjected to hydrothermal treatment at 180 °C for 15 hours. After cooling, large aggregates were removed by vacuum filtration through a 0.22 μm microporous membrane. Finally, the filtrate was dialyzed for 48 hours using a 3500 Da MWCO membrane. The process for the synthesis of rGO-QDs is shown in Figure 3.4.5.

Result: The resulting solution exhibited a strong blue photoluminescence under UV light (365 nm), indicating successful formation of quantum-confined domains. The XRD pattern revealed a broad 002 peak centered around ~24°, consistent with reduced graphene oxide nanosheets of nanometer-scale thickness. However, to ensure accuracy and validate the properties, further structural and electrochemical characterizations were performed and are detailed in Chapter 4.

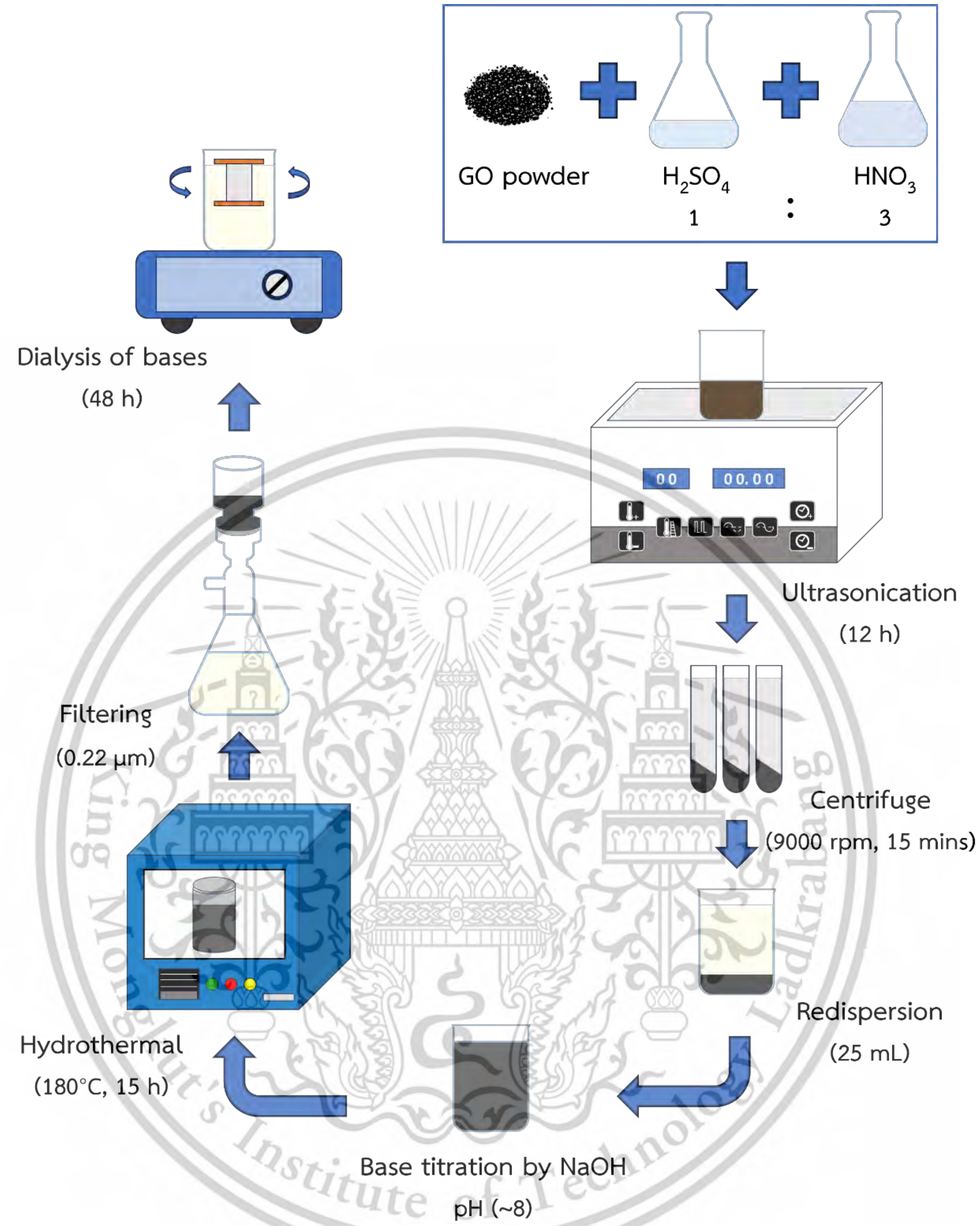

Figure 3.4.5 Synthesis process of rGO-QDs using acid treatment, ultrasonication, and hydrothermal reduction.

3.5 Supercapacitor Fabrication

A symmetric coin-cell supercapacitor (CR2032 type) was fabricated using two identical electrodes. Each electrode was prepared by coating a slurry composed of activated carbon, acetylene black, rGO, and polyvinylidene fluoride (PVDF) binder in N-methyl-2-pyrrolidone (NMP) solvent. The mass ratio of the components was maintained at 80:5:5:10. The slurry was coated onto a stainless steel foil current collector, dried at 80 °C overnight, pressed, and punched into circular discs with a diameter of approximately 16 mm.

The electrolyte was prepared by dispersing rGO-QDs in a 3 M potassium hydroxide (KOH) solution, forming a homogeneous rGO-QD/KOH suspension that enhances ionic conductivity and electrochemical performance.

The coin-cell assembly followed the standard CR2032 stacking configuration as follows:

1. Negative case (bottom cap)
2. Spring and spacer (to ensure compression and contact)
3. Anode electrode disc
4. Separator (soaked with rGO-QD/KOH electrolyte)
5. Cathode electrode disc
6. Positive case (top cap)

All components were stacked and sealed using a coin-cell crimping machine to ensure tight contact and minimize internal resistance. The separator functioned as both an ionic conductor and an electronic insulator. The assembled coin cells were further dried at 60 °C under vacuum for 12 h before testing to remove residual moisture. The internal architecture of the device is illustrated in Figure 3.5.1.

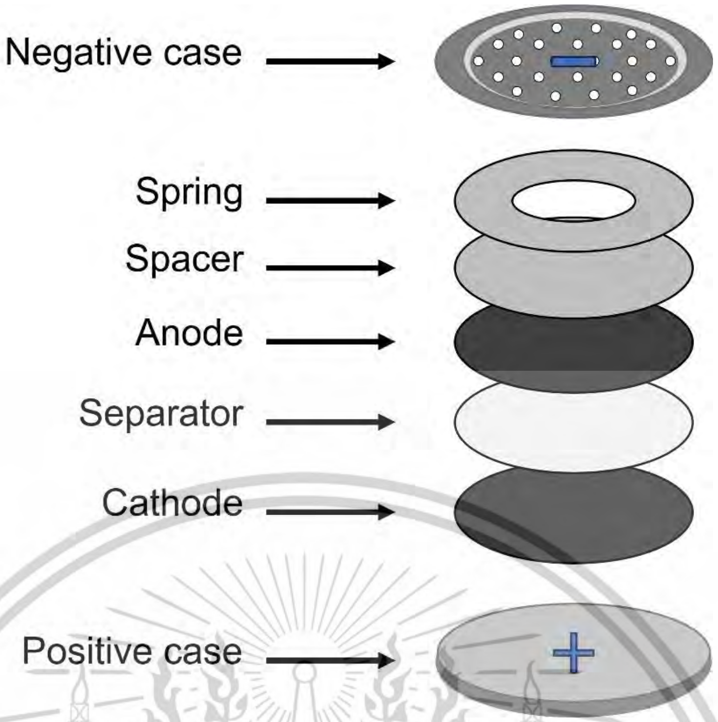

Figure 3.5.1 Schematic illustration of the internal components and assembly structure of a symmetric coin cell supercapacitor (CR2032 type).

Chapter 4

Results and Discussion

4.1 Structural Characterization of rGO-QDs

In order to elucidate the structural modifications induced by reduction and quantum-dot formation, we characterized GO, rGO, and rGO-QDs using Raman spectroscopy, X-ray diffraction (XRD), and transmission electron microscopy (TEM). Raman spectroscopy identifies structural disorder via the D band (~1350 cm^{-1}) and graphitic order via the G band (~1580 cm^{-1}) [60]. The intensity ratio (I_D/I_G) provides a quantitative measure of disorder and was used to monitor defect evolution across the three materials. XRD probes changes in crystalline spacing: for example, high-temperature hydrothermal reduction of GO is known to decrease the interlayer d-spacing (shifting the GO (001) peak to the rGO (002) reflection) and thus restore graphitic order [14]. In our study, the XRD pattern of rGO-QDs exhibited a broad peak at ~24.9°, corresponding to the (002) plane of graphitic carbon, indicating partial restoration of the sp^2 carbon structure (see Figure 4.1.2). TEM provides direct images of the dot morphology and size distribution. The rGO-QDs exhibited an average particle size of approximately 4.14 nm, with narrow size distribution and good dispersion, confirming successful quantum dot formation (see Figure 4.1.3). Additionally, energy-dispersive X-ray spectroscopy (EDX) results further confirm that the hydrothermal reduction effectively removed oxygenated functional groups, as reflected by the significant increase in the carbon.

By comparing these spectroscopic and imaging results across GO, rGO, and rGO-QDs, we can track the evolution of structural order and defect density induced by the chemical treatments. Overall, the characterization results validate the synthesis of nanoscale rGO-QDs with restored graphitic domains, increased defect density from quantum dot formation, and high structural uniformity, supporting their suitability for optical and electrochemical applications.

4.1.1 Raman Spectroscopy Analysis

Raman spectroscopy was employed to investigate the structural changes and defect densities of GO, rGO, and rGO-QDs, as illustrated in Figure 4.1.1. The Raman spectra of all samples exhibit two characteristic peaks: the D-band located around 1350 cm^{-1}, which corresponds to the breathing modes of sp^2 carbon atoms in rings and is associated with defects and disorder in the graphene lattice, and the G-band near 1600 cm^{-1}, which represents the in-plane vibrational modes of sp^2 hybridized carbon atoms. The intensity ratio between these two peaks (I_D/I_G) serves as a key indicator of the defect density and degree of graphitic order in the carbon-based materials.

For GO, the measured I_D/I_G ratio was approximately 1.01, reflecting the substantial presence of structural defects introduced during the oxidation process, primarily due to the incorporation of oxygen-containing functional groups that disrupt the sp^2 network. Upon thermal reduction, the I_D/I_G ratio of rGO increased to 1.07, suggesting that the partial removal of these oxygen functionalities generated new edge defects, thereby increasing the overall defect density [61].

Interestingly, the rGO-QDs sample showed a significantly lower I_D/I_G ratio of 0.91. This reduction in the defect-related D-band intensity indicates an improvement in structural order, likely due to the hydrothermal treatment at 180 °C, which facilitates the restoration of sp^2 carbon domains and enhances graphitic reorganization. The formation of quantum dots with nanoscale dimensions further contributes to this increased ordering through quantum confinement effects [62,63]. These effects are known to promote rehybridization of carbon atoms and enhance crystallinity, leading to improved material properties.

This trend is consistent with the findings reported by Buatong *et al.* (2023) [14], who observed a similar decrease in I_D/I_G ratio for rGO-QDs synthesized under hydrothermal conditions. The improved graphitic ordering observed in rGO-QDs is significant, as it can lead to enhanced electronic conductivity and optical performance, both of which are crucial for applications in optoelectronics, sensing, and energy devices.

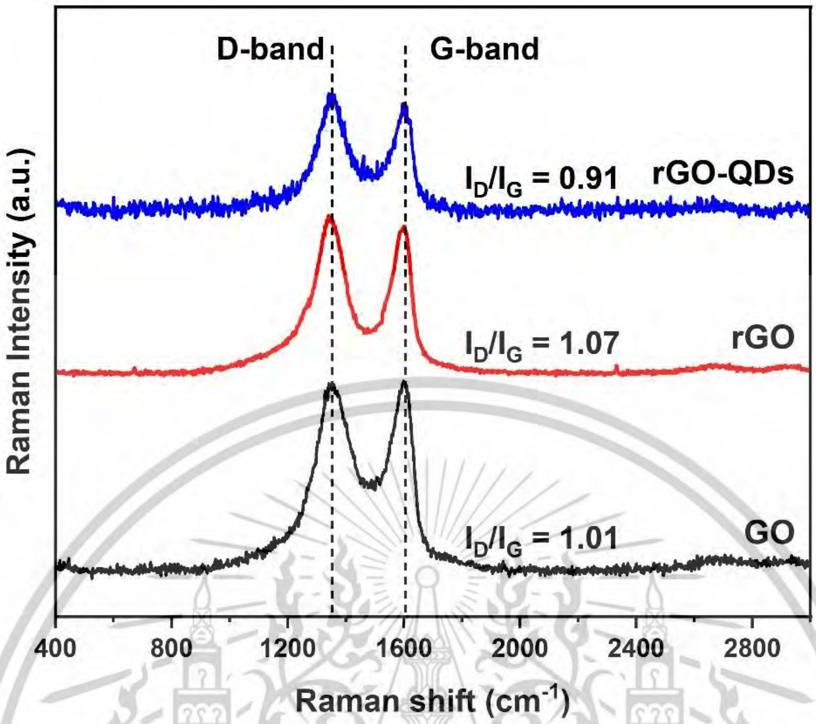

Figure 4.1.1 Raman spectra of GO, rGO, and rGO-QDs showing D and G bands with corresponding I_D/I_G ratios.

In summary, the Raman analysis confirms that while the reduction of GO to rGO initially introduces additional defects [64], the subsequent transformation into rGO-QDs via hydrothermal treatment results in a more ordered carbon structure with fewer defects. This structural evolution highlights the critical role of synthesis conditions and nanoscale morphology in tuning the quality and functionality of graphene-based quantum dots.

4.1.2 X-ray Diffraction (XRD) Analysis

X-ray diffraction (XRD) was utilized to analyze the crystalline structure, interlayer spacing, and crystallite size of the GO, rGO, and rGO-QDs samples. The corresponding XRD patterns are presented in Figure 4.1.2, while the key structural parameters derived from the diffraction data are summarized in Table 4.1.1.

In the case of graphene oxide (GO), a sharp diffraction peak was observed at $2\theta \approx 11.5°$, corresponding to the (001) reflection plane. The associated interlayer spacing (d-spacing) was calculated to be approximately 7.69 Å, which is indicative of the expanded structure resulting from the incorporation of oxygen-containing functional groups between the graphene layers [65]. This spacing reflects the presence of oxygen-containing functional groups and intercalated water molecules that expand the GO layers. This structural expansion is also reflected in the relatively large crystallite size of 39.71 Å, as derived from the Scherrer equation. The presence of a weaker peak near $2\theta \approx 42°$ corresponds to the (100) plane, typically attributed to the in-plane periodicity of the carbon lattice.

Upon reduction to rGO, the (001) peak disappears, and a new, broader peak emerges at $2\theta \approx 24.3°$, corresponding to the (002) reflection plane. The shift of this peak and the reduction in d-spacing to 3.65 Å indicate the removal of interlayer oxygen species and a partial reformation of the graphitic domains. This structural rearrangement is accompanied by a marked decrease in crystallite size to 9.84 Å, and a narrower full width at half maximum (FWHM) of approximately 0.8253°, suggesting improved ordering compared to GO, albeit with some residual disorder.

For rGO-QDs, the diffraction pattern features a very broad (002) peak centered at $2\theta \approx 24.9°$. The d-spacing further decreases to 3.57 Å, and the FWHM increases significantly to 11.97°, signifying a pronounced reduction in crystallite size to 7.10 Å. The broadening of the peak and its low intensity indicate a loss of long-range order, consistent with the nanoscale size and amorphous nature of the quantum dots. This broadening effect is characteristic of nanostructured materials such as quantum dots, where the reduced dimensions limit the long-range crystallographic coherence. The observed decrease in crystallite size and increase in peak broadness reflect the impact of quantum confinement and size-induced lattice distortion in rGO-QDs.

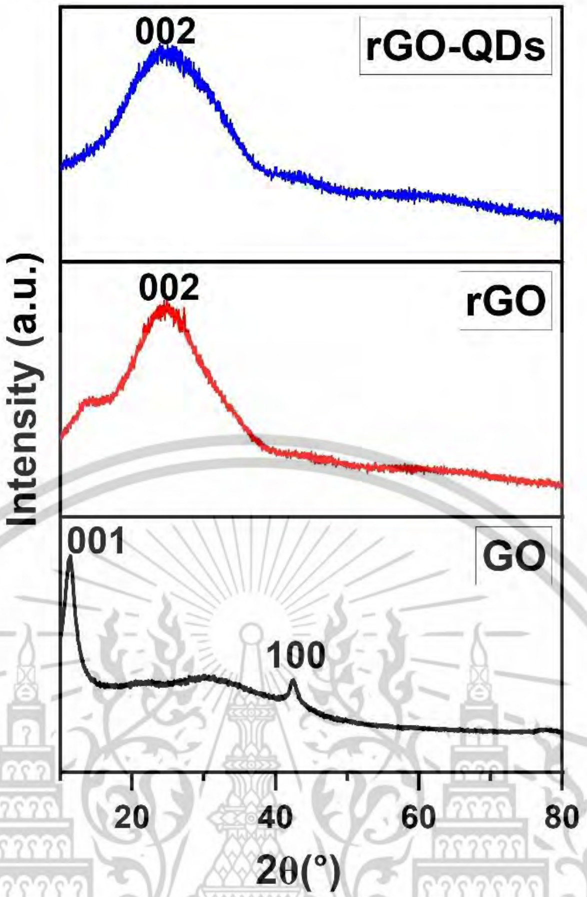

Figure 4.1.2 XRD patterns of GO, rGO, and rGO-QDs showing shifts in diffraction peaks corresponding to structural evolution and reduction in crystallite size.

Overall, the XRD analysis reveals a clear progression from the well-ordered, oxygen-rich GO structure to the partially restored graphitic nature of rGO, and finally to the nanoscale, quantum-confined structure of rGO-QDs. The results confirm the successful synthesis of graphene-based quantum dots with reduced interlayer spacing and minimal crystalline domains, aligned with the expected structural transition upon reduction and size minimization.

Table 4.1.1 Summary of XRD parameters including 2θ values, d-spacing, FWHM, and crystallite size for GO, rGO, and rGO-QDs.

Sample	2θ (°)	d-spacing (Å)	FWHM (°)	(hkl)	Crystallite Size (Å)
GO	11.5012	7.68772	2.1000	001	39.71
rGO	24.3404	3.65454	0.8253	002	9.84
rGO-QDs	24.9046	3.57236	11.9687	002	7.10

4.1.3 Transmission Electron Microscopy (TEM) Analysis

Transmission electron microscopy (TEM) was employed to investigate the morphological and nanostructural characteristics of the synthesized rGO-QDs. Figure 4.1.3 presents a comprehensive set of TEM and HRTEM images, along with particle size distribution and interlayer spacing analysis, to validate the quantum dot formation and graphitic structure restoration.

As shown in Figure 4.1.3(a), the low-magnification TEM image reveals nearly transparent, wrinkled graphene-based sheets, consistent with the morphology of reduced graphene oxide. These features suggest successful exfoliation and thinning of GO during the reduction process, yielding few-layered structures with enhanced transparency an indicator of high-quality rGO formation. The visible folds and overlaps further support the presence of flexible, ultrathin carbon sheets.

At higher magnification, the high-resolution TEM (HRTEM) image in Figure 4.1.3(b) confirms the crystalline nature of the rGO-QDs through the observation of well-defined lattice fringes. These fringes are indicative of sp^2-hybridized carbon domains that remain intact after the hydrothermal treatment. The restoration of such domains is vital for maintaining the desirable electronic and optical properties of the quantum dots.

Figure 4.1.3(c) illustrates the particle size distribution of the rGO-QDs, showing a relatively narrow range of sizes from approximately 2.5 to 6.5 nm. The majority of particles are centered around 3.5 nm, and the average particle diameter was calculated to be 4.14 nm [66]. This uniformity in particle size is particularly important for ensuring consistent quantum confinement effects, which directly influence the optical absorption, emission behavior, and electronic conductivity of the material [67].

A close-up image of the lattice fringes is shown in Figure 4.1.3(d), where the measured interlayer spacing is approximately 3.41 Å. This value is characteristic of graphitic materials and indicates the successful partial restoration of the graphitic stacking order in rGO-QDs. Such tight spacing enhances the electrical pathways within the structure, contributing to improved conductivity an essential parameter for applications in supercapacitors and energy-related devices.

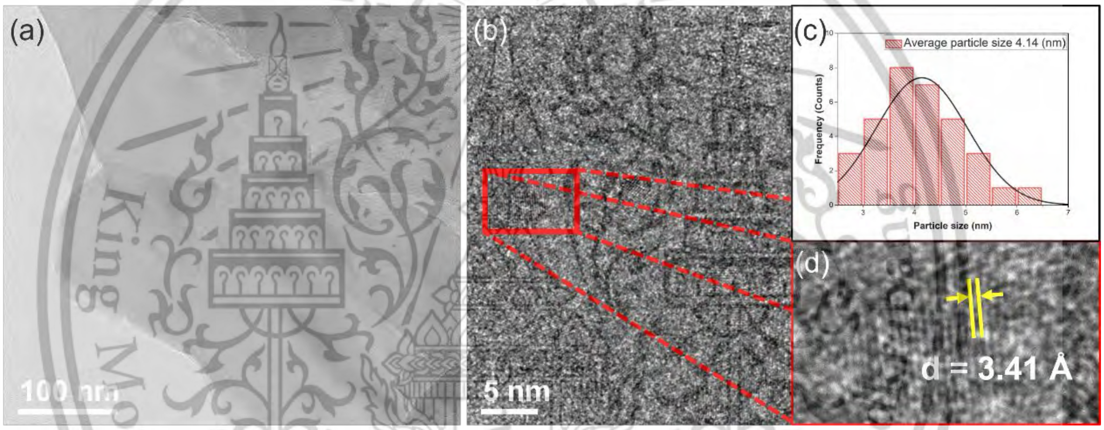

Figure 4.1.3 (a) TEM image of rGO-QDs, (b) HRTEM image showing lattice fringes of crystalline carbon domains, (c) particle size distribution indicating an average size of 4.14 nm, and (d) close-up image showing interlayer spacing of 3.41 Å.

Overall, the TEM results confirm that the rGO-QDs possess a nanoscale, highly crystalline structure with uniform particle size and graphitic features. These structural attributes are expected to significantly enhance the electrochemical and optoelectronic performance of the material, making it suitable for integration into advanced energy storage and sensing platforms.

4.1.4 Energy Dispersive X-ray Spectroscopy (EDX) Analysis

The elemental composition of the GO and rGO-QDs samples was determined by EDX. The GO precursor was found to contain 64.32 at.% carbon and 34.20 at.%

oxygen (C:O ≈ 1.88), whereas the rGO-QDs contained 80.10 at.% carbon and only 16.01 at.% oxygen (C:O ≈ 5.00). In other words, reduction increased the carbon content by ~15.8% and markedly decreased the oxygen content by ~18.2%, causing the C/O atomic ratio to rise from ~1.9 to 5.0. Such a large increase in the C/O ratio signifies effective deoxygenation of the GO: many oxygenated functional groups have been removed. Although a small portion of oxygen remains in the rGO-QDs (16.01%), the significant reduction in oxygen content suggests that most oxygenated groups have been successfully removed during the reduction process. In practical terms, this high carbon fraction (≈80%) corresponds to a predominantly graphitic composition in the QDs, consistent with a restoration of extended sp^2-bonded carbon networks.

This trend is fully consistent with prior studies of GO reduction. For example, Chuah *et al.* report GO with C:O ≈1.90 (44.9% C, 23.6% O) and rGO with C:O ≈2.70 (60.4% C, 22.3% O) after phytoreduction [68]. In that work the higher C/O ratio in rGO was explicitly attributed to removal of surface oxygen (i.e. deoxygenation) by the reducing agent. Likewise, Kalil *et al.* noted that treating GO (C/O 2.15) with a reducing agent raised the C/O ratio to 2.80, providing direct evidence of reduction [69]. These examples echo the same behavior seen here: the carbon-to-oxygen ratio of GO increases dramatically upon reduction. Typical well-oxidized GO materials have C/O ratios in the range ~2–3 (O/C ≈0.33–0.5), whereas fully reduced graphene (or GQDs) often exhibit C/O ratios on the order of 5 or higher (O/C ≈0.2). In fact, one study reports rGO with O/C ≈0.2 (C/O ≈5) after extensive reduction, compared to ~0.4 (C/O ≈2.5) for GO, remarkably similar to our findings. Thus, the substantial rise in C/O from 1.88 to 5.00 here is in line with expectations for highly reduced graphene materials.

The implication of these EDX results is that the reduction process has largely restored the sp^2-hybridized carbon lattice. Oxygen-containing groups in GO (such as epoxides, hydroxyls, and carboxyls) introduce sp^3-like disruptions and defect sites. Their removal during reduction “cleans” the carbon network, increasing the fraction of contiguous sp^2 domains. In other words, a higher C/O ratio corresponds to fewer sp^3-bonded C–O moieties and more purely graphenic (sp^2) carbon. This interpretation is supported by the literature: elevated C/O ratios in reduced samples are consistently linked with re-formation of graphitic carbon. For instance, Chuah *et al.* (2020) explicitly note that the higher C/O in rGO indicates oxygen was “effectively removed by the extract" [68], which implies restoration of sp^2 character. Likewise, studies of GQDs report EDX carbon contents of ~80–82% after reduction [70], reflecting a predominantly carbonaceous (sp^2) structure. In summary, the marked increase in carbon fraction and C:O ratio from GO to rGO-QDs indicates a high degree of reduction, yielding a more ordered, sp^2-rich carbon framework in the QDs.

4.2 Optical Properties of rGO-QDs

The optical properties of rGO-QDs were investigated to evaluate their potential for optoelectronic and energy-related applications. Quantum dots derived from graphene-based materials exhibit unique size-dependent optical behaviors due to quantum confinement and edge effects, which distinguish them from their bulk counterparts. In this study, UV–visible (UV–Vis) absorption spectroscopy and photoluminescence (PL) spectroscopy were employed to characterize the light absorption and emission characteristics of the synthesized rGO-QDs. These techniques provide insight into the electronic structure, energy band transitions, and quantum efficiency of the material.

UV–Vis spectroscopy reveals information about the optical absorption edge, π–π^* transitions in aromatic C=C bonds, and n–π^* transitions associated with residual oxygen-containing groups. The spectral features and absorption peak positions are closely related to the conjugated domain size and the degree of reduction in the rGO-QDs. Photoluminescence spectroscopy, on the other hand, was used to evaluate the fluorescence properties of the quantum dots. The PL behavior of rGO-QDs is highly dependent on particle size, surface states, and chemical composition. The quantum dots synthesized in this work exhibit strong and tunable PL emission, highlighting their suitability for use in sensing, bioimaging, and optoelectronic devices.

The detailed findings from both spectroscopic techniques are presented and discussed in the following subsections.

4.2.1 UV–Vis Absorption Spectroscopy

Ultraviolet–visible (UV–Vis) absorption spectroscopy was employed to investigate the evolution of optical transitions during the structural transformation from graphite to GO, rGO, and finally rGO-QDs. The corresponding absorption spectra are shown in Figure 4.2.1.

Graphite, in its pristine form, displayed minimal absorbance in the UV–Vis region, reflecting the absence of significant π→π* transitions due to its extended sp^2 carbon domains and lack of functionalization. Upon oxidation to form GO, a prominent absorption peak emerged at approximately 230 nm, corresponding to the π→π* transition of aromatic C=C bonds in the disrupted sp^2 network. Additionally, a shoulder near 300 nm was observed, which is attributed to n→π* transitions of C=O groups introduced during oxidation [71].

After chemical reduction, the UV–Vis spectrum of rGO revealed a red shift of the main absorption peak to around 267 nm. This shift is indicative of partial restoration of the conjugated π-electron system due to the removal of oxygen-containing groups, suggesting a successful reduction of GO.

The rGO-QDs exhibited two distinct features: a dominant absorption peak at 267 nm and a weaker shoulder around 398 nm. The peak at 267 nm indicates the preserved π-conjugated system within the nanoscale domains, while the shoulder at 398 nm is associated with surface and edge states, consistent with quantum confinement effects and defect-related transitions in carbon-based quantum dots. These features confirm the formation of discrete nanostructures with localized energy states, enhancing light-matter interaction at specific energies.

The inset in Figure 4.2.1 presents visual confirmation of the optical behavior of rGO-QDs. The solution appears yellowish under ambient light but displays strong blue fluorescence when exposed to 365 nm UV light, further validating the presence of quantum-confined structures with excitation-responsive optical emission [72].

Overall, the UV–Vis absorption analysis highlights the progressive evolution of electronic structure from bulk graphite to functionalized and size-confined carbon nanomaterials. The appearance of new absorption features in rGO-QDs and the spectral red shifts serve as strong indicators of successful reduction, fragmentation, and quantum dot formation.

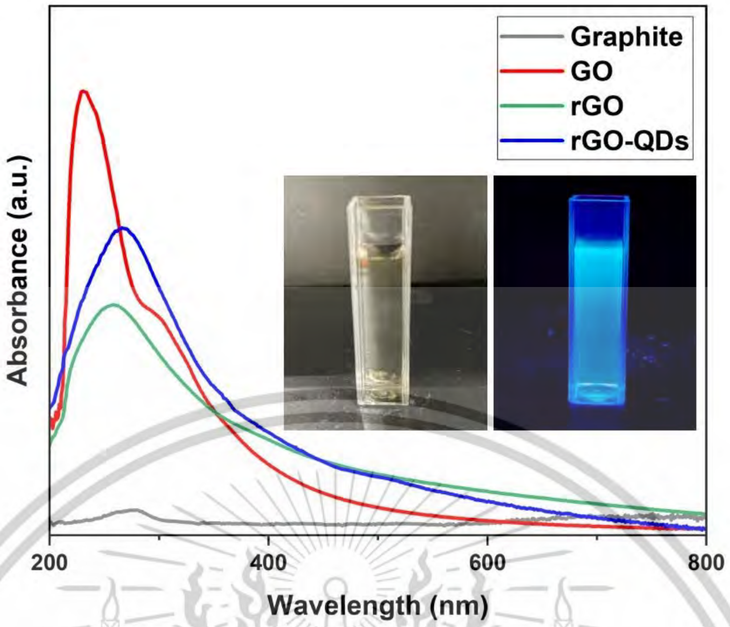

Figure 4.2.1 UV–Vis absorption spectra of graphite (grey), GO (red), rGO (green), and rGO-QDs (blue). Inset: Photographs of rGO-QDs solution under ambient light (left) and UV light at 365 nm (right), showing strong blue fluorescence under UV excitation.

4.2.2 Photoluminescence (PL) Spectroscopy

Figure 4.2.2 illustrates the normalized photoluminescence spectra of rGO-QDs under excitation wavelengths from 320 to 410 nm. As the excitation is tuned from 320 nm to 410 nm, the emission peak systematically red-shifts from about 505 nm to 553 nm, and the PL intensity varies (with a maximum at ~340 nm excitation). The relatively broad PL peak suggests a distribution of sp² domains or surface states, which is common in chemically synthesized QDs. This excitation-dependent emission indicates a broad distribution of emissive sites or dot sizes, as is commonly observed in carbon-based QDs [73]. In our samples, higher-energy excitation (shorter wavelength) preferentially excites smaller sp² clusters, yielding blue–green emission (higher photon energy), while longer-wavelength excitation accesses larger clusters that emit at lower energy (longer wavelength). This behavior where the emission maximum can be "tuned" by the excitation wavelength has been reported by Liu *et al.* (2021) and others for graphene-derived QDs [35]. This result not only confirms the size-dependent optical properties of rGO-QDs but also reflects their quantum confinement behavior, a hallmark of zero-dimensional carbon nanostructures. This emission behavior corresponds to the nanoscale size (~4.14 nm) of the rGO-QDs, which falls well within the quantum confinement regime responsible for size-dependent photoluminescence. Overall, the gradual red shift in PL with increasing excitation (and thus effective dot size) reflects the quantum confinement effect: larger QDs have narrower bandgaps and emit redder light.

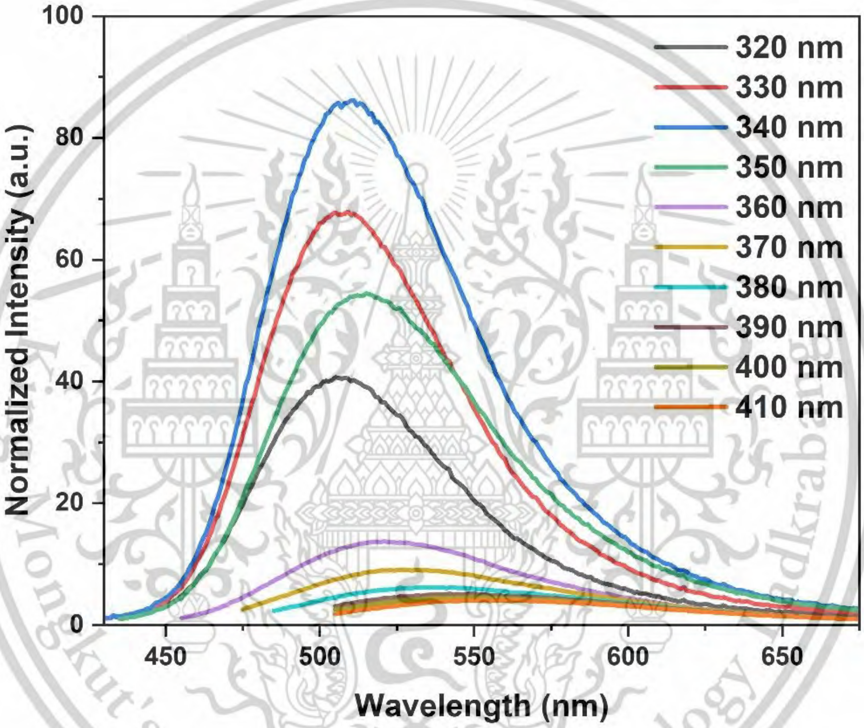

Figure 4.2.2 Normalized PL spectra of rGO-QDs excited at various wavelengths (320–410 nm).

Figure 4.2.3 presents the Tauc plot ($(\alpha h\nu)^2$ vs. photon energy) derived from UV–Vis absorption spectra, which allows estimation of the direct optical bandgap energies of the samples. The rGO-QDs exhibit a significantly widened bandgap of approximately 3.82 eV, compared to 3.42 eV for GO and 3.10 eV for rGO, as shown in Figure 4.2.3. The bandgap for graphite was found to be the lowest, at approximately 0.09 eV, indicating that the bandgap widens as the material becomes more nanoscale and quantum confined. This trend confirms that as the carbon structure transitions from bulk to nanoscale dimensions, the electronic transitions shift to higher energies, in line with established quantum mechanical models.

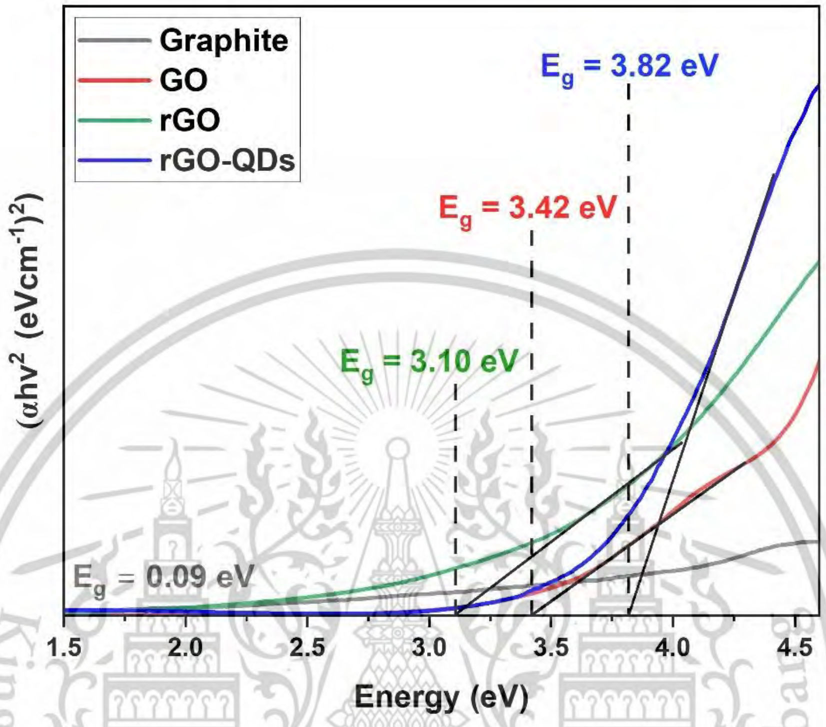

Figure 4.2.3 Tauc plot used to determine the optical bandgap of graphite, GO, rGO, and rGO-QDs.

To further quantify the confinement effect, the Brus equation was used to estimate the radius of the sp² clusters responsible for the observed photoluminescence (PL):

$$E = E_{bg} + \left[\frac{h^2}{8m_e r^2} + \frac{h^2}{8m_h r^2}\right] - \frac{1.8e^2}{4\varepsilon_0 \varepsilon r} \tag{2}$$

where:

- E is the size-dependent bandgap energy (eV),
- E_{bg} is the bandgap of bulk graphite (~0.09 eV),
- h is Planck's constant (6.626 × 10^{-34} J·s),
- r is the radius of the QD (in meters),

- m_e and m_h are the effective masses of the electron and hole, respectively. In this study, values of $m_e = m_h = 0.03m_0$, (where m_0 is the free electron mass) were assumed based on commonly accepted parameters for carbon-based nanomaterials.

By applying this model, the emission energy values observed from PL spectra were converted into corresponding quantum dot sizes. As shown in Table 4.2.1, the PL emission energies decrease from 2.46 eV (505 nm emission at 320 nm excitation) to 2.24 eV (553 nm emission at 410 nm excitation). These energy values correspond to calculated radii ranging from approximately 1.59 to 1.66 nm (i.e., diameters between 3.18 and 3.32 nm). These estimated particle sizes are in good agreement with the average size derived from TEM analysis (~4.14 nm), reinforcing the conclusion that quantum confinement governs the optical response of the rGO-QDs. This agreement across spectroscopic and microscopic data further strengthens the reliability of the optical model applied.

This quantitative correlation between particle size and optical bandgap strongly supports the existence of size-tunable quantum behavior in the synthesized rGO-QDs, a characteristic also reported in similar graphene quantum dot studies [35,74].

Table 4.2.1 Effect of excitation wavelength on PL emission and corresponding rGO-QD size estimation.

Excitation wavelength (nm)	Excitation energy (eV)	Emission wavelength (nm)	Emission energy (eV)	Radius (nm)	Diameter (nm)
320	3.88	505	2.46	1.59	3.18
330	3.76	509	2.44	1.60	3.20
340	3.65	511	2.43	1.60	3.20
350	3.54	515	2.41	1.60	3.20
360	3.45	521	2.38	1.61	3.22
370	3.35	528	2.35	1.62	3.24
380	3.26	538	2.31	1.63	3.26
390	3.18	549	2.26	1.65	3.30

400	3.10	553	2.24	1.66	3.32
410	3.03	553	2.24	1.66	3.32

Figure 4.2.4 shows the relationship between the PL bandgap energy (from Table 4.2.1) and $1/(\text{radius}^2)$. The data fall on a straight line, confirming the expected $E \propto 1/r^2$ dependence from quantum confinement. The linear fit (red line) indicates that the modest change in radius (~0.06 nm) between the samples produces the observed ~0.22 eV shift in bandgap, in agreement with effective-mass theory. In other words, the larger the dot (smaller $1/r^2$), the smaller the bandgap and the more red-shifted the emission, consistent with prior studies [35]. The extracted radii (~1.6 nm) and diameters (~3.2 nm) agree well with the TEM/HRTEM measurements of a few-nanometer QDs and are comparable to values reported for graphene/GOQDs in the literature. It should be noted, however, that emissions beyond ~500 nm may also involve surface or defect-related states, particularly in oxygen-rich carbon systems. Indeed, in our case the PL peak saturates near 553 nm (at the longest excitation), suggesting that further red emission may be partially influenced by surface-trap states, as discussed by Guo *et al.* (2017) [73]. Nonetheless, the overall trends excitation tunable emission and a clear size–energy inverse-square relationship confirm that our rGO-QDs exhibit pronounced quantum-confinement behavior.

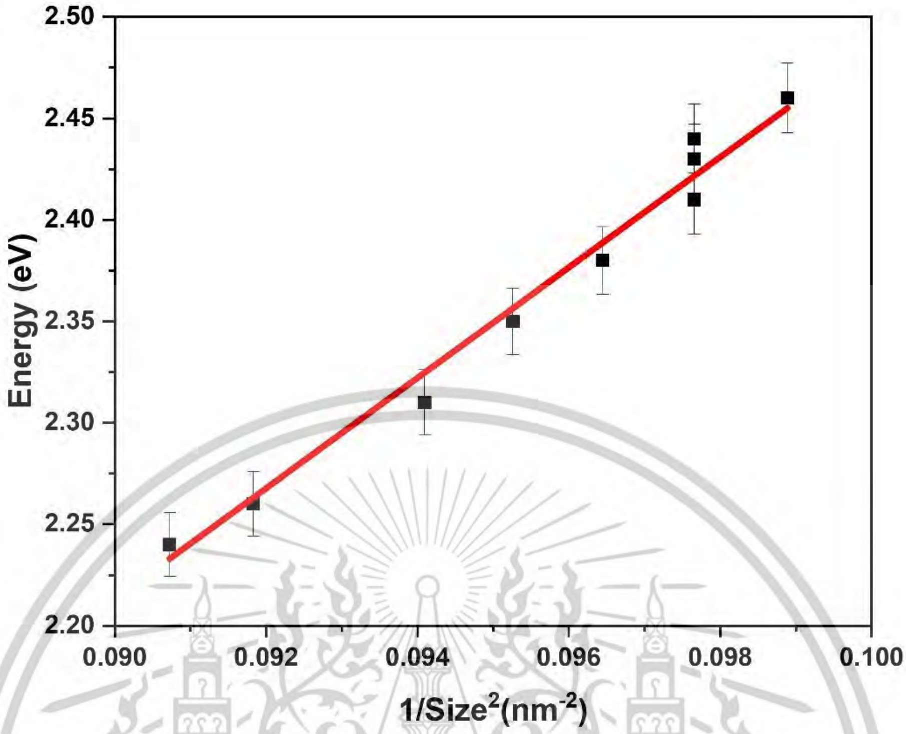

Figure 4.2.4 Linear correlation between PL emission energy and $1/r^2$ of rGO-QDs, validating the quantum confinement model.

According to the calculation results in Table 4.2.1, the sizes of rGO-QDs were estimated to be within the range of 3.18 to 3.32 nm, which aligns with the size distribution observed in Figure 2.3.1(b) and the TEM image in Figure 2.2.2(d). The emission peaks spanning 505–553 nm correspond to rGO-QD sizes between 3.18 and 3.32 nm. The strongest fluorescence emission, recorded at 511 nm upon excitation at 340 nm in Figure 2.3.1(b), was associated with an rGO-QD size of approximately 3.20 nm, which closely matches the average size determined from TEM analysis in Figure 2.3.1(b).

4.3 Electrochemical Properties of rGO-QDs

The electrochemical behavior of reduced graphene oxide quantum dots (rGO-QDs) plays a critical role in determining their performance in energy storage and electronic applications. Owing to their high surface-to-volume ratio, abundant edge sites, and restored sp^2-hybridized carbon networks, rGO-QDs exhibit unique charge transport and ionic conduction characteristics.

In this study, both electronic and ionic transport properties were systematically investigated. The ionic conductivity and Hall effect measurements provided insights into charge carrier mobility, concentration, and type, thereby revealing the fundamental electrical nature of the rGO-QDs. These intrinsic properties are essential for understanding how rGO-QDs behave under electrochemical stimuli and how efficiently they can support charge movement.

Furthermore, the electrochemical activity of rGO-QDs was evaluated via cyclic voltammetry (CV), galvanostatic charge–discharge (GCD), and electrochemical impedance spectroscopy (EIS). These techniques enabled assessment of their capacitive behavior, conductivity, and interfacial charge-transfer processes. Key parameters such as specific capacitance, charge–discharge stability, and internal resistance were derived to quantify their performance.

The detailed results and analysis of the ionic conductivity and Hall effect, followed by electrochemical testing of symmetric coin cell supercapacitors incorporating rGO-QDs, are presented in the following subsections.

4.3.1 Ionic conductivity and Hall effect

The ionic conductivity of rGO-QDs in aqueous form was evaluated using electrochemical impedance spectroscopy (EIS). The measurements were conducted over a frequency range of 100 kHz to 0.01 Hz, with temperature variations controlled from room temperature to 80°C. To analyze the impedance data, an equivalent circuit model was employed, incorporating Rs (solution resistance), Ret (charge transfer resistance), CPE (constant phase element), and Warburg elements, allowing for a comprehensive assessment of ionic transport mechanisms. This model highlights the influence of both bulk and interfacial effects on the overall ionic conductivity of the material [75,76]. Figure 4.3.1 presents the EIS results of rGO-QDs, including Nyquist plots and Arrhenius-type plots, which illustrate the temperature dependence of ionic conductivity.

Figure 4.3.1(a) presents the Nyquist plot analysis of rGO-QDs measured at various temperatures (25, 30, 40, 50, 60, 70, and 80°C) over a frequency range of 100 kHz to 0.01 Hz, providing valuable insights into their electrochemical behavior. The inset in Figure 4.3.1(a) depicts the EIS measurement setup for evaluating the ionic conductivity of rGO-QDs. The system employed a frequency range of 100 kHz to 0.01 Hz and consisted of a Pt sheet working electrode, a reference electrode, a Pt sheet counter electrode, and a temperature probe immersed in the rGO-QDs solution. The intercept on the real impedance axis in the Nyquist plot represents the solution resistance (Rs), indicating the internal resistance of the rGO-QDs aqueous system.

The Nyquist plot exhibited semicircular arcs, representing both bulk and charge transfer resistances, which are essential for understanding the ionic transport mechanisms within rGO-QDs [77]. As the temperature increased, the semicircles became smaller, indicating a decrease in resistance. This reduction corresponds to enhanced ion mobility, driven by the greater thermal energy available at higher temperatures, which facilitates the movement of ions and charge carriers within the rGO-QDs [78]. The inverse relationship between resistance and temperature aligns with fundamental electrochemical properties, as higher temperatures promote increased ionic diffusion, leading to improved ionic conductivity [79].

The equivalent circuit model used to analyze the impedance data incorporates key components such as series resistance (Rs), charge transfer resistance (Rct), a constant phase element (CPE), and Warburg elements (W, Ws) to account for ion resistance, capacitance, and diffusion effects. This model effectively captures the complex electrochemical interactions occurring within rGO-QDs at varying temperatures [80]. These findings have significant implications for the application of rGO-QDs in electronic and optoelectronic devices. The observed increase in ion mobility at higher temperatures suggests that rGO-QDs are well-suited for applications requiring efficient charge transport, such as supercapacitors and batteries [81]. The ability to model impedance behavior using an equivalent circuit provides a structured approach for optimizing the electrochemical performance of rGO-QDs in various applications [82]. The ionic conductivity ($\boldsymbol{\sigma}$) of rGO-QDs in aqueous form was calculated using the equation:

$$\boldsymbol{\sigma} = \frac{L}{R_S A} \tag{3}$$

Where L is the distance between electrodes (cm), R_S is the intercept value on the real impedance axis from EIS spectra (Ω), and A represents the electrode area (cm²). The

R_s values were derived from the Nyquist plot intercept on the real impedance axis, indicating the internal resistance of the system. Figure 4.3.1(b) provides a magnified view of the Nyquist plot at higher frequencies, illustrating the variation of R_s values with temperature. The R_s values of rGO-QDs aqueous solution were 622.4, 368.2, 336.5, 250.8, 169.6, 114.9, and 60.2 Ω at 25, 30, 40, 50, 60, 70, and 80°C, respectively. The observed decrease in R_s with increasing temperature aligns with the principle that higher thermal energy enhances ionic conductivity by facilitating charge carrier movement [80,83].

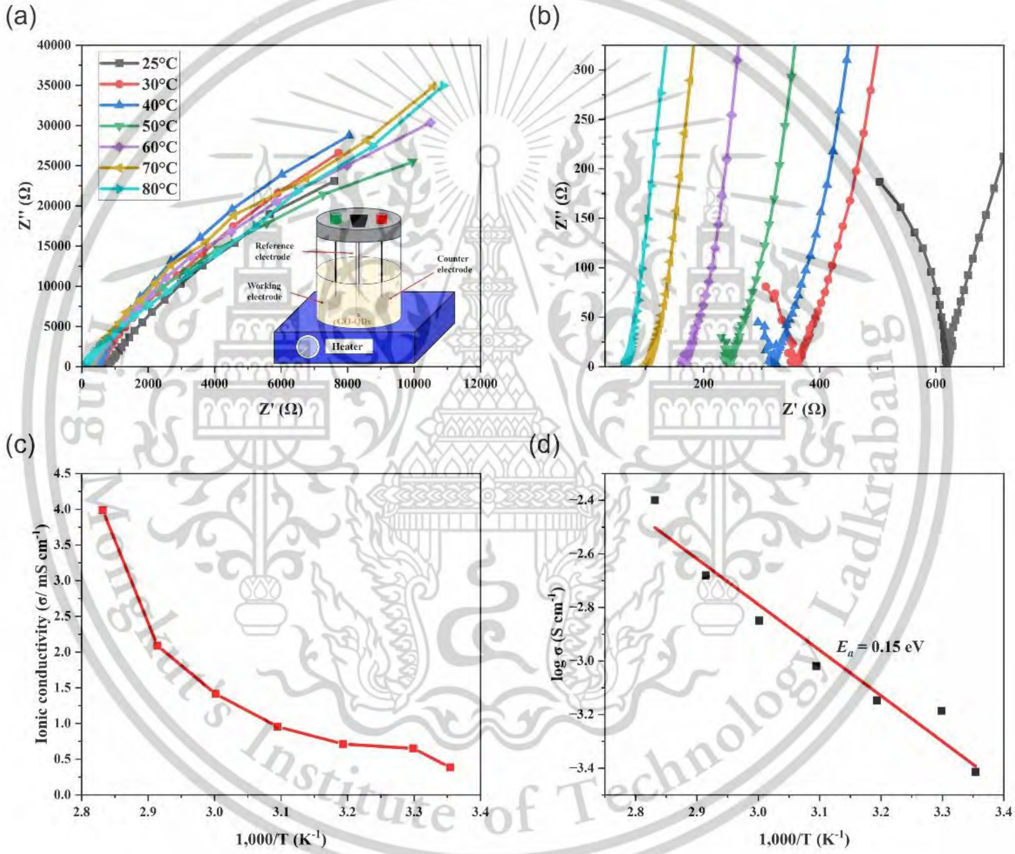

Figure 4.3.1 Ionic conductivity analysis of rGO-QDs. The inset in (a) shows the measurement setup for ionic conductivity. (a) Nyquist plot depicting impedance behavior at different temperatures, (b) magnified Nyquist plot at higher frequencies, (c) Arrhenius plot of ionic conductivity versus inverse temperature (1,000/T), and (d) logarithmic Arrhenius plot with activation energy (E_a = 0.15 eV).

Based on the Nyquist plot analysis, the decrease in charge transfer resistance with increasing temperature indicates that higher temperatures enhance ionic transport within rGO-QDs. This temperature-dependent behavior is critical for maintaining or improving electrical conductivity in electronic applications such as supercapacitors and batteries [77,84]. Figure 4.3.1(c) illustrates the Arrhenius plot, which depicts the temperature dependence of ionic conductivity in rGO-QDs. The calculated ionic conductivity (**σ**) values were 0.39, 0.65, 0.71, 0.96, 1.41, 2.09, and 3.99 mS/cm at 25, 30, 40, 50, 60, 70, and 80°C, respectively. As the inverse temperature (1000/T) increases, the ionic conductivity follows an Arrhenius-type behavior, similar to other ionic materials, indicating that ionic transport in rGO-QDs is thermally activated [85]. The temperature dependence of ionic conductivity in rGO-QDs can be described by the Arrhenius equation:

$$\sigma = \sigma_0 e^{-\frac{E_a}{kT}} \tag{4}$$

where:

- σ is a pre-exponential factor,
- σ_0 is the activation energy,
- k is the Boltzmann constant,
- T is the absolute temperature.

At higher temperatures, the increased thermal energy enhances ion mobility, leading to improved ionic conductivity [86]. Conversely, at lower temperatures, the reduction in thermal energy restricts ion hopping, limiting ionic transport within rGO-QDs [85]. Additionally, the amorphous phase present in rGO-QDs contributes to the increase in ionic conductivity, as it provides greater free volume for ion migration, further reinforcing the Arrhenius-type behavior [87]. The Arrhenius plot confirms that the ionic conductivity of rGO-QDs is thermally activated, emphasizing their potential for applications that require stable and efficient ionic transport across different temperatures, such as in batteries and supercapacitors, where maintaining conductivity is essential for optimal device performance [88].

Figure 4.3.1(d) presents the logarithmic Arrhenius plot, demonstrating a linear relationship between log σ and 1000/T. The calculated activation energy (E_a) of 0.15 eV confirms that the ionic conductivity of rGO-QDs is thermally activated, with higher temperatures facilitating greater ion mobility [83,89]. The strong correlation coefficient ($R^2 = 0.95$) further validates the consistency and reliability of the data. These findings confirm that rGO-QDs enhance electrical conductivity at elevated temperatures, improving ionic transport efficiency, which is essential for supercapacitor applications [75,90]. The results are consistent with previous studies that have reported similar thermally activated ionic conduction mechanisms in polymer electrolytes and nanocomposites [76,91]. The observed increase in ionic conductivity at higher temperatures is attributed to enhanced ion mobility, which is crucial for electrochemical devices such as batteries and supercapacitors, where efficient ionic transport plays a key role in charge and discharge cycles [77,92].

Figure 4.3.2(a) presents the sheet resistance analysis of GO and rGO-QDs over the temperature range of 310 K to 400 K. For GO, the sheet resistance shows a sharp decline between 310 K and approximately 350 K, followed by a plateau, indicating a thermally activated conduction mechanism in which increasing temperature enhances carrier mobility, thereby reducing resistance [93,94]. The initially high sheet resistance of GO at lower temperatures is likely due to the presence of oxygen-containing functional groups, which impede charge transport by introducing defects and disrupting the π-conjugation network within the GO structure, thus limiting its conductivity [95]. As the temperature increases, the thermal energy facilitates charge carrier movement, leading to a significant improvement in electrical conductivity. This trend aligns with previous studies that have reported similar thermally activated behavior in GO and rGO based materials [7,96]. Beyond 350 K, the plateau in sheet resistance suggests that the material has reached a saturation point in carrier mobility, meaning further increases in temperature do not significantly enhance conductivity. This behavior is commonly observed in conductive materials, where factors such as defect density and electronic structure impose intrinsic limitations on conductivity improvements at higher temperatures [19,24].

For rGO-QDs, the observed extremely low sheet resistance despite the presence of a wide bandgap of 3.82 eV (as seen in Figure 4.2.3) can be attributed to the dominance of hopping conduction mechanisms. The reduction process effectively restored the π-conjugation network and removed oxygen-containing functional groups, thereby creating conductive pathways that enable efficient charge transport [97]. Unlike conventional semiconductors, where a wide bandgap typically correlates with high resistance, defect-mediated hopping conduction in rGO-QDs facilitates enhanced electrical conductivity. This behavior is consistent with previous findings [98], which reported a significant improvement in conductivity following the removal of oxygen functional groups in rGO materials. Furthermore, the ability to tune the bandgap of rGO by modifying functional group content highlights the interplay between the quantum confinement effect and restored conductivity in rGO-QDs [11].

The Hall effect was analyzed using the relationship described by Equation (5):

$$R_H(t) = \pm\frac{1}{e}\frac{p\mu_p{}^2 - n\mu_n{}^2}{\left(p\mu_p + n\mu_n\right)^2} \tag{5}$$

where e is the elementary charge, μ_n and μ_p are the mobilities of negative and positive charge carriers, respectively, and n and p represent the concentrations of negative and positive charge carriers, respectively. The sign of the Hall coefficient (R_H) is used to determine the majority charge carrier type in the material: a positive R_H ($R_H > 0$) indicates p-type carriers (holes as the dominant charge carriers), while a negative R_H ($R_H < 0$) signifies n-type carriers (electrons as the dominant charge carriers). Figure 4.3.2(b) presents the Hall coefficient (R_H) variation for GO and rGO-QDs as a function of temperature. The results for GO showed n-type conductivity at room temperature, a transition to p-type conductivity in the range of 320 K to 350 K, and a reversion to n-type behavior from 360 K to 400 K. The fluctuations between positive and negative values indicate that both electrons and holes contribute to conduction, resulting in mixed-type behavior, which underscores the unstable electronic properties of GO. In contrast, rGO-QDs exhibited a stable p-type conductivity across all measured temperatures, with positive R_H values persisting up to 400 K, indicating that holes remain the dominant charge carriers. This consistent p-type behavior suggests that rGO-QDs offer stable charge transport characteristics, which is essential for ionic conduction applications where predictable and reliable charge carrier behavior is crucial for device performance and efficiency.

Figure 4.3.2(c) illustrates the temperature-dependent charge carrier concentration (CCC) for GO and rGO-QDs. The carrier concentration in GO varied from 6.51×10^{13} to 1.47×10^{15} /m² over the temperature range of 310 K to 400 K. However, significant fluctuations were observed, including notable dips and even negative values around 350 K, indicating unstable carrier dynamics. This instability is likely due to carrier recombination and transitions between electron and hole conduction mechanisms [99,100]. The variation in carrier concentration suggests that charge transport in GO is inconsistent across different temperatures, posing challenges for its use in electronic applications. The presence of oxygen-containing functional groups in GO contributes to complex interactions that negatively impact carrier mobility and stability, leading to the observed fluctuations [92,101]. Such instability is a critical drawback for applications that require stable and predictable charge transport, as performance variability can significantly affect the reliability of electronic devices [89,101].

Additionally, the charge carrier concentration (CCC) of rGO-QDs ranged from 1.87×10^{15} to 5.96×10^{15} /m² over the temperature range of 310 K to 400 K. Unlike GO, rGO-QDs exhibited improved stability in carrier concentration, which can be attributed to the reduction process that removes oxygen functional groups, thereby restoring a more stable electronic structure [7,82]. This enhanced structural stability results in better conductivity and more consistent charge transport performance, making rGO-QDs highly suitable for ionic conduction applications that require stable behavior across varying thermal conditions [3,8,73,102–104].

Figure 4.3.2(d) presents the temperature-dependent charge carrier mobility for GO and rGO-QDs. In GO, the carrier mobility ranged from −227.29 cm²/V·s to 33.40 cm²/V·s over the temperature range of 310 K to 400 K. As the temperature increased, the mobility decreased, which is a typical behavior observed in semiconductors, where phonon scattering at higher temperatures disrupts charge transport, thereby reducing carrier mobility. This decline in mobility further limits GO's performance in high-temperature applications. In contrast, the carrier mobility of rGO-QDs ranged from 82.42 cm²/V·s to 308.58 cm²/V·s over the same temperature range. Unlike GO, rGO-QDs exhibited significantly higher and more stable mobility, which can be attributed to their more stable carrier concentration and restored π-conjugation network after the reduction process. This enhancement in mobility demonstrates the superior charge transport properties of rGO-QDs, even at elevated temperatures. The ability of rGO-QDs to maintain high and stable mobility across a broad temperature range makes them particularly suitable for high-performance ionic conduction devices, where efficient and consistent charge transport is essential for reliable operation under varying thermal conditions.

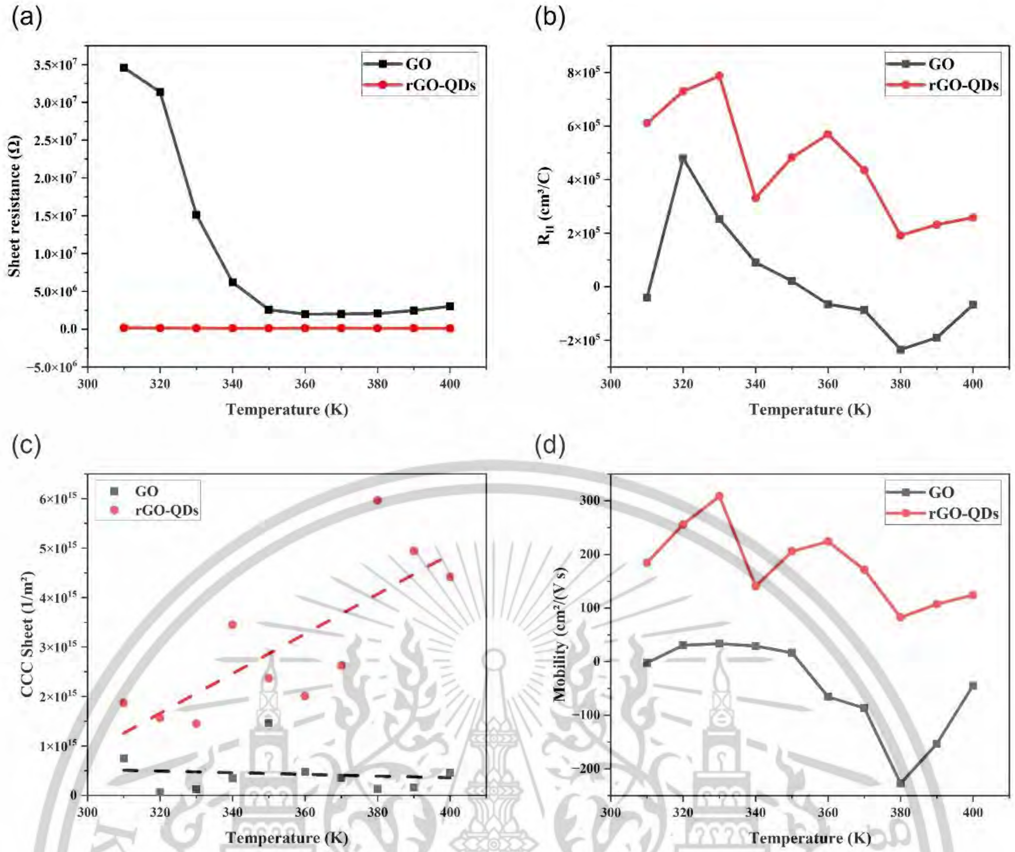

Figure 4.3.2 Temperature dependence of (a) sheet resistance, (b) Hall coefficient (RH), (c) charge carrier concentration (CCC), and (d) mobility for GO and rGO-QDs.

4.3.2 Electrochemical Properties

Figure 4.3.3 presents the electrochemical properties of the supercapacitor device, comparing the performance of a KOH-based electrolyte with that of a KOH/rGO-QDs electrolyte. The supercapacitor device was fabricated in a CR2032 coin-cell configuration, assembled symmetrically using electrodes composed of acetylene black, activated carbon, rGO, and PVDF in NMP at a weight ratio of 5:80:5:10.

Figure 4.3.3(a) and (b) illustrate the Nyquist plots, showing the impedance behavior of the supercapacitor device with KOH electrolyte and KOH/rGO-QDs electrolyte, respectively. The internal resistance (R_S) of the supercapacitor with KOH electrolyte was measured at 1.23 Ω, whereas the device using KOH/rGO-QDs electrolyte exhibited a significantly lower R_S of 0.38 Ω. This 3.2-fold reduction in R_S indicates that the enhanced ionic conductivity of rGO-QDs contributes to reduced internal resistance. The high surface area of rGO-QDs increases the number of active ion-transport sites, and their restored π-conjugated carbon network facilitates rapid ion diffusion and charge transfer. These properties collectively enhance specific capacitance and ion mobility.

From the Nyquist data, the double-layer capacitance (C_{dl}) was determined using the equation:

$$C_{dl} = \frac{1}{(R_{ct})(2\pi f)} \tag{6}$$

where f is the relaxation frequency and R_s is the charge transfer resistance. The R_{ct} values were 80.3 Ω for the KOH device and 0.57 Ω for the KOH/rGO-QDs device. The relaxation frequency increased significantly from 56.70 Hz (KOH) to 5,510 Hz (KOH/rGO-QDs), suggesting much faster charge transfer kinetics. As a result, the C_{dl} of the KOH/rGO-QDs device was 50.5 μF, which is 1.44 times greater than that of the KOH device (35.1 μF), confirming improved capacitive behavior.

Figure 4.3.3(c) and (d) illustrate the Warburg impedance behavior, which appears as a linear tail in the low-frequency region of the Nyquist plot. The Warburg impedance (Z_W) is described by the equation:

$$Z_W = (1 - j)\sigma_W \omega^{-1/2} \tag{7}$$

Where Z_W represents the Warburg impedance, σ_W is the Warburg coefficient, and ω is the angular frequency, given by $\omega = 2\pi f$. The slope (σ_W) obtained from the plot of $\omega^{-1/2}$ versus Z_W was 0.58 $\Omega s^{1/2}$ for the KOH/rGO-QDs device, whereas the KOH-based device exhibited a much higher σ_W value of 55.51 $\Omega s^{1/2}$. The significantly lower σ_W for the KOH/rGO-QDs device indicates faster ion diffusion and enhanced ionic conductivity, highlighting the beneficial role of rGO-QDs in facilitating efficient charge transport within the electrolyte.

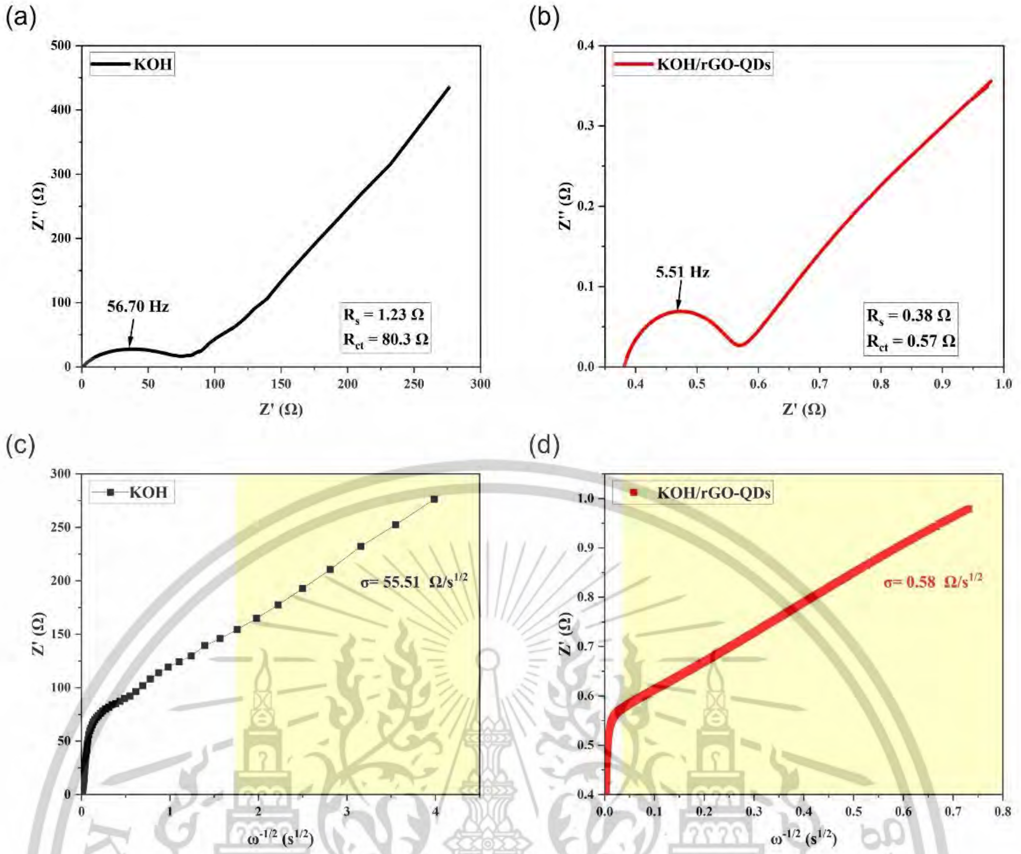

Figure 4.3.3 EIS analysis of KOH and KOH/rGO-QDs electrolytes: (a) Nyquist plot of KOH electrolyte device, (b) Nyquist plot of KOH/rGO-QDs device, (c) Warburg impedance plot of KOH electrolyte, and (d) Warburg impedance plot of KOH/rGO-QDs.

Figure 4.3.4(a) and (b) present the cyclic voltammetry (CV) plots for supercapacitor devices utilizing KOH electrolyte and KOH/rGO-QDs electrolyte, respectively. The CV curves were recorded by sweeping the potential window from 0 V to 0.1 V, while varying the applied electric voltage at scan rates of 5, 10, 20, and 30 mV/s. The KOH device showed a narrow potential window of about −1.25 mV to 2.0 mV, while the rGO-QDs device expanded this window to −50 mV to 40 mV. The broader CV area observed for the rGO-QDs system indicates greater capacitive charge storage, attributed to faster ion transfer and higher accessible surface area.

Figure 4.3.4(c) and (d) show the galvanostatic charge-discharge (GCD) curves at current densities from 0.5 to 5 A/g. Both devices exhibited symmetric triangular shapes, indicating good capacitive reversibility. At a current density of 5 A/g, the discharge time for the KOH/rGO-QDs device (100 s) exceeded that of the KOH-only device (80 s), confirming higher energy storage capacity.

Specific capacitance (C_{sp}) (F/g) was calculated using:

$$C_{sp} = \frac{I \times \Delta t}{m \times \Delta V} \tag{8}$$

where:

- I is the constant discharge current (A),
- Δt is the discharge time (s),
- ΔV is the voltage change during discharge (V),
- m represents the mass of the active material (g).

Figure 4.3.4(e) presents the specific capacitance (C_{sp}) vs. current density for both systems. The KOH/rGO-QDs device exhibited specific capacitances of 25 to 55 F/g, while the KOH-only device yielded 5 to 48 F/g. The highest value (55.0 F/g at 0.5 A/g) for the rGO-QDs device demonstrates their superior electrochemical performance. Figure 4.3.4(f) displays a practical demonstration: two coin cell supercapacitors with KOH/rGO-QDs electrolyte connected in series successfully powered two red LEDs. This confirms the practical viability of rGO-QDs-enhanced electrolytes for low-power energy storage applications.

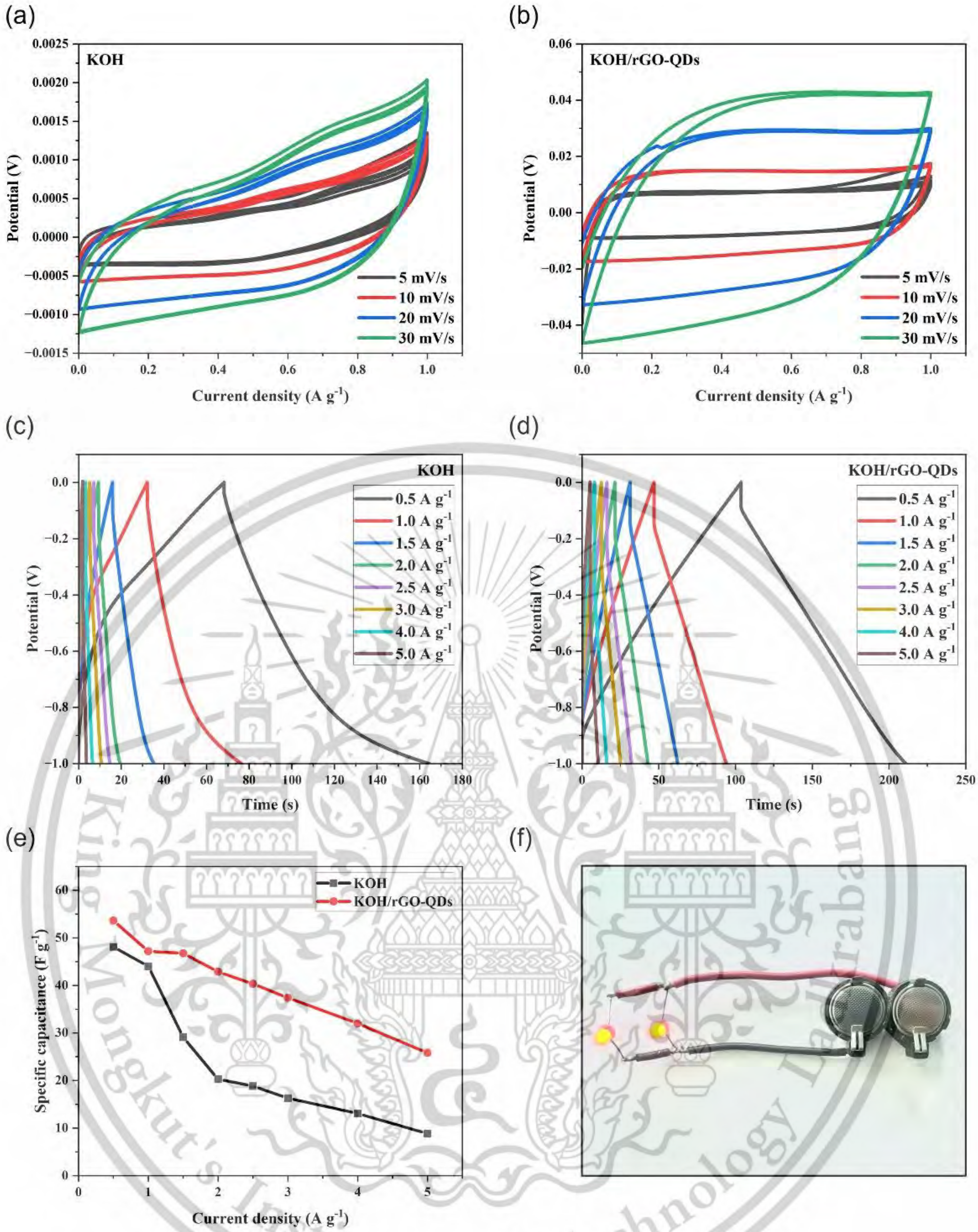

Figure 4.3.4 Electrochemical performance of KOH and KOH/rGO-QDs supercapacitors: cyclic voltammetry (a, b), discharge-charge curves (c, d), specific capacitance vs. current density (e), and (f) LED demonstration powered by two coin-cell supercapacitors in series.

Chapter 5

Conclusions

This research initially set out to enhance the thermoelectric performance of bismuth telluride (Bi_2Te_3) through the incorporation of reduced graphene oxide quantum dots (rGO-QDs) as a nanoscale composite additive. The core motivation was to address the intrinsic limitations of Bi_2Te_3 such as its relatively high thermal conductivity by introducing rGO-QDs, which exhibit unique electronic and thermal transport behavior derived from quantum confinement and high surface activity. It was anticipated that rGO-QDs would reduce the thermal conductivity of the composite while maintaining or enhancing electrical conductivity, leading to an improved thermoelectric figure of merit (ZT).

However, during the experimental phase, several key challenges were encountered. These included significant difficulties in compacting and sintering Bi_2Te_3 into high-quality pellets suitable for thermoelectric measurement, as well as limited access to specialized equipment required for accurately measuring Seebeck coefficient, electrical conductivity, and thermal conductivity under controlled conditions. These technical and logistical obstacles ultimately rendered the continuation of the thermoelectric focus unfeasible within the available research environment.

Rather than abandoning the study, the direction was revised to concentrate on the fundamental material of interest rGO-QDs while exploring a new application domain that shares similar material requirements: electrochemical energy storage. In particular, the study focused on investigating rGO-QDs as additives in supercapacitor electrolyte systems. This transition allowed the research to retain its scientific relevance and rigor, while contributing new knowledge to a related but distinct field.

The synthesis of rGO-QDs was carried out via a hydrothermal process, with systematic optimization of parameters such as pH, ultrasonication time, and purification methods. The final optimized synthesis yielded rGO-QDs with an average size of approximately 3-4 nm, strong blue fluorescence under UV illumination, and structural features indicative of restored π-conjugation. Characterization using UV-Vis spectroscopy, photoluminescence (PL), Raman spectroscopy, X-ray diffraction (XRD), transmission electron microscopy (TEM) and and energy-dispersive X-ray spectroscopy (EDX) confirmed the successful formation of well-dispersed, graphitic carbon-based quantum dots exhibiting quantum confinement effects. In addition to their optical and structural features, the electrochemical properties of the synthesized rGO-QDs were explored by incorporating them into a 3 M potassium hydroxide (KOH) solution to form a hybrid electrolyte for symmetric coin-cell supercapacitors. Electrochemical impedance spectroscopy (EIS) revealed that the presence of rGO-QDs significantly increased the ionic conductivity of the electrolyte and reduced the internal resistance of the system. These enhancements are attributed to the improved ion transport pathways enabled by the nanodots' high surface area, edge-active sites, and surface functional groups, which facilitate both electrostatic and pseudocapacitive interactions.

Performance tests of the assembled supercapacitors including cyclic voltammetry, galvanostatic charge–discharge (GCD), and capacitance retention demonstrated that the rGO-QD-enhanced electrolyte achieved a specific capacitance of up to 55 F/g, which is markedly higher than that of the pure KOH system. Furthermore, the device showed improved charge–discharge characteristics, lower equivalent series resistance (ESR), and greater stability over repeated cycles. These results not only validate the electrochemical compatibility of rGO-QDs but also illustrate their multifunctionality as both optical and ionic conductors in energy storage applications.

In summary, although the original thermoelectric enhancement of Bi_2Te_3 composites could not be achieved due to technical limitations, this study successfully refocused on the core innovation rGO-QDs and demonstrated their potential as high-performance materials for electrochemical energy storage. The research contributes valuable insights into the synthesis, structure–property relationships, and functional applications of carbon-based quantum dots. It also underscores the importance of adaptability in research, showing how scientific value can still be derived even when the initial experimental path proves impractical.

Looking forward, the results from this study lay a strong foundation for future work on multifunctional nanomaterials. Further exploration may include developing hybrid systems that combine rGO-QDs with conductive polymers or metal oxides, scaling the synthesis process for industrial applications, and integrating these nanomaterials into full-device systems such as flexible energy storage units or hybrid optoelectronic–electrochemical devices. The insights gained from this research thus represent not only a successful pivot in experimental focus but also a meaningful contribution to the advancement of sustainable and scalable nanomaterials for energy conversion and storage.

References

1. J. Zhu, D. Yang, Z. Yin, Q. Yan, and H. Zhang, "Graphene and Graphene-Based Materials for Energy Storage Applications," Small **10**, 3480–3498 (2014).
2. F. Liu, T. Tang, Q. Feng, M. Li, Y. Liu, N. Tang, W. Zhong, and Y. Du, "Tuning photoluminescence of reduced graphene oxide quantum dots from blue to purple," J. Appl. Phys. **115**, 164307 (2014).
3. D. Lee, J. Seo, X. Zhu, J. Lee, H.-J. Shin, J. M. Cole, T. Shin, J. Lee, H. Lee, and H. Su, "Quantum confinement-induced tunable exciton states in graphene oxide," Sci. Rep. **3**, 2250 (2013).
4. S. Li, T. Fan, X. Liu, F. Liu, H. Meng, Y. Liu, and F. Pan, "Graphene Quantum Dots Embedded in Bi_2Te_3 Nanosheets To Enhance Thermoelectric Performance," ACS Appl. Mater. Interfaces **9**, 3677–3685 (2017).
5. K. Ahmad, C. Wan, M. A. Al-Eshaikh, and A. N. Kadachi, "Enhanced thermoelectric performance of Bi2Te3 based graphene nanocomposites," Appl. Surf. Sci. **474**, 2–8 (2019).
6. T. Seesan, C. Sriwong, and C. Ruttanapun, "Fabrication, optical and ion conduction properties of reduced graphene oxide quantum dots and application in electrolyte supercapacitor devices," Mater. Sci. Eng. B **315**, 118099 (2025).
7. M. Hasani and M. Montazer, "Cationization of cellulose/polyamide on UV protection, bio-activity, and electro-conductivity of graphene oxide-treated fabric," J. Appl. Polym. Sci. **134**, 45493 (2017).
8. S. Zhang, Y. Li, H. Song, X. Chen, J. Zhou, S. Hong, and M. Huang, "Graphene quantum dots as the electrolyte for solid state supercapacitors," Sci. Rep. **6**, 19292 (2016).
9. M. Pumera, A. Ambrosi, A. Bonanni, E. L. K. Chng, and H. L. Poh, "Graphene for electrochemical sensing and biosensing," TrAC Trends Anal. Chem. **29**, 954–965 (2010).
10. H. Hu, H. Quan, B. Zhong, Z. Li, Y. Huang, X. Wang, M. Zhang, and D. Chen, "A Reduced Graphene Oxide Quantum Dot-Based Adsorbent for Efficiently Binding with Organic Pollutants," ACS Appl. Nano Mater. **1**, 6502–6513 (2018).

11. Y. Jin, Y. Zheng, S. G. Podkolzin, and W. Lee, "Band gap of reduced graphene oxide tuned by controlling functional groups," J. Mater. Chem. C **8**, 4885–4894 (2020).
12. R. Al-Gaashani, A. Najjar, Y. Zakaria, S. Mansour, and M. A. Atieh, "XPS and structural studies of high quality graphene oxide and reduced graphene oxide prepared by different chemical oxidation methods," Ceram. Int. **45**, 14439–14448 (2019).
13. Y. Yang, H. Shen, J. Yang, X. Ren, K. Gao, and Z. Wang, "Enhanced Conductivity and Flexibility in Reduced Graphene Oxide Paper by Combined Chemical-Thermal Reduction," J. Electron. Mater. **50**, 6991–6999 (2021).
14. N. Buatong, C. Ruttanapun, and C. Sriwong, "Synthesis of reduced graphene oxide quantum dots from graphene oxide via hydrothermal process and theirs structural, luminescence and magnetic properties," J. Taiwan Inst. Chem. Eng. **142**, 104667 (2023).
15. N. O. Weiss, H. Zhou, L. Liao, Y. Liu, S. Jiang, Y. Huang, and X. Duan, "Graphene: An Emerging Electronic Material," Adv. Mater. **24**, 5782–5825 (2012).
16. U. Chasanah, W. Trisunaryanti, Triyono, H. S. Oktaviano, I. Santoso, and D. A. Fatmawati, "Study of green reductant effects of highly reduced graphene oxide production and their characteristics," Commun. Sci. Technol. **7**, 103–111 (2022).
17. J. Shen, Y. Zhu, X. Yang, and C. Li, "Graphene quantum dots: emergent nanolights for bioimaging, sensors, catalysis and photovoltaic devices," Chem. Commun. **48**, 3686–3699 (2012).
18. N. Mahmoudi, F. Ostadhossein, and A. Simchi, "Physicochemical and antibacterial properties of chitosan-polyvinylpyrrolidone films containing self-organized graphene oxide nanolayers," J. Appl. Polym. Sci. **133**, (2015).
19. J. Zhou, Y. Yan, Y. Zhang, Y. Zhang, D. Zhang, H. Lin, Y. Chen, B. Zhao, and J. Xiong, "Amino-terminated hyperbranched polymer functionalized graphene oxide with in situ trapped silver nanoparticles for high-performance antibacterial nonwoven fabric," J. Appl. Polym. Sci. **140**, e53466 (2023).
20. P. Gozali Balkanloo, K. Mohammad Sharifi, and A. Poursattar Marjani, "Graphene quantum dots: synthesis, characterization, and application in wastewater treatment: a review," Mater. Adv. **4**, 4272–4293 (2023).
21. C. Zhao, X. Song, Y. Liu, Y. Fu, L. Ye, N. Wang, F. Wang, L. Li, M. Mohammadniaei, M. Zhang, Q. Zhang, and J. Liu, "Synthesis of graphene quantum dots and their applications in drug delivery," J. Nanobiotechnology **18**, 142 (2020).

22. K. Maneesai, K. Silakaew, S. Khammahong, C. Phrompet, C. Sriwong, C. Thanachayanont, and C. Ruttanapun, "Temperature-dependent electrical transport, Hall effect, and Seebeck properties of bulk chemically reduced graphene oxide with bipolar charge carrier materials," AIP Adv. **13**, 035333 (2023).

23. S. Chung, R. A. Revia, and M. Zhang, "Graphene Quantum Dots and Their Applications in Bioimaging, Biosensing, and Therapy," Adv. Mater. **33**, 1904362 (2021).

24. M. Santiago-Calvo, V. Blasco, C. Ruiz, R. París, F. Villafañe, and M. Á. Rodríguez-Pérez, "Improvement of thermal and mechanical properties by control of formulations in rigid polyurethane foams from polyols functionalized with graphene oxide," J. Appl. Polym. Sci. **136**, 47474 (2019).

25. T. Chiba, H. Yabuki, and M. Takashiri, "High thermoelectric performance of flexible nanocomposite films based on Bi2Te3 nanoplates and carbon nanotubes selected using ultracentrifugation," Sci. Rep. **13**, 3010 (2023).

26. F. Usmani, "Development of tin selenide and bismuth telluride based graphene composites for thermoelectric applications," (2020).

27. F. Usmani, "Development of tin selenide and bismuth telluride based graphene composites for thermoelectric applications," (2020).

28. M. Zhao, D. Kim, V. L. Nguyen, J. Jiang, L. Sun, Y. H. Lee, and H. Yang, "Coherent Thermoelectric Power from Graphene Quantum Dots," Nano Lett. **19**, 61–68 (2019).

29. S. Li, T. Fan, X. Liu, F. Liu, H. Meng, Y. Liu, and F. Pan, "Graphene Quantum Dots Embedded in Bi2Te3 Nanosheets To Enhance Thermoelectric Performance," ACS Appl. Mater. Interfaces **9**, 3677–3685 (2017).

30. S. Zhang, L. Sui, H. Dong, W. He, L. Dong, and L. Yu, "High-Performance Supercapacitor of Graphene Quantum Dots with Uniform Sizes," ACS Appl. Mater. Interfaces **10**, 12983–12991 (2018).

31. X. Shi, Z.-Z. Yin, J. Xu, S. Li, C. Wang, B. Wang, Y. Qin, and Y. Kong, "Preparation, characterization and the supercapacitive behaviors of electrochemically reduced graphene quantum dots/polypyrrole hybrids," Electrochimica Acta **385**, 138435 (2021).

32. W. Hu, K. He, S. Wu, T. Chen, X. Yu, Y. Liang, M. Zheng, Y. Xiao, H. Dong, Y. Liu, and H. Hu, "Ordered sandwich silicon quantum dot/Fe3O4/reduced graphene oxide

architectures for high-performance lithium-ion batteries," J. Alloys Compd. **943**, 168947 (2023).

33. N. I. M. Fauzi, Y. W. Fen, F. B. K. Eddin, and W. M. E. M. M. Daniyal, "Structural and Optical Properties of Graphene Quantum Dots–Polyvinyl Alcohol Composite Thin Film and Its Potential in Plasmonic Sensing of Carbaryl," Nanomaterials **12**, 4105 (2022).
34. A. I. Ekimov and A. A. Onushchenko, "Quantum Size Effect in Three-Dimensional Microscopic Semiconductor Crystals," JETP Lett. **118**, S15–S17 (2023).
35. Z. Liu, F. Li, Y. Luo, M. Li, G. Hu, X. Pu, T. Tang, J. Wen, X. Li, and W. Li, "Size Effect of Graphene Quantum Dots on Photoluminescence," Molecules **26**, 3922 (2021).
36. L. Najafi, B. Taheri, B. Martín-García, S. Bellani, D. D. Girolamo, A. Agresti, R. Oropesa-Nuñez, S. Pescetelli, L. Vesce, E. Calabrò, M. Prato, A. E. D. R. Castillo, A. D. Carlo, and F. Bonaccorso, "MoS_2 Quantum Dot/Graphene Hybrids for Advanced Interface Engineering of a $CH_3NH_3PbI_3$ Perovskite Solar Cell with an Efficiency of over 20%," ACS Nano **12**, (2018).
37. S. Bellani, L. Najafi, B. Martín-García, A. Ansaldo, A. E. D. R. Castillo, M. Prato, I. Moreels, and F. Bonaccorso, "Graphene-Based Hole-Selective Layers for High-Efficiency, Solution-Processed, Large-Area, Flexible, Hydrogen-Evolving Organic Photocathodes," J. Phys. Chem. C **121**, (2017).
38. A. Reheman, Y. Tursun, D. Talifu, H. Maimaiti, K. Kadeer, and A. Abulizi, "Facile One-Step Sonochemical Synthesis and Photocatalytic Properties of Graphene/Ag3PO4 Quantum Dots Composites," Nanoscale Res. Lett. **13**, (2018).
39. N. H. Kwon, J. M. Lee, T.-H. Gu, X. Jin, and S.-J. Hwang, "Synergetic Hybridization Effect of Homogeneously Mixed Inorganic and Graphene Nanosheets on the Photocatalytic Activity of Semiconductor," Sol. RRL **5**, (2020).
40. M. Wei, Y. Hong, D. Han, L. Yang, H. Liu, and L. Su, "One-Step Hydrothermal Synthesis of ZnS Quantum Dots-Reduced Graphene Oxide Composites with Enhanced Photocatalytic Activity," Phys. Status Solidi A **215**, (2018).
41. J. Wang, K. Zhang, S. Hao, H. Xia, and M. Lavorgna, "Simultaneous reduction and surface functionalization of graphene oxide and the application for rubber composites," J. Appl. Polym. Sci. **136**, (2018).

42. S.-W. Moon and Y. Chae, "Colorful graphene-based wearable e-textiles prepared by co-dyeing cotton fabrics with natural dyes and reduced graphene oxide," Sci. Rep. **14**, (2024).
43. W. Dai, W. Xiong, J. Yu, S. Zhang, B. Li, L. Yang, T. Wang, X. Luo, J.-P. Zou, and S. Luo, "Bi_2MoO_6 Quantum Dots In Situ Grown on Reduced Graphene Oxide Layers: A Novel Electron-Rich Interface for Efficient CO_2 Reduction," ACS Appl. Mater. Amp Interfaces **12**, (2020).
44. F. Gao, Y. Liu, C. Lei, C. Liu, H. Song, Z. Gu, P. Jiang, S. Jing, J. Wan, and C. Yu, "The Role of Dendritic Mesoporous Silica Nanoparticles' Size for Quantum Dots Enrichment and Lateral Flow Immunoassay Performance," Small Methods **5**, (2021).
45. X. Liu, Y. Zhou, J. Lin, X. Xiao, Z. Wang, L. Jia, M. Li, K. Yang, J. Fan, W. Yang, and G. Li, "Directional Growth and Density Modulation of Single-Atom Platinum for Efficient Electrocatalytic Hydrogen Evolution," Angew. Chem. **136**, e202406650 (2024).
46. H. P. Phan, V. T. Le, V. H. Nguyen, D. H. Nguyen, V. D. Nguyen, N. V. Nguyen, and V. H. Nguyen, "Design of hetero-nanojunction of RGO/\(\alpha\)-Fe\(_2\)O\(_3\) nanofibers for ethanol gas sensor," Commun. Phys. **33**, 103–103 (2023).
47. M. Wei, Y. Hong, D. Han, L. Yang, H. Liu, and L. Su, "One-Step Hydrothermal Synthesis of ZnS Quantum Dots-Reduced Graphene Oxide Composites with Enhanced Photocatalytic Activity," Phys. Status Solidi A **215**, 1800082 (2018).
48. Y. R. Kumar, K. Deshmukh, K. K. Sadasivuni, and S. K. K. Pasha, "Graphene quantum dot based materials for sensing, bio-imaging and energy storage applications: a review," RSC Adv. **10**, 23861–23898 (n.d.).
49. F. A. Permatasari, M. A. Irham, S. Z. Bisri, and F. Iskandar, "Carbon-Based Quantum Dots for Supercapacitors: Recent Advances and Future Challenges," Nanomaterials **11**, 91 (2021).
50. D. Pan, J. Zhang, Z. Li, and M. Wu, "Hydrothermal Route for Cutting Graphene Sheets into Blue-Luminescent Graphene Quantum Dots," Adv. Mater. **22**, 734–738 (2010).
51. D. Khalafallah, J. Miao, M. Zhi, and Z. Hong, "Structuring graphene quantum dots anchored CuO for high-performance hybrid supercapacitors," J. Taiwan Inst. Chem. Eng. **122**, 168–175 (2021).

52. D. Qu, M. Zheng, J. Li, Z. Xie, and Z. Sun, "Tailoring color emissions from N-doped graphene quantum dots for bioimaging applications," Light Sci. Appl. **4**, e364–e364 (2015).
53. M. Choi, J. An, H. Lee, H. Jang, J. H. Park, D. Cho, J. Y. Song, S. M. Kim, M.-W. Oh, H. Shin, and S. Jeon, "High figure-of-merit for ZnO nanostructures by interfacing lowly-oxidized graphene quantum dots," Nat. Commun. **15**, 1996 (2024).
54. T. Du, J. She, X. Yang, Y. Zhao, S. Zhou, and J. Zhao, "Role of functionalization in the fluorescence quantum yield of graphene quantum dots," Appl. Phys. Lett. **122**, (2023).
55. N. Sohal, S. Singla, S. J. Malode, S. Basu, B. Maity, and N. P. Shetti, "Bioresource-Based Graphene Quantum Dots and Their Applications: A Review," ACS Appl. Nano Mater. **6**, (2023).
56. S. Campuzano, P. Yáñez-Sedeño, and J. M. Pingarrón, "Carbon Dots and Graphene Quantum Dots in Electrochemical Biosensing," Nanomaterials **9**, (2019).
57. G. Tan, W. G. Zeier, F. Shi, P. Wang, G. J. Snyder, V. P. Dravid, and M. G. Kanatzidis, "High Thermoelectric Performance SnTe–In2Te3 Solid Solutions Enabled by Resonant Levels and Strong Vacancy Phonon Scattering," Chem. Mater. **27**, 7801–7811 (2015).
58. P. Tian, L. Tang, K. S. Teng, and S. P. Lau, "Graphene quantum dots from chemistry to applications," Mater. Today Chem. **10**, 221–258 (2018).
59. S. Zhu, J. Zhang, C. Qiao, S. Tang, Y. Li, W. Yuan, B. Li, L. Tian, F. Liu, R. Hu, H. Gao, H. Wei, H. Zhang, H. Sun, and B. Yang, "Strongly green-photoluminescent graphene quantum dots for bioimaging applications," Chem. Commun. **47**, 6858–6860 (2011).
60. D. López-Díaz, J. A. Delgado-Notario, V. Clericò, E. Diez, M. D. Merchán, and M. M. Velázquez, "Towards Understanding the Raman Spectrum of Graphene Oxide: The Effect of the Chemical Composition," Coatings **10**, 524 (2020).
61. D. Perumal, E. L. Albert, N. Saad, T. Y. Y. Hin, R. M. Zawawi, H. F. Teh, and C. A. Che Abdullah, "Fabrication and Characterization of Clinacanthus nutans Mediated Reduced Graphene Oxide Using a Green Approach," Crystals **12**, 1539 (2022).
62. M. Lodde, R. P. J. van Veldhoven, E. Verhagen, and A. Fiore, "The effect of In(Ga)As/GaAs quantum dots on the optical loss of photonic crystal cavities," J. Appl. Phys. **135**, 063103 (2024).

63. C. E. Jee, M. K. Chow, and S. P. Yeap, "Fabrication of flexible carbon dioxide gas sensor with conductive polymer/reduced graphene oxide hybrids: Effects of substrate type and mass ratio," J. Appl. Polym. Sci. **140**, e53415 (2023).
64. H. J. Sim, Z. Li, P. Xiao, and H. Lu, "The Influence of Lateral Size and Oxidation of Graphene Oxide on Its Chemical Reduction and Electrical Conductivity of Reduced Graphene Oxide," Molecules **27**, 7840 (2022).
65. P. Das, S. Ibrahim, K. Chakraborty, S. Ghosh, and T. Pal, "Stepwise reduction of graphene oxide and studies on defect-controlled physical properties," Sci. Rep. **14**, 294 (2024).
66. S. Dorontić, S. Jovanović, and A. Bonasera, "Shedding Light on Graphene Quantum Dots: Key Synthetic Strategies, Characterization Tools, and Cutting-Edge Applications," Materials **14**, 6153 (2021).
67. H. Saleem, A. Saud, and S. J. Zaidi, "Sustainable Preparation of Graphene Quantum Dots from Leaves of Date Palm Tree," ACS Omega **8**, 28098–28108 (2023).
68. R. Chuah, S. C. B. Gopinath, P. Anbu, M. N. Salimi, A. R. W. Yaakub, and T. Lakshmipriya, "Synthesis and characterization of reduced graphene oxide using the aqueous extract of Eclipta prostrata," 3 Biotech **10**, 364 (2020).
69. H. Kalil, S. Maher, T. Bose, and M. Bayachou, "Manganese Oxide/Hemin-Functionalized Graphene as a Platform for Peroxynitrite Sensing," J. Electrochem. Soc. **165**, G3133 (2018).
70. S. Tanwar, A. Sharma, and D. Mathur, "A graphene quantum dots–glassy carbon electrode-based electrochemical sensor for monitoring malathion," Beilstein J. Nanotechnol. **14**, 701–710 (2023).
71. S. Gurunathan, J. W. Han, A. A. Dayem, V. Eppakayala, and J.-H. Kim, "Oxidative stress-mediated antibacterial activity of graphene oxide and reduced graphene oxide in Pseudomonas aeruginosa," Int. J. Nanomedicine **7**, 5901–5914 (2012).
72. X. Wu, F. Tian, W. Wang, J. Chen, M. Wu, and J. X. Zhao, "Fabrication of highly fluorescent graphene quantum dots using L-glutamic acid for in vitro/in vivo imaging and sensing," J. Mater. Chem. C Mater. Opt. Electron. Devices **1**, 4676–4684 (2013).
73. R. Guo, T. Li, and S. Shi, "Electron transition pathways of graphene oxide quantum dots unraveled by emission wavelength dependent photoluminescence lifetime," RSC Adv. **7**, 19701–19706 (2017).

74. J. Shen, Y. Zhu, X. Yang, and C. Li, "Graphene quantum dots: emergent nanolights for bioimaging, sensors, catalysis and photovoltaic devices," Chem. Commun. **48**, 3686 (2012).

75. C. Zhang, J. Su, J. Hu, and L. Zhang, "Si@S-doped C anode with high cycling stability using PVA-g-PAA water soluble binder for lithium-ion batteries," J. Appl. Polym. Sci. **137**, 48764 (2020).

76. M. Pavličková, S. Đurđić, M. Hatala, D. Stanković, Ľ. Švorc, P. Veteška, and P. Gemeiner, "Pad printing inks based on reduced graphene oxide and various cellulose binders: Rheological properties, printability and application in electrochemical sensors," J. Appl. Polym. Sci. **140**, e54570 (2023).

77. S. Das and A. Ghosh, "Symmetric electric double-layer capacitor containing imidazolium ionic liquid-based solid polymer electrolyte: Effect of TiO2 and ZnO nanoparticles on electrochemical behavior," J. Appl. Polym. Sci. **137**, 48757 (2020).

78. P. Huo, Z. Xun, S. Ni, Y. Liu, G. Wang, and J. Gu, "Crosslinked quaternized poly(arylene ether sulfone) copolymer membrane applied in an electric double-layer capacitor for high energy density," J. Appl. Polym. Sci. **136**, 47759 (2019).

79. F. C. Tavares, D. S. Dörr, A. Pawlicka, and C. Oropesa Avellaneda, "Microbial origin xanthan gum-based solid polymer electrolytes," J. Appl. Polym. Sci. **135**, 46229 (2018).

80. Y. Li and Y. Zheng, "Preparation and electrochemical properties of polyaniline/reduced graphene oxide composites," J. Appl. Polym. Sci. **135**, 46103 (2018).

81. H. Ji, S. Dhomkar, R. Wu, J. Ludwig, Z. Lu, D. Smirnov, M. C. Tamargo, G. W. Bryant, and I. L. Kuskovsky, "Long spin-flip time and large Zeeman splitting of holes in type-II ZnTe/ZnSe submonolayer quantum dots," J. Appl. Phys. **124**, 144306 (2018).

82. J. Wang, H. Li, L. Zhang, X. Lai, W. Wu, and X. Zeng, "In situ preparation of reduced graphene oxide reinforced acrylic rubber by self-assembly," J. Appl. Polym. Sci. **136**, 47187 (2019).

83. S. P. Ega, S. N. Karri, and P. Srinivasan, "Polyanilines from spent battery powder and activated carbon: Electrodes for asymmetric supercapacitor cell," J. Appl. Polym. Sci. **139**, e52864 (2022).

84. J. Mohanta, D. K. Padhi, and S. Si, "Li-ion conductivity in PEO-graphene oxide nanocomposite polymer electrolytes: A study on effect of the counter anion," J. Appl. Polym. Sci. **135**, 46336 (2018).
85. H. Syawal, N. K. Farhana, Z. L. Goh, S. Bashir, N. M. Saidi, E. Rachagan, S. Ramesh, and R. Kasi, "Highly efficient dye-sensitized solar cells: A comparative study with two different system of solvent-free binary room-temperature ionic liquid-based electrolytes," J. Appl. Polym. Sci. **138**, 51312 (2021).
86. M.-A. AL-Akhras, S. E. Alzoubi, A. A. Ahmad, R. Ababneh, and A. Telfah, "Studies of composite films of polyethylene oxide doped with potassium hexachloroplatinate," J. Appl. Polym. Sci. **138**, 49757 (2021).
87. E. Ruiz-Colón, M. Pérez-Pérez, and D. Suleiman, "Transport properties of blended sulfonated poly(styrene-isobutylene-styrene) and isopropyl phosphate membranes," J. Appl. Polym. Sci. **136**, 47009 (2019).
88. Shalu, S. K. Chaurasia, R. K. Singh, and S. Chandra, "Electrical, mechanical, structural, and thermal behaviors of polymeric gel electrolyte membranes of poly(vinylidene fluoride-co-hexafluoropropylene) with the ionic liquid 1-butyl-3-methylimidazolium tetrafluoroborate plus lithium tetrafluoroborate," J. Appl. Polym. Sci. **132**, (2015).
89. X. Zhao and J. Pionteck, "Electrochemical performance of polydopamine modified PANI/rGO composites: Dependency on preparation sequence," J. Appl. Polym. Sci. **138**, 50663 (2021).
90. S. Acharya, L. Swain, and B. P. Sahoo, "Tunable dielectric characteristics of TPU/PPy composite film and foamyfilm with low loss over a wide range of temperature," J. Appl. Polym. Sci. **140**, e54548 (2023).
91. D. Guo, J. Wang, and J. Lei, "Synthesis and characterization of an acrylate-copolymer-based antistatic agent composed of a single-ion conductive polymer electrolyte," J. Appl. Polym. Sci. **119**, 2674–2682 (2011).
92. S. Ramesh, C. Liew, and K. Ramesh, "Ionic conductivity, dielectric behavior, and HATR–FTIR analysis onto poly(methyl methacrylate)–poly(vinyl chloride) binary solid polymer blend electrolytes," J. Appl. Polym. Sci. **127**, 2380–2388 (2013).
93. M. Albozahid, H. Z. Naji, Z. K. Alobad, J. K. Wychowaniec, and A. Saiani, "Synthesis and characterization of hard copolymer polyurethane/functionalized graphene

nanocomposites: Investigation of morphology, thermal stability, and rheological properties," J. Appl. Polym. Sci. **139**, e53118 (2022).

94. P. Dai, Y. Jiao, H. Ma, X. Zeng, Y. Lu, L. Wang, M. Bao, and M. Zhai, "Radiation synthesis of polysilane-modified graphene oxide for improving thermal conductivity and mechanical properties of silicone rubber," J. Appl. Polym. Sci. **136**, 47776 (2019).
95. L. Ma, D. Zhao, and J. Zheng, "Construction of electrostatic and π–π interaction to enhance interfacial adhesion between carbon nanoparticles and polymer matrix," J. Appl. Polym. Sci. **137**, 48633 (2020).
96. Y. Wang, X. Chen, W. Zhu, X. Huang, X.-Z. Tang, and J. Yang, "A comparison of thermoplastic polyurethane incorporated with graphene oxide and thermally reduced graphene oxide: Reduction is not always necessary," J. Appl. Polym. Sci. **136**, 47745 (2019).
97. D. Joung, L. Zhai, and S. I. Khondaker, "Coulomb blockade and hopping conduction in graphene quantum dots array," Phys. Rev. B **83**, 115323 (2011).
98. O. Akhavan, M. Abdolahad, A. Esfandiar, and M. Mohatashamifar, "Photodegradation of Graphene Oxide Sheets by TiO2 Nanoparticles after a Photocatalytic Reduction," J. Phys. Chem. C **114**, 12955–12959 (2010).
99. X. Xiang, H. Li, Y. Zhu, S. Xia, and Q. He, "The composite hydrogel with "2D flexible crosslinking point" of reduced graphene oxide for strain sensor," J. Appl. Polym. Sci. **138**, 50801 (2021).
100. V. Babaahmadi, R. A. Abuzade, and M. Montazer, "Enhanced ultraviolet-protective textiles based on reduced graphene oxide-silver nanocomposites on polyethylene terephthalate using ultrasonic-assisted in-situ thermal synthesis," J. Appl. Polym. Sci. **139**, 52196 (2022).
101. L. Yang, Z.-G. Chen, G. Han, M. Hong, Y. Zou, and J. Zou, "High-performance thermoelectric Cu2Se nanoplates through nanostructure engineering," Nano Energy **16**, 367–374 (2015).
102. Y. Li, H. Yang, F. Wang, and Y. Huang, "Superior anticorrosion performance of epoxy-based composites with well-dispersed melamine modified graphene oxide," J. Appl. Polym. Sci. **138**, 49866 (2021).

103. Y. Zhang, L. Liu, N. Xi, Y. Wang, Z. Dong, and U. C. Wejinya, "Dielectrophoretic assembly and atomic force microscopy modification of reduced graphene oxide," J. Appl. Phys. **110**, 114515 (2011).

104. U. A. Méndez-Romero, S. A. Pérez-García, X. Xu, E. Wang, and L. Licea-Jiménez, "Functionalized reduced graphene oxide with tunable band gap and good solubility in organic solvents," Carbon **146**, 491–502 (2019).